UNIVERSITY OF SÃO PAULO

INSTITUTE OF GEOSCIENCES

DEFORMATION BAND EVOLUTION ALONG A MAJOR TRANSFER ZONE IN THE CRETACEOUS TUCANO RIFT BASIN, NE BRAZIL

Cleber Peralta Gomes Júnior

Advisor: Prof. Dr. Renato Paes de Almeida

MASTERS DISSERTATION

Post-graduation Program in Geochemistry and Geotectonics: Geotectonics

São Paulo

2018

Cleber Peralta Gomes Júnior

DEFORMATION BAND EVOLUTION ALONG A MAJOR TRANSFER ZONE IN THE CRETACEOUS TUCANO RIFT BASIN, NE BRAZIL

Dissertation submitted to the Institute of
Geosciences at the University of São Paulo
to obtain a master's degree in Geology.
Concentration area: Geotectonics.
Advisor: Prof. Dr. Renato Paes de Almeida.
External coadviser: Prof. Dr. Haakon Fossen (Universitet i Bergen).

SÃO PAULO

2018

Serviço de Biblioteca e Documentação do IGc/USP

Ficha catalográfica gerada automaticamente com dados fornecidos pelo(a) autor(a) via programa desenvolvido pela Seção Técnica de Informática do ICMC/USP

Bibliotecários responsáveis pela estrutura de catalogação da publicação: Sonia Regina Yole Guerra - CRB-8/4208 | Anderson de Santana - CRB-8/6658

PERALTA GOMES JÚNIOR, CLEBER
DEFORMATION BAND EVOLUTION ALONG A MAJOR TRANSFER ZONE IN THE CRETACEOUS TUCANO RIFT BASIN, NE BRAZIL / CLEBER PERALTA GOMES JÚNIOR; orientador RENATO PAES DE ALMEIDA. -- São Paulo, 2018.
92 p.

Dissertação (Mestrado - Programa de Pós-Graduação em Geoquímica e Geotectônica) -- Instituto de Geociências, Universidade de São Paulo, 2018.

1. Subseismic structures. 2. Deformation bands. 3. Rift transfer zone. 4. Tucano Basin. I. PAES DE ALMEIDA, RENATO, orient.
II. Título.

Acknowledgments

Thanks to life, so generous in offering so much and yet always reminding us to be humble to learn and evolve.

To my family, who always gave me support, education and true values to keep me doing this dissertation.

To the professors and coworkers, because they believed and had patience, their contribution and dedication kept me motivated to do a decent job of their effort.

To the friends, because they are the family that we choose and that supports us when encouraging and taking care of each other.

To the Institute of Geosciences and employees, second home that gave me purpose and made me see and experience beyond what I had until then.

Abstract

The Cretaceous Tucano Rift basin exhibits notable examples of subseismic structures, i.e. cataclastic deformation bands and related structures, that help to unravel the pre-Gondwana breakage and South Atlantic opening geologic framework. We investigate the structural kinematic evolution of subseismic structures, their geometry, distribution, frequency, orientation and kinematics within and away from a first order rift transfer zone. The Vaza-Barris rift transfer zone probably acted allowing displacement between arranged *en-echelon* segmented extensional rift axes and connecting major fault-bounded depocenters of minor sub-basins. The great dominance of north to northeast-oriented deformation band faults agrees with the overall structure of the rift, revealing that the majority of the subseismic structures are compatible with the regional stress field responsible for the basin formation. The very steep normal-slip subseismic structures and high rake striation (dip-slip to high-oblique) in slip surfaces are similar both within and away from the transfer zone. Local strike-slip deformation bands are found only along the transfer zone and at the basin borders, possibly recording local stresses related to fault tips and transfer faults, thus suggesting a transtensional strain regime. Different orientation of subseismic structures occur only in pre-rift successions to the east of the area, related to the proximity of major seismic-scale faults and possibly different regional stress fields. Deformation bands within sandstones of the so-called post rift Banzaê Member of the Marizal Formation studied in this work suggests a late rift pulse or continued rifting during the Aptian. Due to cataclasis, these subseismic structures introduce a macro permeability anisotropy in reservoir rocks that should be taken into consideration during well planning and hydrocarbon injection or production situation.

Resumo

A bacia cretácea do tipo Rifte do Tucano exibe exemplos notáveis de estruturas sub-sísmicas, isto é, bandas de deformação cataclásticas e estruturas relacionadas, que ajudam a desvendar a estrutura geológica da ruptura pré-Gondwana e abertura do Atlântico Sul. Investigamos a evolução cinemática estrutural de estruturas sub-sísmicas, sua geometria, distribuição, freqüência, orientação e cinemática dentro e fora de uma zona de transferência de primeira ordem. A zona de transferência de rifte de Vaza-Barris provavelmente agiu permitindo o deslocamento entre eixos de separação extensional *en-echelon* segmentados e conectando grandes depocentros limitados por falhas de sub-bacias menores. A grande dominância das falhas de bandas de deformação orientadas em direção norte-nordeste concorda com a estrutura geral do rifte, revelando que a maioria das estruturas sub-sísmicas são compatíveis com o campo de tensão regional responsável pela formação da bacia. As estruturas sub-sísmicas muito íngremes de deslizamento normal e o alto grau de inclinação (deslizamento-alto a alto-oblíquo) em superfícies de deslizamento são similares dentro e fora da zona de transferência. Bandas locais de deformação por transcorrência são encontradas apenas ao longo da zona de transferência e nas bordas da bacia, possivelmente registrando tensões locais relacionadas à terminações de falhas e falhas de transferência, sugerindo um regime de tensão transtensional. Diferentes orientações de estruturas sub-sísmicas ocorrem apenas em sucessões pré-rifte a leste da área, relacionadas à proximidade de grandes falhas na escala sísmica e possivelmente a diferentes campos de tensão regionais. Bandas de deformação dentro dos arenitos do chamado pós rifte Membro Banzaê da Formação Marizal estudadas neste trabalho sugere um pulso de rifte tardio ou rifte contínuo durante o Aptiano. Devido à cataclase, estas estruturas sub-sísmicas introduzem uma macro anisotropia de permeabilidade nas rochas reservatório que deve ser levada em consideração durante o planejamento de poços e situações de injeção ou produção de hidrocarbonetos.

INDEX

Table of Figures

1. Introduction

The structure of rift transfer zones is known from field observations (Younes and McClay, 2002; Fossen et al., 2005), seismic data (Scott and Rosendahl, 1989), experimental (Schlische and Withjack, 2009) and numerical modeling (Allken et al., 2013). However, most of these studies discuss relatively large-scale aspects of such zones. Little or no attention has been paid to subseismic structures (deformation bands, deformation band zones or clusters, slip surfaces and deformation band faults) with millimeter to meter-scale displacements, which are of particular interest with respect to hydrocarbon production and CO2 sequestration in reservoir-quality rift units. The reason is mainly that most rifts are buried under post-rift sediments and/or seawater, and hence explored by means of seismic data and only scattered well information.

The study area (Fig. 1) hosts notable examples of areas with exposed deformation bands, strain localization structures that form during deformation of highly porous sands and sandstones. We here investigate the structural expression along a first order rift transfer zone and discuss how these structures differ in terms of frequency, distribution, orientation, geometry and kinematics. These structures record local strain and are thus used to address the strain evolution within and away from the transfer zone and infer local stress. The development of subseismic structures may help to unravel the pre-Gondwana breakup and Early Cretaceous opening of South Atlantic. Such structures have been described to influence the permeability of reservoir rocks (Ballas et al., 2015), and a better understanding of them may therefore be of great importance in many hydrocarbon reservoirs.

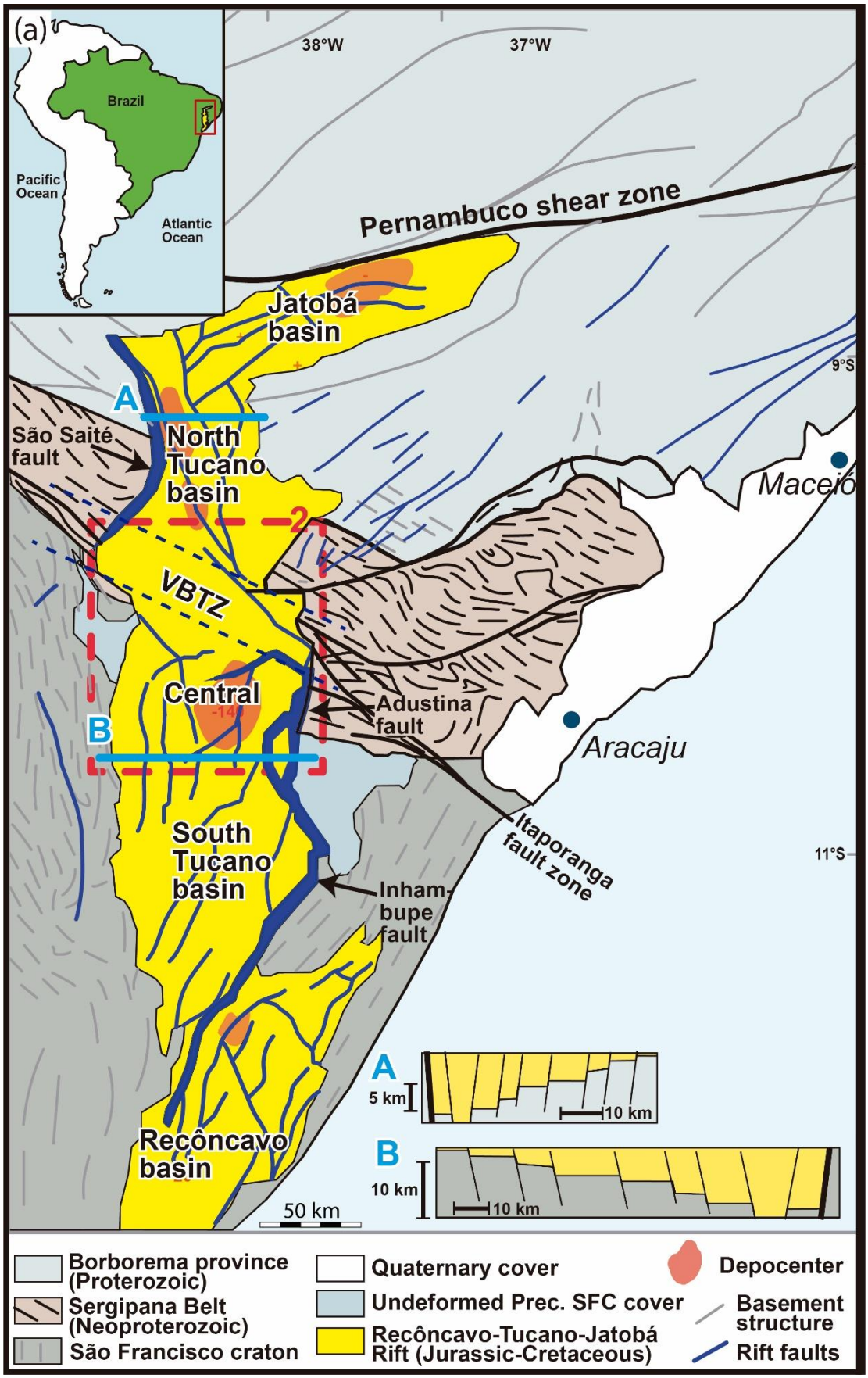

Fig. 1. Recôncavo-Tucano-Jatobá rift system (modified from Magnavita, 1992; Szatmari and Milani, 1999; Gordon et al., 2017).

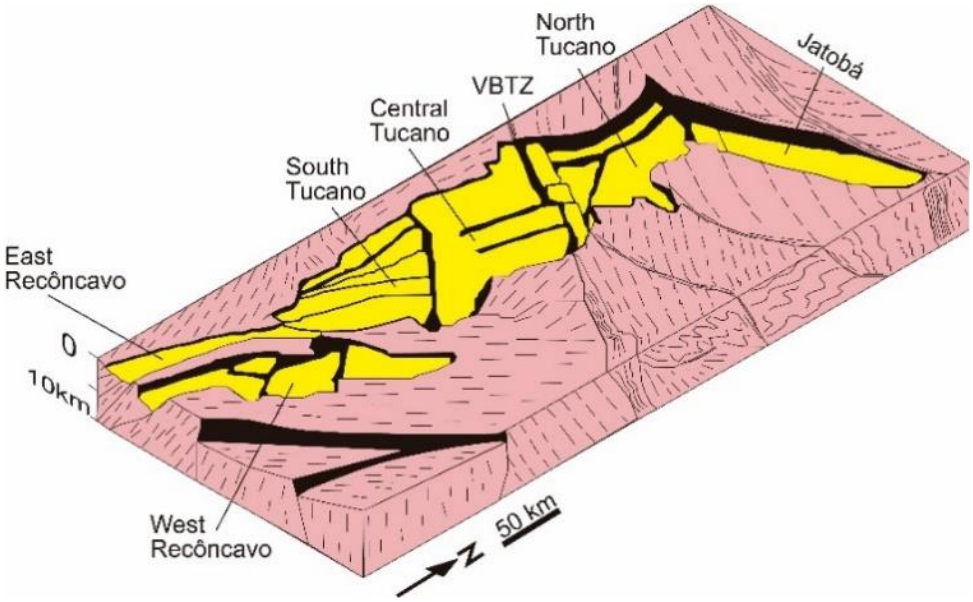

Fig. 2: RTJ rift system block diagram (modified from Milani and Davison, 1988).

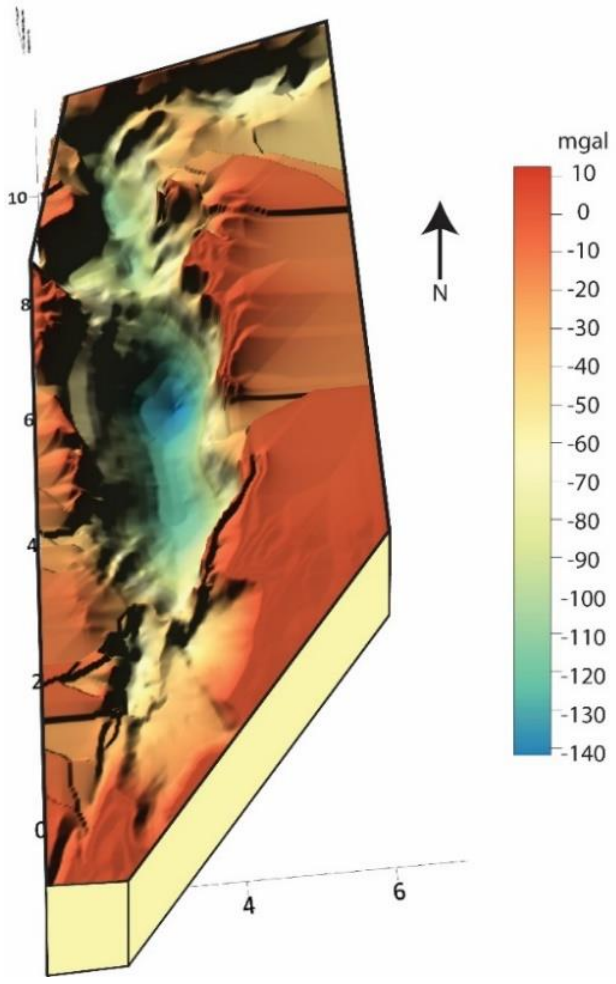

Fig. 3: Gravimetric 3D model. Gravimetric data from Magnavita, 1992.

1.1 Aims

Constrain the geometry and distribution of Central Tucano rift-related faults by mapping and analyzing deformation bands and related subseismic structures with respect to large-scale structures, notably seismic-scale major faults and transfer zones. The work involves the use of existing data (regional gravity, seismic and geological data), remote sensing, fieldwork and microstructural analysis.

Which stratigraphic units contain deformation bands? How the deformation bands develop in different lithologies? How kinematics was developed during faulting? How many rift phases occurred or how long did rifting last? How does the subseismic sandstone deformation influence fluid flow during reservoir production?

Specific Objectives

a) Map and analyze deformation bands and related structures with respect to large-scale structures, notably seismic-scale regional faults and rift transfer zones;
b) Determine the spacing, distribution, orientation and kinematics of the deformation bands and related structures within different stratigraphic units and structural subdomains;
c) Compare deformation bands of both strike-slip and normal-slip sense in the Tucano basin;
d) Compare subseismic deformation along a first order rift transfer zone with overall rift basin;
e) New data on pre-Gondwana breakup and Early Cretaceous South Atlantic opening;
f) Estimate permeability reduction within sandstone reservoirs.

1.2 Methods

1- Compilation of published information regarding rift basins and related transfer zones, as well as deformation bands within sandstones.

2- Compilation of data from the Tucano-Recôncavo-Jatobá rift system stratigraphy, structure and evolution.

3- Field data acquisition from exposed subseismic structures in the Central Tucano Basin within the Vaza-Barris transfer zone and away from it. These features were compared to similar structures observed in the Colorado Plateau in Utah, a classic area of cataclastic deformation bands that was visited by the candidate during a field course promoted by the University of Bergen during the project.

4- Integration of field data with published geological maps, geophysical (gravity and seismic) data and remote sensing to access their large-scale distribution, spacing, orientation and influence on fluid flow within sandstone reservoirs.

5- All data collected during structural mapping of planar and linear subseismic structures strain localization, spacing and distribution was carried out with the aid of FieldMove Clino Pro (Midland Valley Exploration Ltd).

6- Fault slip data from striated (*slickenlines*, *striae* or lineations) slip surfaces was used for strain inversion. The structural analysis was carried out with the aid of the softwares FaultKin 7 (Allmendinger, 2017) and ORIENT 3.7 (Vollmer, 2017), based on M-plane, or *movement plane*, geometry (Twiss and Unruh, 1998; Marrett and Allmendinger, 1990). Fault plane solution (*beachballs*) and kinematic tensors (*average axes*) were calculated from Linked Bingham analysis.

7- Deformation bands may develop a series of short parallel (linking) bands bounded by longer zones of bands forming open networks called "*ladder structures*" (Davis, 1999; Schultz and Balasko, 2003) that tend to develop Riedel geometries and nested patterns with several ladder generations, in which rotation leads to a global sigmoidal configuration (Katz and Weinberger, 2005). These structures helped unravel paleostrain and kinematics sense depending on the plan view.

8- The conjugate sets data allowed to calculate their Line of Intersection (intermediate stress axis) and poles of Bisecting Planes (maximum and minimum stress axes), which was carried out with the aid of the software Stereonet 10 (Allmendinger, 2017).

2. Rift Systems and Transfer Zones

2.1 Rift Systems

Rift systems are distributed worldwide and generally form in extensional tectonic regimes with remarkable mechanical subsidence and faulting due to continental lithosphere stretching, thinning and rupture during rifting. Extensional sedimentary basins (Fig. 4) form as depressions filled by sediments with border uplift bounded by high angle normal faults at least in one side.

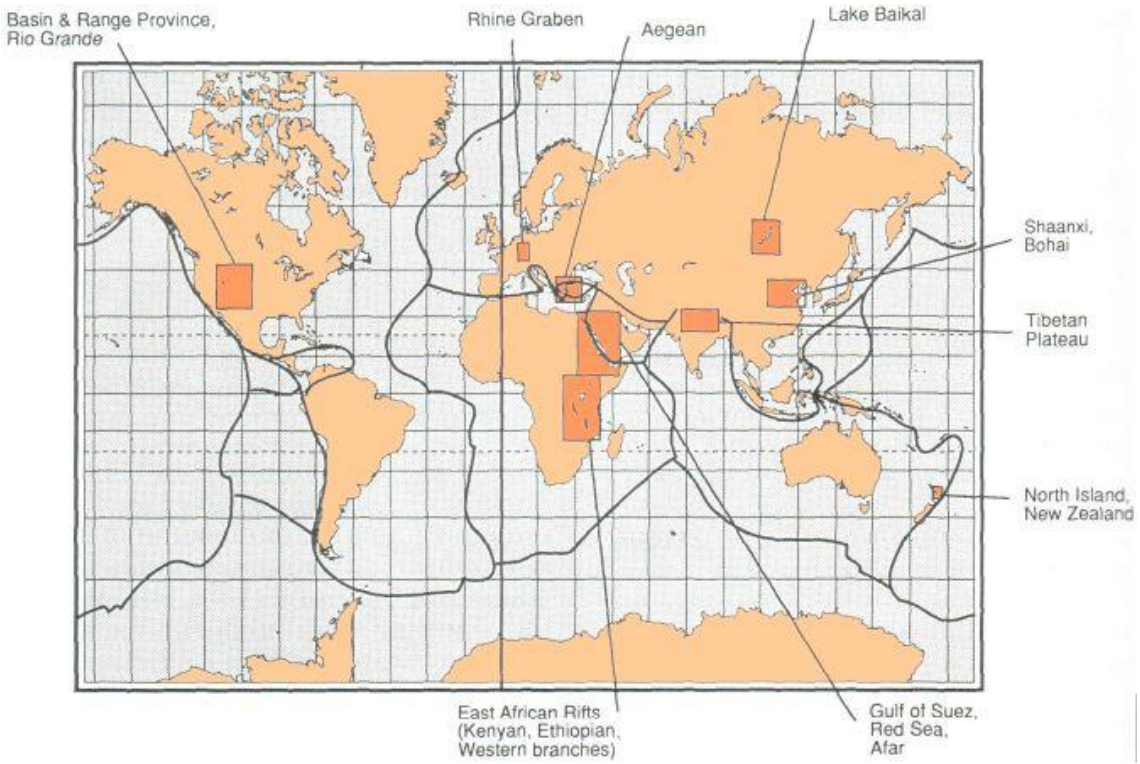

Fig. 4. Extensional sedimentary basins distributed worldwide (Sengör, 1995).

Rift systems can still be active (or modern) nowadays and when lithospheric stretching lasts long enough, they may develop ongoing seafloor spreading and turn into passive margins (Fig. 5). Otherwise, if they fail, they are called fossil or palaeo-rifts (aulacogen or abandoned arm) (Olsen & Morgan,1995).

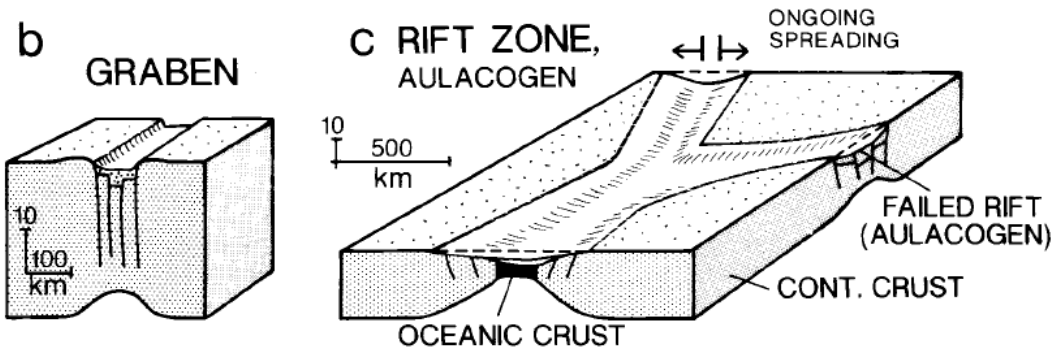

Fig. 5. Divergent boundary basins (Einsele, G., 2000).

The concept of the East African Rift System was proposed by Suess (1891). The term rift valley was coined by Gregory (1894) also to describe the great system of shoulders and valleys, bounded by escarpments and high angle faults characteristic of East Africa. Gregory (1920) defined rift valleys as the results of subsidence between a parallel series of faults and latter, and Dixey (1938, 1946) assumed that rifts were products of uplift and subsequent fracture of the crust formed between fault systems.

The East African Rift System was investigated by seismic surveys (Fig. 6) (Rosendahl, 1987; Scott and Rosendahl, 1989) and several stages of evolution during rifting were then proposed. Initial stretching and thinning of the continental lithosphere would be followed by subsidence of the upper crust and development of asymmetric graben, subdivided in blocks and with large development of the half-graben system. At the beginning, rift shoulders uplift and after this, an opposite face to the system master fault develop, forming an opposite active fault and a passive master fault, so the central region acts as a free block. The large development of shoulders leads to alternation of active phase between master fault and opposite fault, where a free block can undergo subsidence and uplift phases. Then, both faces separate apart from each other and starts the spreading phase.

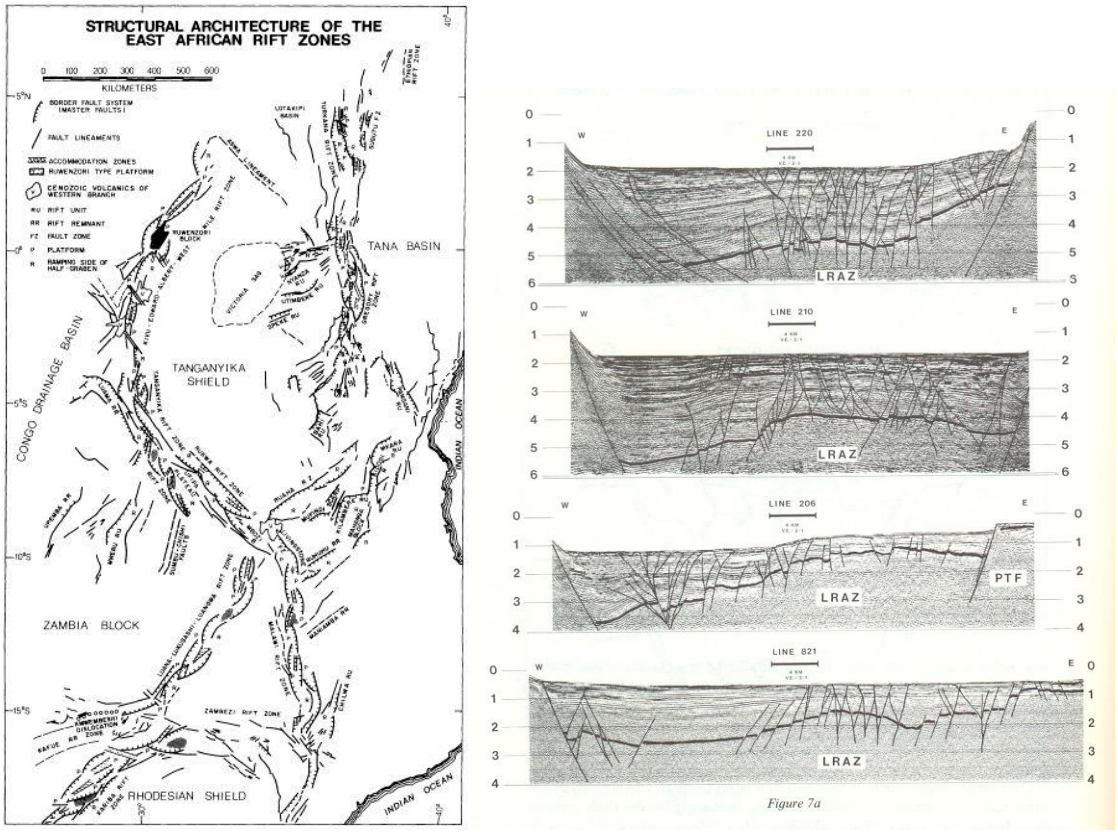

Fig. 6. Seismic surveys and profiles along the Tanganyika Lake (from Rosendahl, 1987).

An alternative classification (Prosser, 1993) suggests that distinct stages of rift and post-rift systems could occur repeatedly during the evolution of rift systems. The evolution of rift systems would progressively include pre-rift, initial rift, rift climax, immediate post-rift and late post-rift stratigraphic sequences (Fig. 7). However, it is unclear how post-rift sequences may occur during rifting, being not properly distinguished these two terms. A more consistent classification (Gawthorpe & Leeder, 2000) divides rift evolution into different phases: initial phase, interaction and linkage phase, through-going fault (tectonic) phase and post-tectonic phase (Fig. 8).

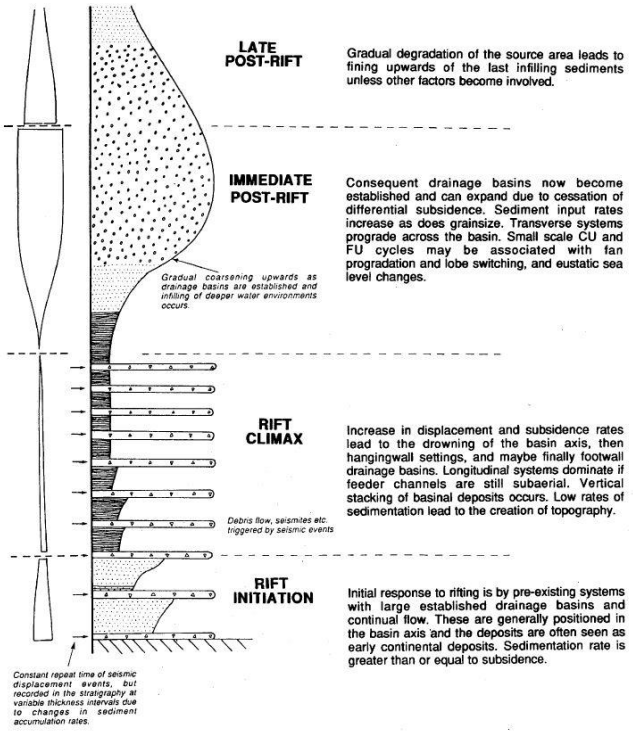

Fig. 7. Idealized log of the vertical lithostratigraphy through the rift basin center (from Prosser, 1993).

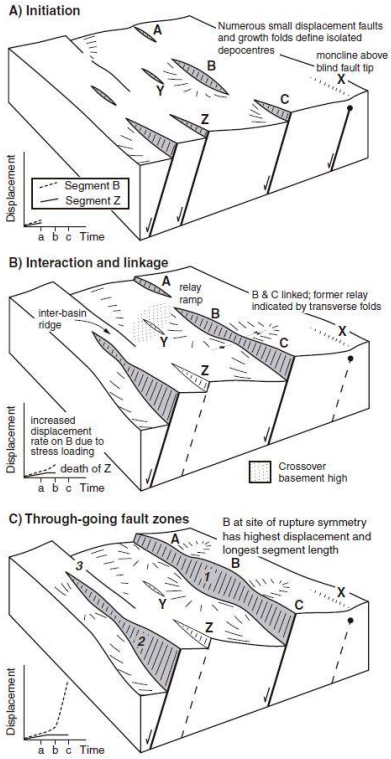

Fig. 8. Schematic 3D evolution of a normal fault array (from Gawthorpe & Leeder, 2000).

Lithospheric-scale initial models such as pure (symmetric) shear (McKenzie, 1978) and simple (asymmetric) shear (Wernicke, 1981) were fundamental for the development of the following studies regarding rift systems (Fig. 9). Simple shear in the brittle crust and pure shear in the ductile lithosphere combined mechanisms are both important during extension (Allen & Allen, 2005). Pure shear is a perfect co-axial planar strain that does not involve rotation of strain axes or a marker from its original position, keeping the volume constant, since it compensates shortening in one direction by extension in another. Simple shear involves planar strain with constant volume too but not co-coaxial, thus involving rotation of a marker from its original position, so strain axes orientation varies during strain evolution (Fossen, 2018).

Further studies in continental extension terranes, based on simple shear extension mechanisms, suggests that major detachment faults (Lister, 1986) lead to an inherent asymmetry of extensional structure, uplift and subsidence patterns (Fig. 10). Evolutionary characteristics of the system are related to rheological variations and their influence on the brittle-ductile transition of the crust. Master faults tend to be planar until the brittle-ductile transition of the crust, where below this limit the faults evolve as listric faults. Displacement of the focus of crustal thinning is associated with the thinning of the lithospheric mantle, thus also explaining the asymmetry involved in this type of basin. Variation in crustal thickness may occur due to the low angle of master faults that are associated with changes in density and flexural rigidity of the rocks to explain the development of the basin.

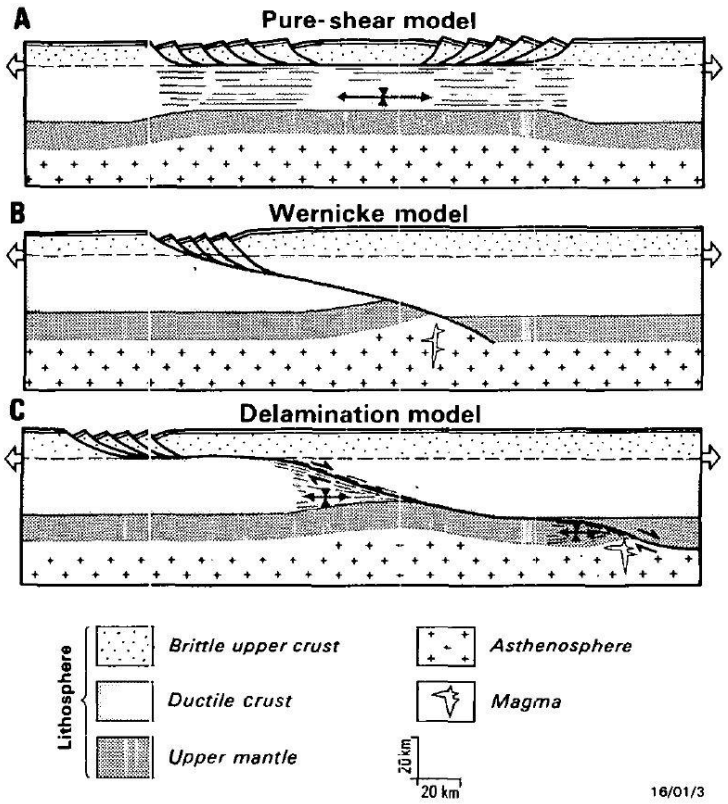

Fig. 9. Geodynamic models for continental extension (from Lister et al. 1986).

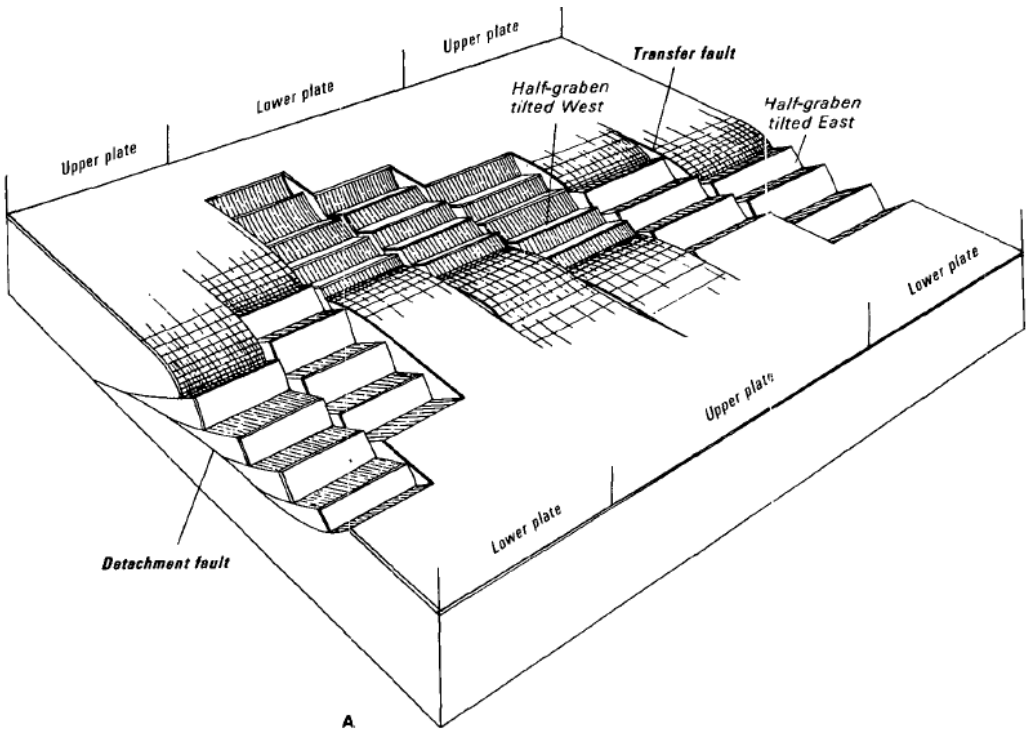

Fig. 10. Changes from upper plate to lower plate occurring across transfer faults (from Lister, 1986).

The beginning of the rift process is associated with a local increase in temperature, which changes the depth of the geotherms making them shallower. The upper crust, of low-velocity and low-density, reacts like a zone of weakness that undergoes intense thinning and extension caused by the deformation of the mid-inferior crust. The evolution of this scenario leads to a superficial dome that culminates in a series of small faults. After initial deformation, the rate of extension within the upper crust increases and results in the generation of space and formation of the primary horst and graben system. The process may be non-continuous, with changes in the crust and lithosphere always based on the evolution of distinct velocity, density and viscosity zones.

The role of mantle dynamics during rifting controls whether active (mantle involved) or passive (mantle not involved) rifts are formed. Active rifts occur due to the high temperature anomaly responsible for primary deformation, where elastic properties of the lithosphere are responsible for flexural uplift of the shoulders in response to subsidence and thinning of the upper crust and the formation of graben. In active rifts, there is intense volcanism with the ascension of the asthenosphere being independent of the magnitude of the lithospheric extension. They are characterized by crustal swelling (causing dome or large continental plateaus) and lower subsidence rate due to the great addition of material in the crust (Sengör, 1995). Passive rifts occur due to the occurrence of a regional stress field of sufficient magnitude to exceed the boundary of the local resistance envelope, resulting in an extensional deformation process of the lithosphere. In passive rifts, the local stress field is connected to the plate border and to the lithostatic forces. The mass movement of the asthenosphere in the system takes place passively (due to the lithosphere extension) and is responsible for the lithospheric thinning and fracturing of upper brittle crust. In this context partial fusion of the asthenosphere can occur in small portions, which advances with the course of the extension. These systems are characterized by rapid subsidence and uplift of the shoulders associated with block rotation (by faulting), flexural rigidity, lateral thermal flow or local magma production (Sengör, 1995).

Rift basins can be distinguished by the thermal structure of the lithosphere under the system, thickness of the crust and thermal gradient of the lithosphere determining stretching pattern and subsidence rates (Sengör, 1995; Allen & Allen, 2005): African type with normal crustal thickness and heat flow (30-35 km, ~60mW/m²), slow extension for long periods of time, high angle master faults, small total area with elongated and narrow systems with deep individual basins; Basin and Range type with thick crust at the

beginning of extension and high heat flow (~60 km thick, ~100mW/m²), rapid extension for short periods of time, low angle master faults and large overall area with large basin systems with many small basins associated with ductile extension at lower levels and the exhumation of core complexes; and Aegean-type with intermediate crustal thickness and heat flow (~45 km, ~80mW/m²) with large rifts but composed of deeper basins.

More recent, numerical geodynamic modelling has become an important tool to predict basic properties of non-volcanic rifted margins (Fig. 11). Numerical modelling has been used to compare 'type I' margins (such as the Iberia-Newfoundland conjugates), where large tracts of continental mantle lithosphere are exposed at the sea floor, and 'type II' margins (such as some ultrawide central South Atlantic margins), where thin continental crust spans wide regions below which continental lower crust and mantle lithosphere have apparently been removed. Neither corresponds to uniform extension, instead, either crust or mantle lithosphere has been preferentially removed. In type I, depth-dependent extension results in crustal-necking breakup before mantle-lithosphere breakup and in type II, the converse is true, whereas in the latter underplating may occur (Huismans and Beaumont, 2011).

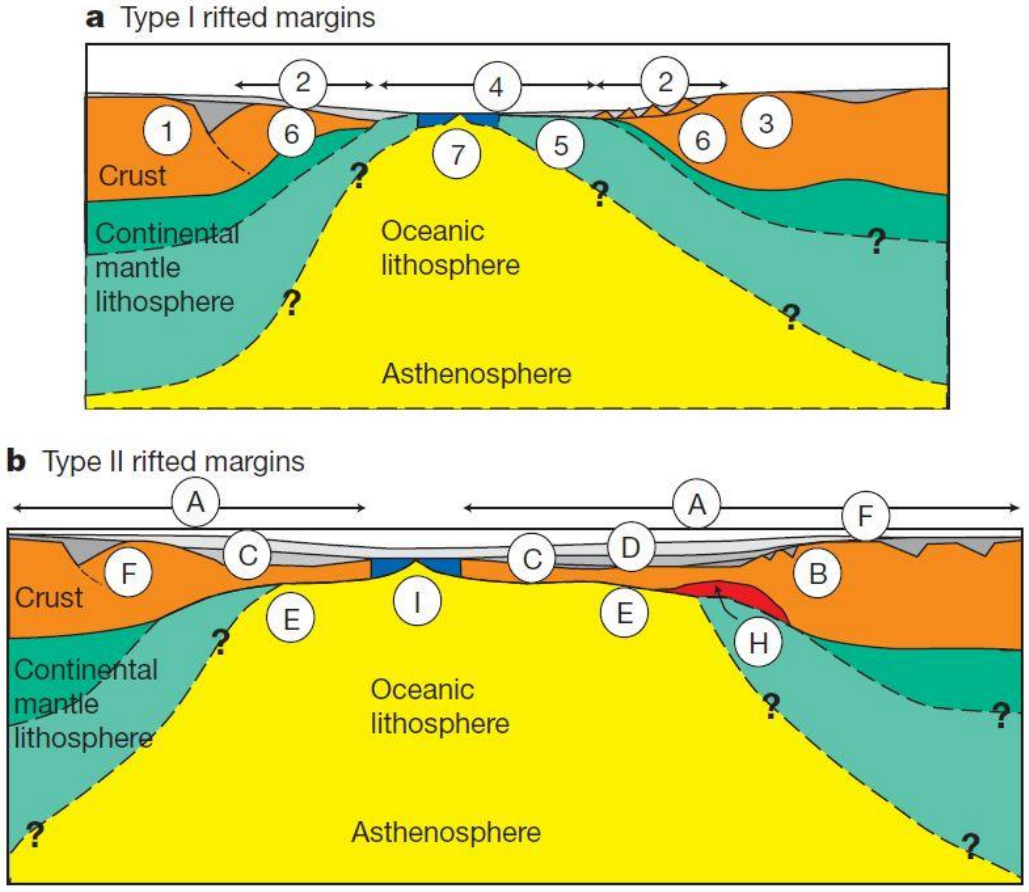

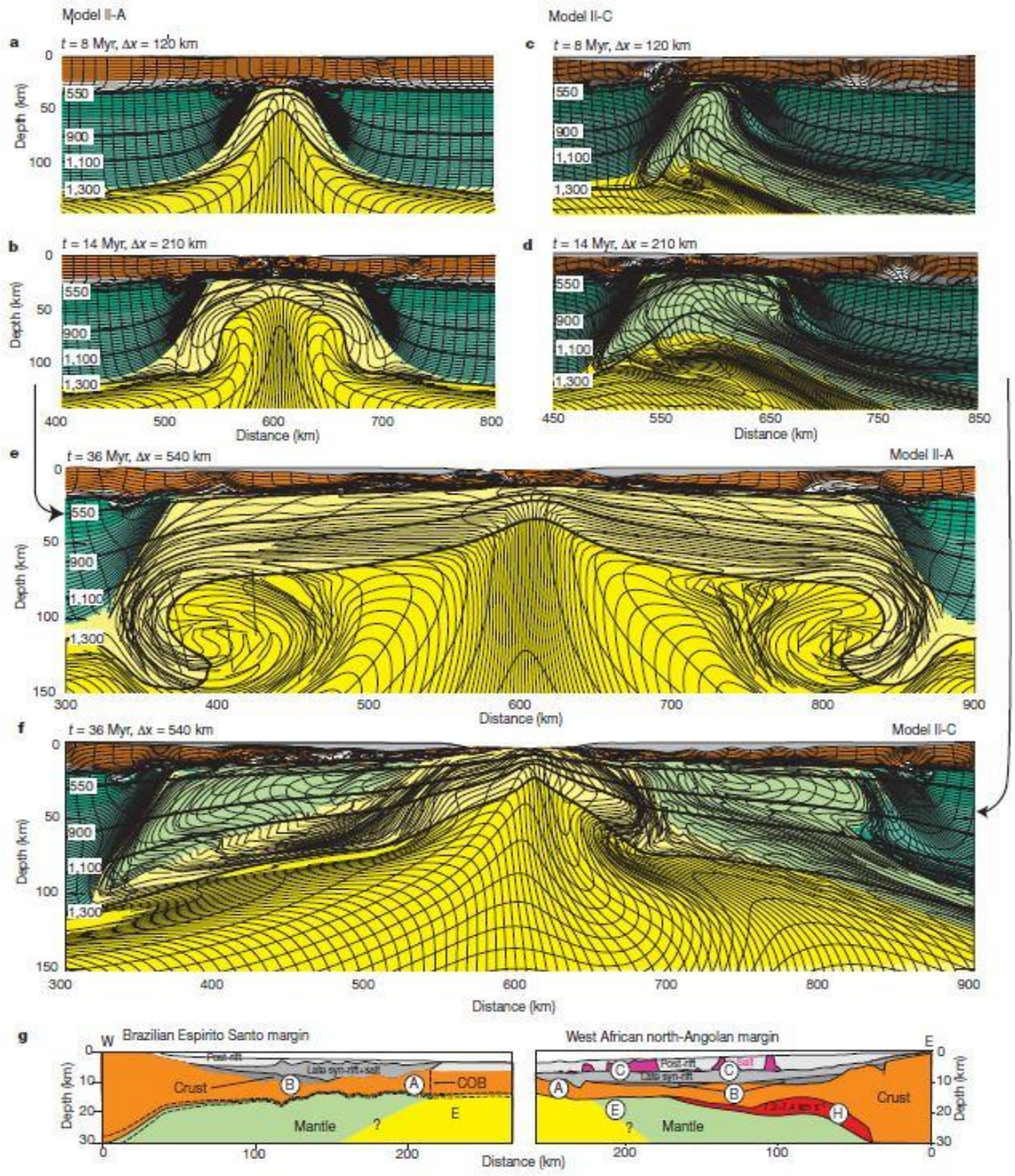

Fig. 11. Characteristic properties of type I and type II margins (above) and detailed type II margins (below) (from Huismans and Beaumont, 2011).

2.2 Transfer Zones

Transfer zones are integral components of continental rifts, separating first-order compartments of contrasting structural expression and connecting basin-bounding master faults. Several geometrically different types of transfer zones have been described in the literature (Rosendahl et al., 1986; Morley, 1990), and a particularly common type is the conjugate overlapping type (Morley, 1990), where two oppositely dipping master fault and their associated depocenters switch locations from one side of the basin to the other across the transfer zone.

Early researches on extensional basin margins (Gibbs, 1984) defined transfer zones as areas that limit structural units and accommodate different structural domains in an extensional zone. Transfer faults trends at a high angle to the margins, accommodating different slip rates between extension and in many cases as either latter faults or rift integral components. Transfer faults offset marginal features and allow margins to switch from upper-plate to lower-plate characteristics along strike (Lister, 1986). They act similarly to oceanic transform faults linking axial extensional fault segments and accommodate mismatches between both high- and low-angle normal faults nucleating at different places along strike. Thus, they transfer strain from one basin unit (e.g. half-graben) to another (Rosendahl et al., 1986).

Transfer zones would differ from accommodation zones (Rosendahl, 1987), because accommodation zones did not consider the temporal evolution of the fault system and how these changes affect the geometry of the basin. Transfer faults influence the variations of graben subsidence and uplift of shoulders where geometry can be varied (Figs. 12 and 13), directly linked to the deformation of the zone affected by the extension. They constitute areas of discrete deformation, characterized by the formation of planes and small faults, that can reactivate preexisting zones of weakness.

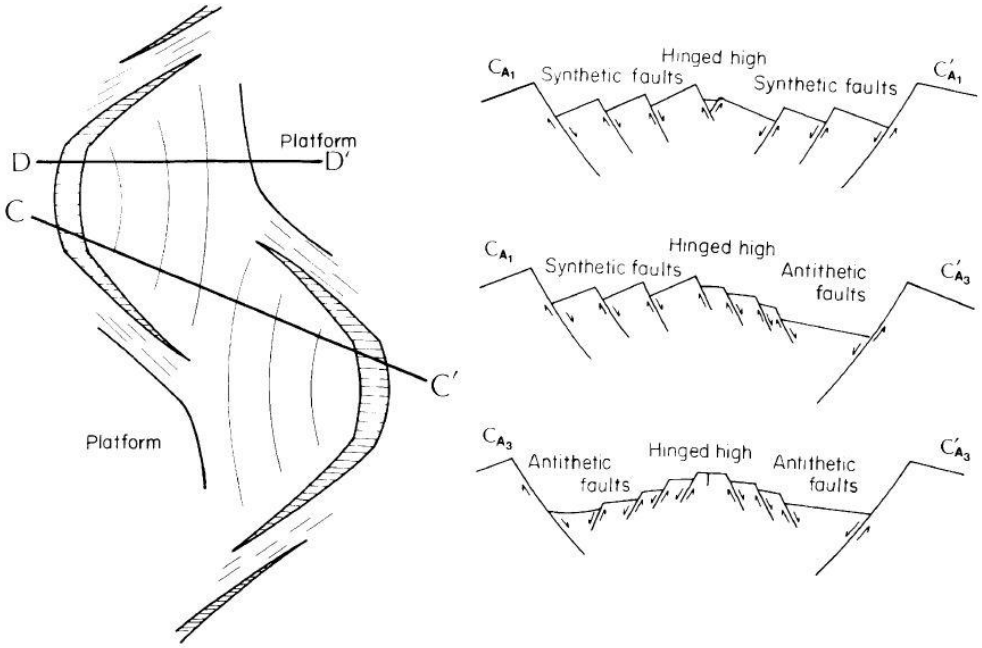

Fig. 12. Overlapped two facing opposing half-graben and associated hinged ridge or hinged high (from Rosendahl et al., 1986).

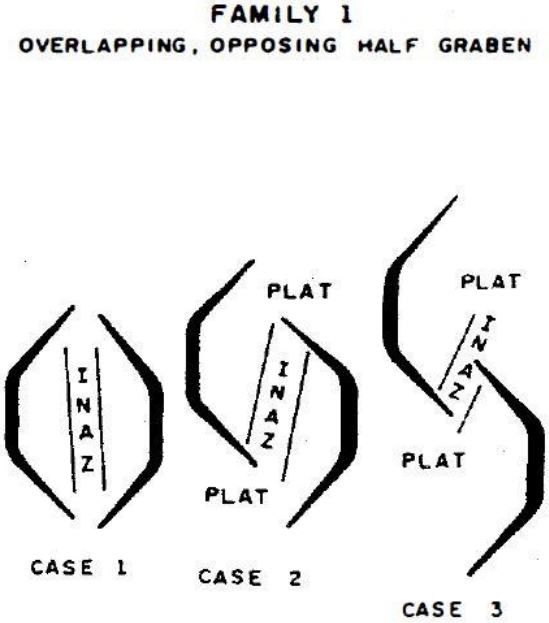

Fig. 13. Overlapping transfer zones (Scott and Rosendahl, 1989).

A commonly used classification of transfer zones (Morley, 1990) includes three main criteria: primary subdivision by relative orientation of throw of the major faults (synthetic and conjugate); secondary subdivision of conjugate transfer zones into where

the normal faults dip toward each other (convergent) and where occur between faults that dip away from each other (divergent); and the tertiary subdivision by fault terminations in map view; fault tips approach, or they overlap, completely overlap ("collateral") or are in line ("collinear") (Fig. 14). Orthogonal transfer zones are often associated with fault terminations (Schlische & Withjack, 2009) and may invert basin depocenters (Fig. 15a) when linking overlapped opposite dipping major faults (Magnavita, 1992).

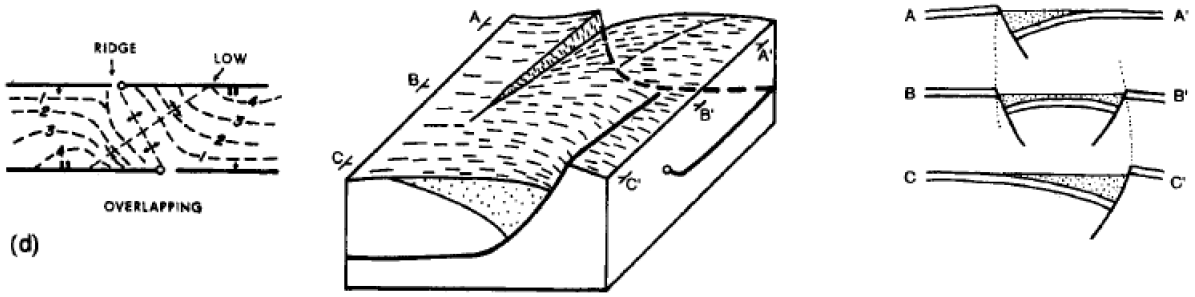

Fig. 14. Conjugate overlapping transfer zone (from Morley, 1990).

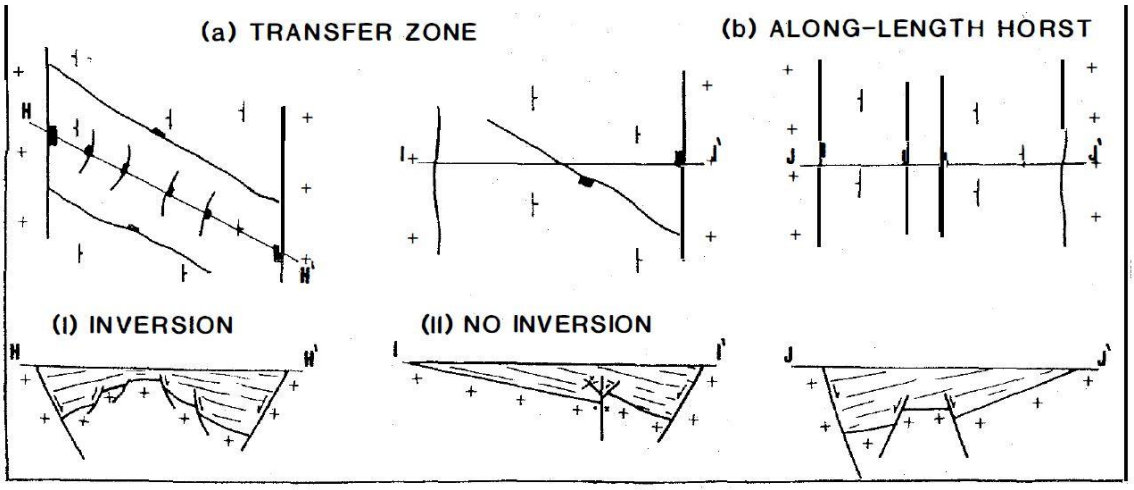

Fig. 15. Transfer zones map-view and cross-section (Magnavita, 1992).

3. Structures

3.1 Introduction

Deformation bands and related structures are found in many upper-crustal tectonic and non-tectonic regimes within highly porous sand(stones) (Aydin and Johnson, 1983; Fossen et. al, 2007, 2017). These structures are particularly relevant for this study because the Tucano basin hosts notable examples of cataclastic deformation bands and related structures that help unravel the strain evolution in the study area.

3.2 Subseismic structures: deformation bands, clusters, slip surfaces and faults

Deformation bands are localized mm-scale tabular, although non-discrete, strain deformational structures that form in rocks with high porosity, firstly described (Aydin and Johson, 1983) in sandstones of the Triassic-Jurassic of the Colorado Plateau, Utah, US. One of the objectives in the study of deformation bands is to obtain information about the physical conditions during deformation from structural and petrographic observations of deformation bands. Another is to be able to predict the type of deformation band in a given reservoir based on its lithological characteristics, depth of burial during deformation and other relevant geological information (Fossen, 2010).

Deformation bands are commonly arranged as Riedel structures (Katz et. al 2005), forming conjugate sets and also developing ladder-style internal linking bands (Schultz et al., 2003). The ladder structures can rotate during cataclastic shear-zone evolution (Katz et al., 2005) and when they reach several meters of thickness the term “radiator” rock is proposed (Davis, 1999).

Deformation bands can accumulate over time to form deformation bands zones (or clusters), a group of interconnected deformation bands within a network producing certain spatial distribution or arrangement. At some point, and particularly if strain hardening occurs, deformation bands or clusters can develop slip surfaces along or deformation band faults which much larger displacements may accumulate. Once slip surfaces form, a fault is formed, a surface created by brittle failure of rock with an offset along markers. An expected sequence of progressive shear strain increase would develop

deformation bands, clusters, slip surfaces and major faults (Fig. 16). Faults have an average Dmax / L ratio (maximum displacement / length) greater than deformation bands (Schultz and Fossen, 2002).

\\\\\\\\\\\\\\\

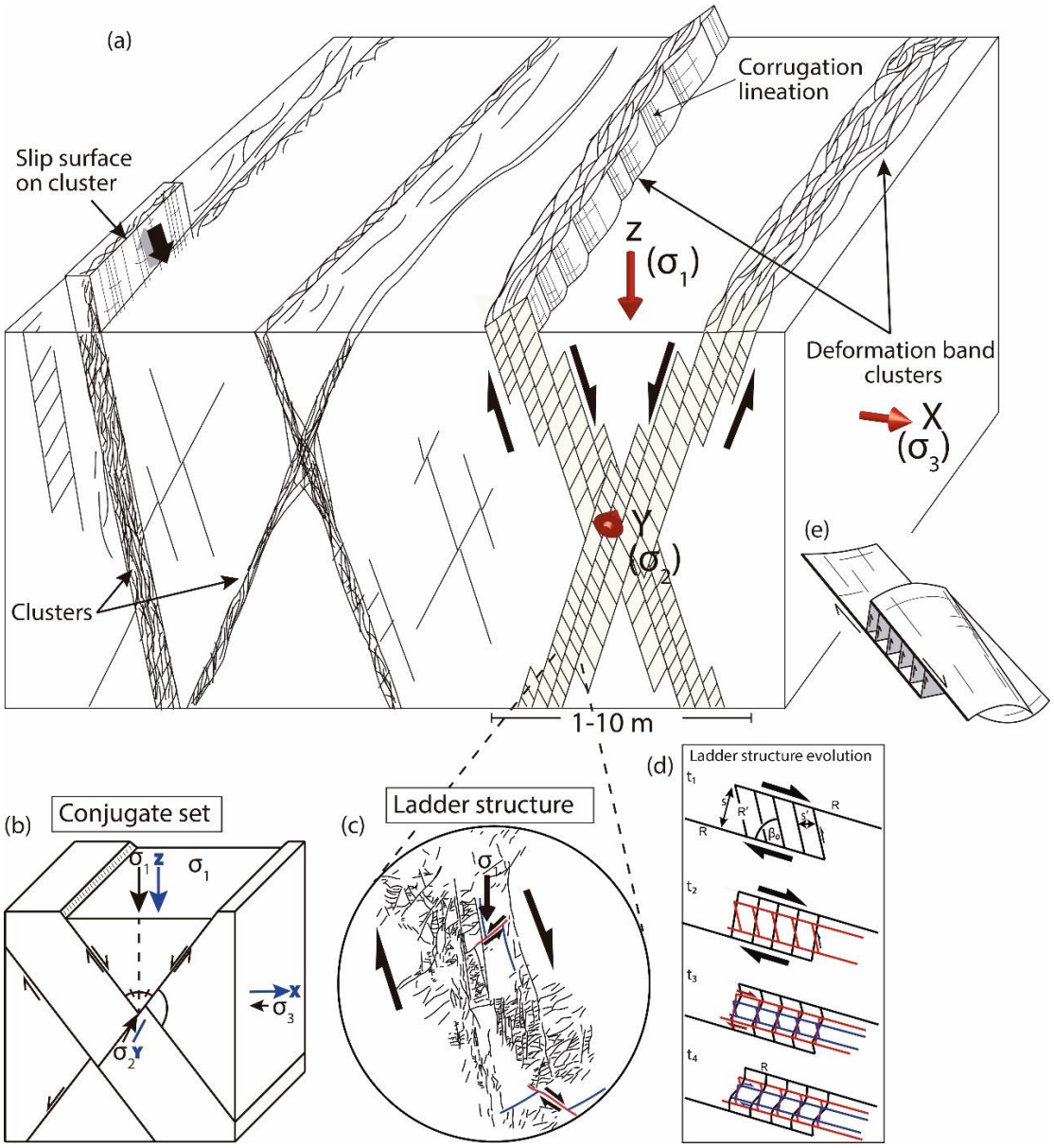

Fig. 16. Block diagram showing normal sense ladder structures on vertical profile and \anastomosed pattern in map view (modified from Fossen, 2018). Stress related to conjugate sets are shown (right and bottom left). Cataclastic shear zone with rotational ladder structures (left): R and R' are synthetic and antithetic shear bands, respectively, and β_0 is the initial angle between them (bottom right figure modified from Katz et al., 2005).

The deformation bands within the Colorado Plateau (Utah) and the Tucano basin are both cataclastic deformation bands (Figs. 17-19), thus involving cataclasis and permeability reduction, grouping into clusters and developing slip surfaces and faults.

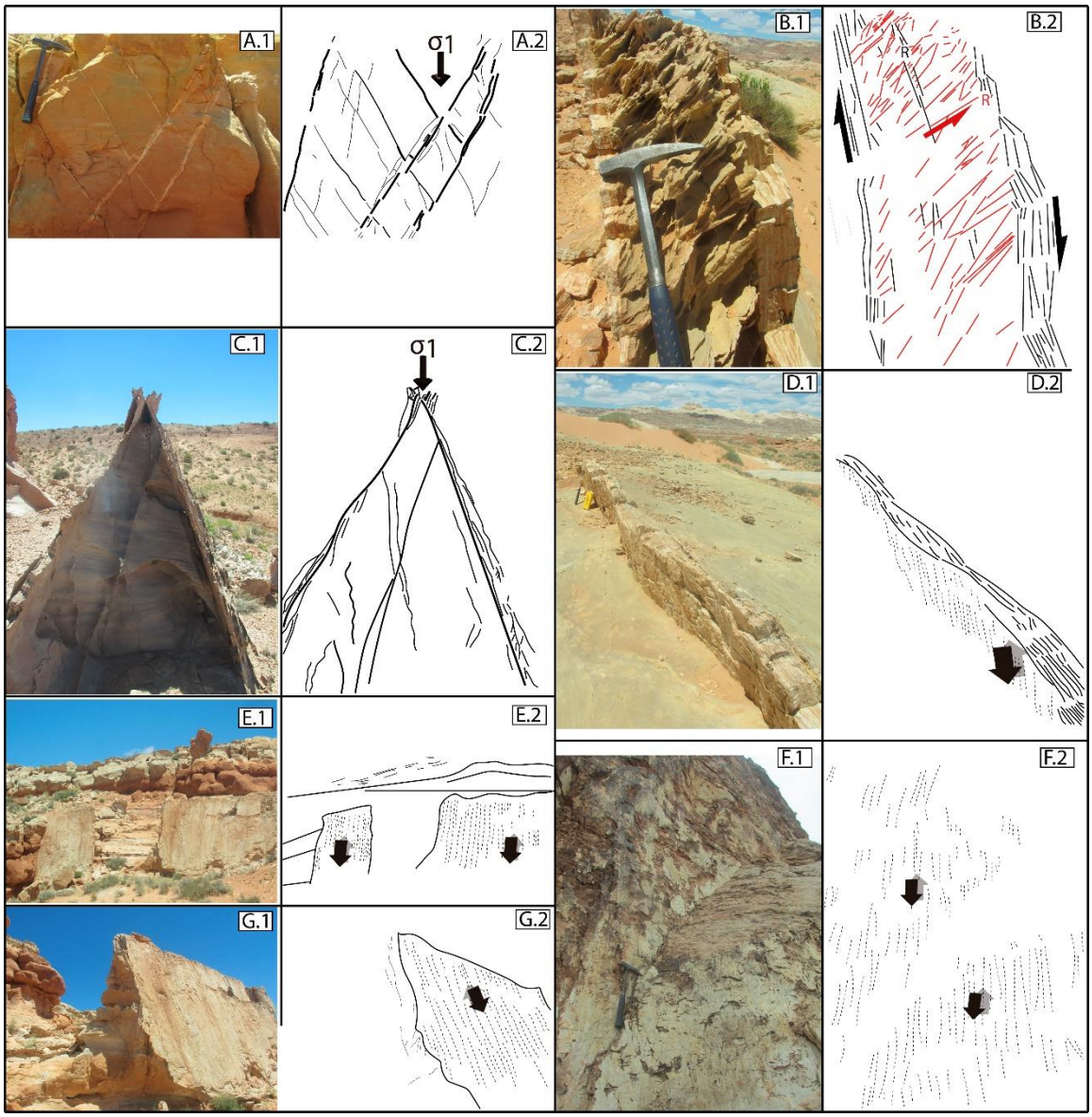

Fig. 17. Subseismic structures within the Colorado Plateau – Utah: A) deformation band conjugate sets. B) ladder-style linking bands. C) erosional features of conjugate sets known as tepee. D) deformation band cluster. E) Aydin's Wall slip surface. F) Slip surface near Courthouse Fault. G) Aydin's wall detail.

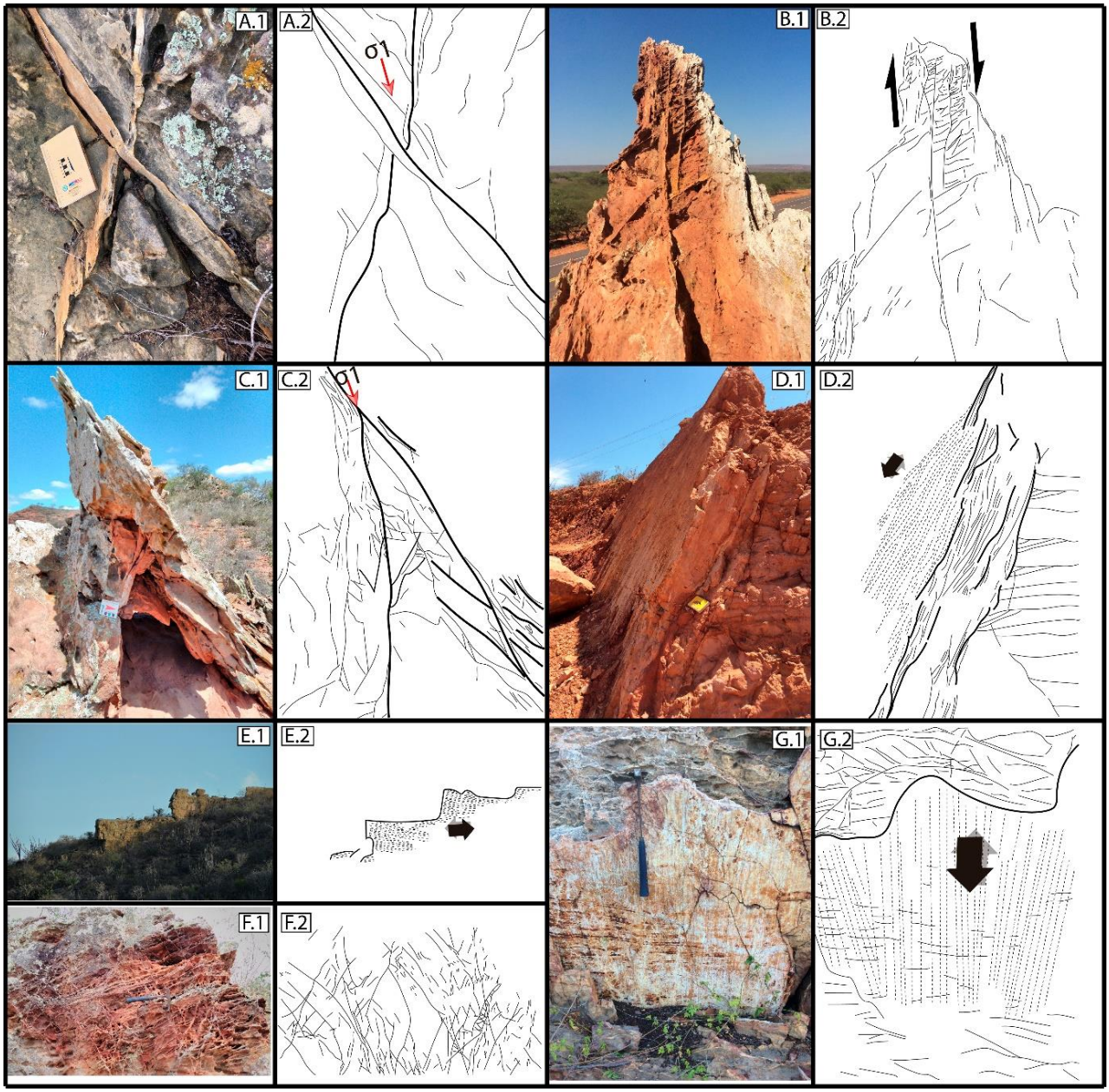

Fig. 18. Subseismic structures within the Tucano Basin. A: Deformation band conjugate sets. B: Steep dip-slip deformation band cluster with normal sense ladder structures. C: Deformation bands conjugate sets geomorphological features known as *tepee*. D: Deformation band cluster nearby fault core. E: Steep and thick deformation band clusters. F: thick deformation band conjugate sets. G: Steep slip surface.

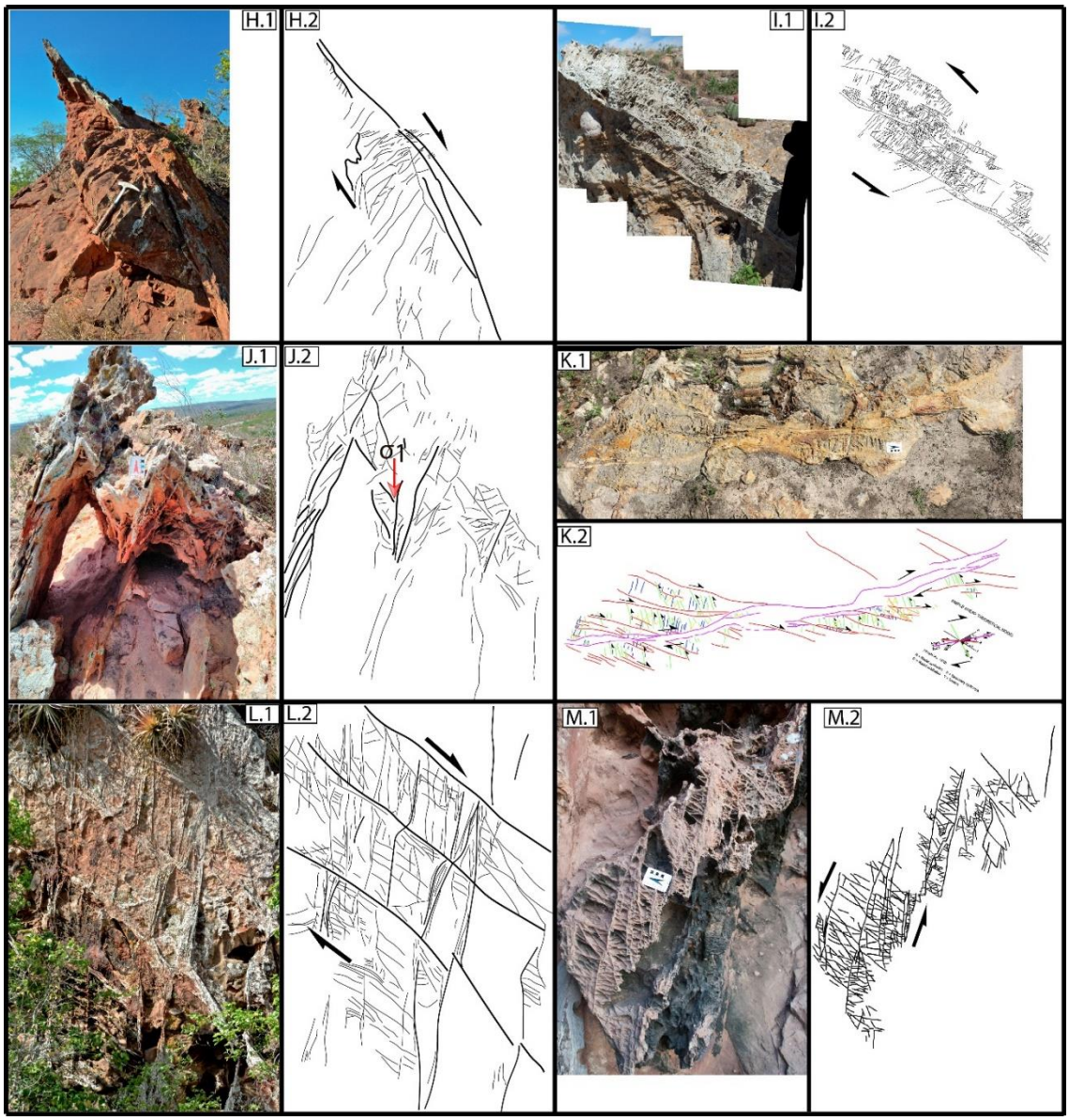

Fig. 19. Subseismic structures within the Tucano Basin. H: Normal sense ladder structures. I: Low angle dipping deformation band cluster with reverse sense rotated ladder structures. J: Double *tepees*. K: Strike-slip deformation band cluster with horizontal ladder structures. L: 10-meters high confining deformation bands with linking-bands in ladder-like geometry. M: deformation bands developing normal sense ladder structures.

Fault Damage Zone

The fault damage zone is a zone surrounding the fault slip surface or fault core in which the host rock has been deformed, and where the deformation can be related to the fault (Fig. 16). The intensity of deformation bands increases towards failure (Schueller et al., 2013).

In Goblin Valley, southeastern Utah, a 6-meter fault (Fig. 20) shows remarkable deformation band zones (or clusters) with developed ladder-style linking-bands in the fault damage zone (Fossen and Hesthammer, 1997). It is possible to see that the gray sandstone (at the top) contains many more deformation bands than the underlying sandy siltstone, which also reflects the preference of formation of deformation bands in coarse and porous sediments.

Meter-scale faults and their damage zones with associated deformation bands are also found within the Tucano Basin (Fig. 21), more pronounced within coarser sandstones where erosional processes develop geomorphological features known as *tepee* (Figs. 18c and 19j).

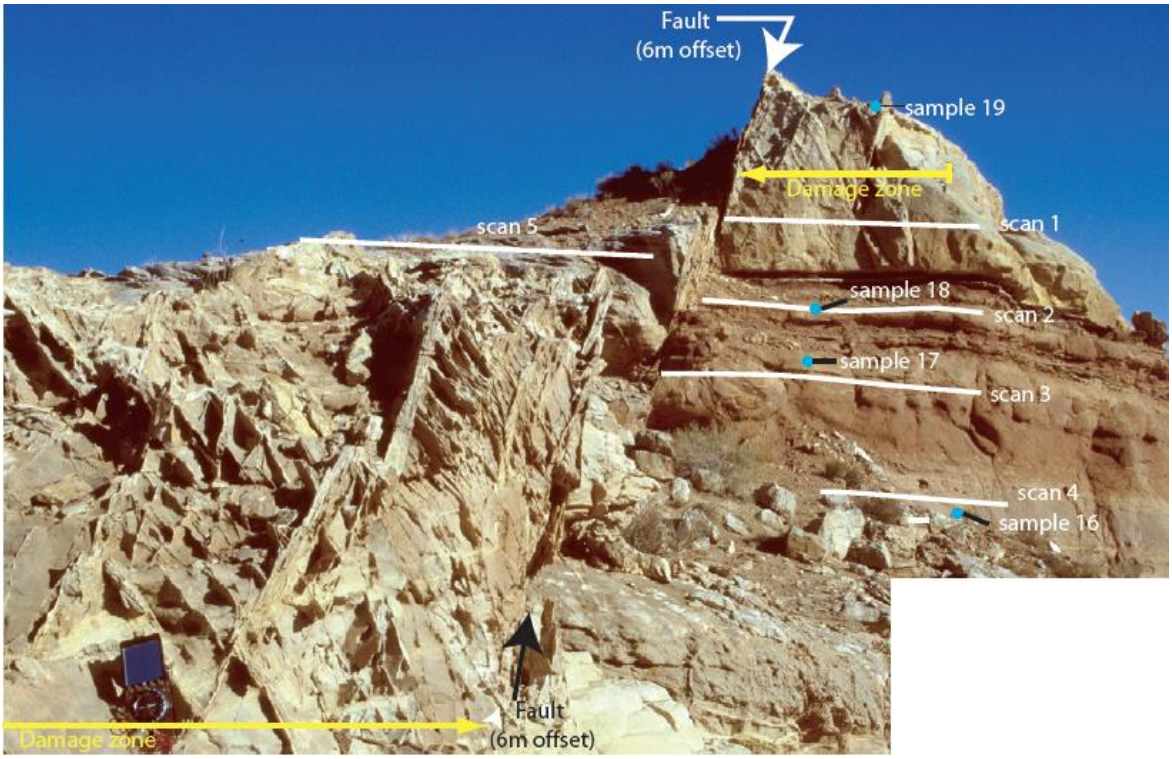

Fig. 20. The 6 meters fault, Goblin Valley, Utah. Attention for the variation of intensity of deformation bands due to grain size, porosity and grain sorting (Fossen et al., 2016b).

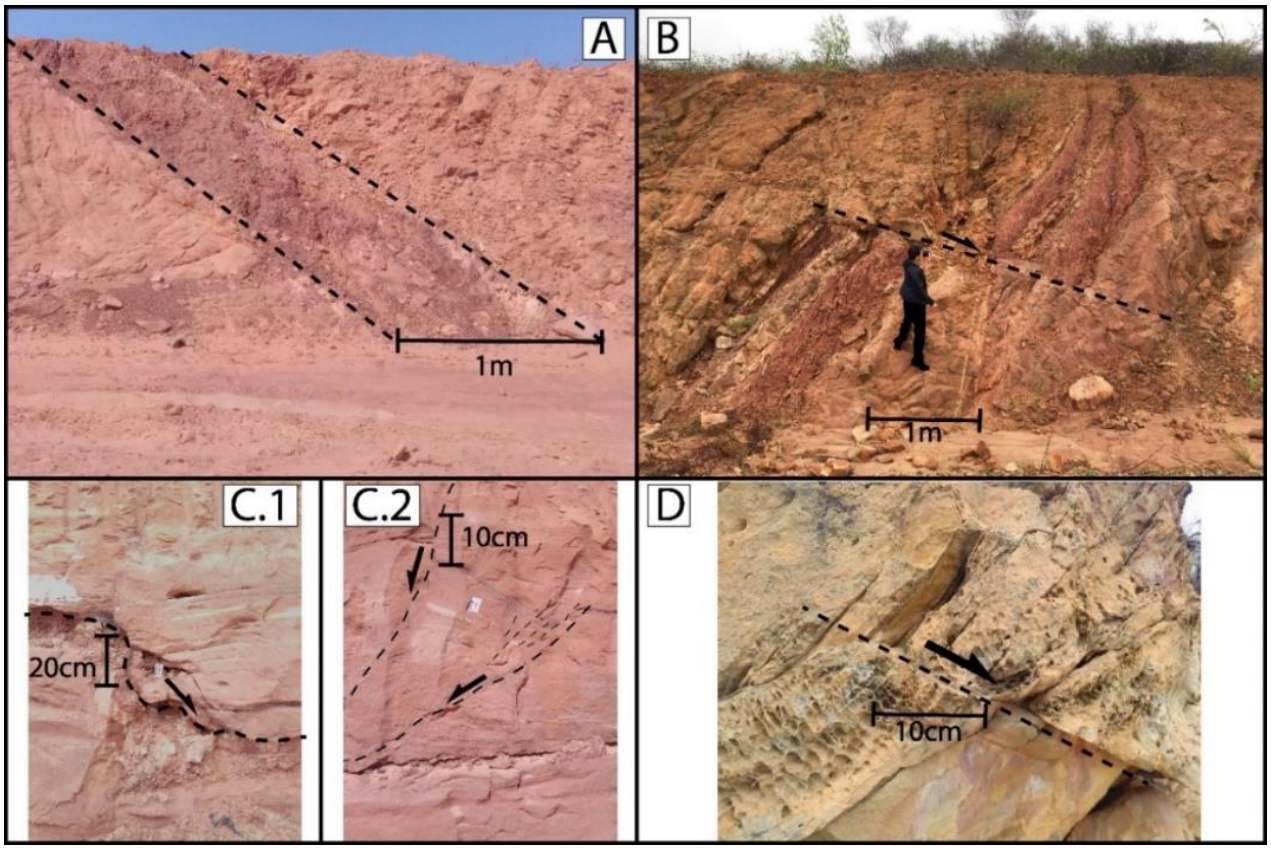

Fig. 21. Subseismic-scale faults within the Tucano Basin. A: Fault core (gouge) and associated deformation bands. B: normal fault on the road to Aribicé. C: subtle faults and deformation bands within fine sediments below the coarser sandstones where we observed the *tepee* geometry. D: deformation bands and fracturing.

3.3 Deformation mechanisms of deformation bands

The frictional, or brittle, regime is dominant in the upper crust, above the brittle-ductile transition zone (~10-15 km in depth). Brittle deformation mechanisms usually involve granular flow and may involve cataclastic flow (Fossen et al., 2007). Granular, or particulate, flow allows translation and rotation of grains to accommodate frictional slip along grain boundaries (frictional sliding). Shear stress depends on the contact surface area, the orientation of this surface, and the angle of repose, which is a factor controlled by the friction between individual sand grains. The higher the friction between grains, the higher the angle of repose (Fossen et al., 2016b). Frictional sliding can be distributed over the whole rock or localized to a few millimeters to tens of meters wide zones or bands.

Fracturing result when differential stress exceeds its rupture strength and is very common on brittle deformation of non-porous rocks. Porous rocks can also develop fractures when stress on grain contact areas is high enough, where intragranular fractures dominate deformation bands. While fractures may increase permeability, cataclastic deformation bands reduce permeability due to grain comminution.

Several mechanisms can operate during the formation of deformation bands (Fig. 22). Grain rearrangement or disaggregation is a common nondestructive mechanism where the grains roll and translate by frictional slip along the primary contacts between the grains. This deformation mechanism is called particulate or granular flow. When phyllosilicates are represented in the rock, a fabric may form in the band, and the band becomes a phyllosilicate deformation band. Some bands also show evidence of dissolution, a mechanism that results in what is known as chemical compaction. The minimum depth for significant cataclasis occurrence is estimated at approximately 1 km, although the critical depth varies with several physical parameters (Fossen, 2010).

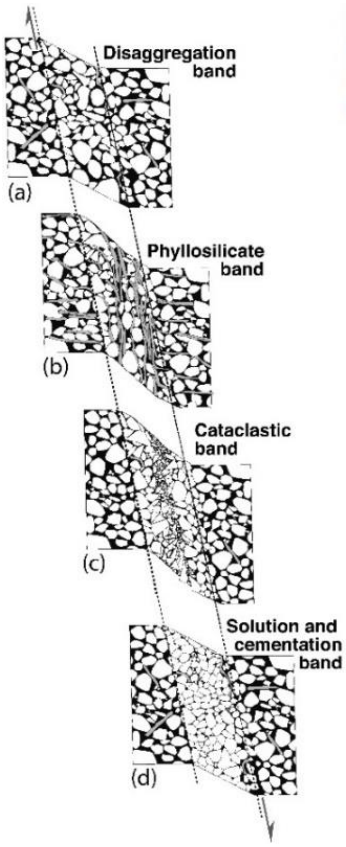

Granular flow	Shallow depth, low eff. stress, poor lithification
Cataclastic flow	>1 km depth, some lithification, high confining pressure
Dissolution (Qtz)	>2–3 km depth, >90 °C, locally along faults due to fluid flow
Cementation	For quartz, same as above. Calcite shallower

Variable	Granular flow → Cataclasis
Burial depth (confining stress)	Shallow → Deep
Lithification	Unconsolidated → Well lithified
Fluid overpressure	High → Low
Cement strength	$FeO(OH)$ (low) → $CaCO_3$ → SiO_2 (high)
Grain roundness	Angular → Rounded
Grain sorting	Poor → Good
Mineralogy (grain strength)	Strong → Weak
Phyllosilicate content	High → None
Tectonic regime	Extensional → Contractional

Fig. 22. Four different classes of deformation bands that occur in deformed sand and sandstones (left – Fossen et al., 2007) and deformation bands formation mechanisms

(right above - Fossen, 2010). Variables controlling the degree of cataclasis in deformation bands (right below - Fossen et al., 2017).

Important factors controlling the formation of deformation bands are confining pressure (burial depth), deviatoric stress (tectonic regime), pore fluid pressure and host rock properties, controlled by degree of lithification, mineralogy, grain size distribution, grain sorting and grains shape (Fossen et al., 2007).

Several types of syn-depositional deformational structures contain localized deformational structures known as disaggregation bands. In pure quartzitic sandstones with uniform grain size distribution, disaggregation bands are hard to be seen. Abundant field examples from Utah show that such bands can be related to the vertical movements linked to the charge and expulsion of fluids, forming a pre-tectonic set of deformational structures located in deformed sandstones that can easily be neglected or misinterpreted as tectonic structures in petroleum reservoirs. Plug measurements and investigation of thin sections show that they have little or no effect on fluid flow. In contrast, disaggregation bands formed as a response to tectonic stress at the larger confining pressures in the same lithology show 3 to 4 orders of magnitude in permeability reduction. This makes it important to differentiate between non-sedimentary and tectonic deformation bands. They should also be separated because only bands formed in relation to a tectonic stress can be used to predict proximity to major faults and evaluation of the extent of failure in a reservoir (Fossen, 2010).

Cataclasis

Cataclasis involves brittle fragmentation (or comminution) of minerals or grains, with rotation of grain fragments, grain boundary frictional sliding, grain flaking and fracturing, grain size reduction, crushing and commonly volume change (Sibson, 1977).

Wider brittle or cataclastic shear zones involve moderate cataclastic deformation, where the fragments resulting from grain crushing flow during shearing (cataclastic flow). Along slip or fault surfaces, intense cataclasis in thin zones involve extreme grain size reduction. Pulverization occurs during strong grain crushing without evidence of shear offset and it seems to be related to very high strain rates ($>100\ s^{-1}$) and may be related to large earthquake events producing very high rupture rates (Fossen et al., 2016b).

The geometric analyses of subseismic structures (i.e. deformation bands, deformation bands zones (clusters), slip surfaces and faults) allow prediction of kinematics on developing cataclastic shear-zones (Fig. 16). The development of simple Riedel structures and its different generations build patterns that reveal the interaction between different structures. The cross-cutting relations among deformation bands within the Riedel structures are quite useful to understand the sense of slip of each Riedel and anti-Riedel structures.

The Mohr-Coulomb criterion can also be used together with cross-cutting relations amongst deformation bands within the Riedel structures. It is also possible to compare the orientation of deformation bands to theoretical strain calculations (Fig. 16). Progressive development of the Riedel structures due to shear strain increasing can reveal kinematics during deformation bands development. Granular flow and discrete faulting can be coupled as deformation mechanisms. Granular flow may be very important during early stages of shear-zone evolution and discrete faulting can be dominant during late forming stages (Katz et al., 2005).

The Riedel geometry is represented by deformation bands sub-parallel to the shear direction and synthetic to the sense of displacement across the shear-zones (R). When overlapped, they are connected by antithetic deformation bands (R') which tend to form sub-parallel to each other when belonging to the same Riedel structure. As a conjugate set, R and R'-bands create an angle of about $\varphi/2$ and $90 - \varphi/2$ to the general shear-zone direction, respectively. R and R'-bands intersect in an acute angle of $\beta = 90 - \varphi$ where φ is the angle of internal friction (Riedel, 1929).

During simple shear and formation of Riedel structures, R'-deformation bands are primary rotated. The initial angle (β_0) between R and R'-bands follow the Mohr-Coulomb criterion (usually at an angle of 45°). As strain accumulates, granular flow facilitates rotation of R' structures and increasing of β angle. With progression of strain accumulation, new elongated and narrow Riedel structures are formed, overprinting the older structures. The higher strain, the higher is the angle with the R-band direction. Because of the strain difference inside these domains, R'-bands rotate leading to a sigmoidal shape (Katz et al., 2005).

4. Recôncavo-Tucano-Jatobá Rift System

4.1 Geologic Setting

The Recôncavo-Tucano-Jatobá (RTJ) rift system developed in the Late Jurassic to Early Cretaceous during the initial stages of the regional extension that lead to the opening of the South Atlantic (Szatmari et al., 1985, 1987; Magnavita and Cupertino, 1987, 1988; Milani and Davison, 1988; Magnavita et al., 1994; Szatmari and Milani, 1999; Gordon et al., 2017). The rifts structural configuration results from the interplay of regional tensional stresses with the pre-existing fabric of the local basement structures. Its major faults and the alignment of the resulting depocenters follow the NS strike direction of the pre-Brasiliano fabric in the São Francisco craton in its southern part. To the north, the rift changes direction completely, where the Jatobá basin follows the E-W oriented Brasiliano Borborema Province shear zones, notably the Pernambuco shear zone.

The Tucano Basin is usually divided into three N-S oriented half-graben bounded by two transfer zones. The Vaza-Barris Transfer Zone (VBTZ), focused on in this work, separated the central and north Tucano sub-basins and is oriented according to the Brasiliano Sergipe belt fabric (Milani and Davison, 1988; Magnavita et al., 1994; Szatmari and Milani, 1999; Destro et al., 2003; Gordon et al., 2017). The Tucano basin extends approximately 400 km long and 80 km wide, with depocenters that can reach up to 15 km of sedimentary strata with only limited amounts of volcanic rock.

4.2 Stratigraphy

The Tucano basin is filled by siliciclastic successions of continental environments, including lacustrine, deltaic and alluvial sandstones, mudstones and minor conglomerate. Its stratigraphy has been divided into pre, syn and post-rift sequences (Fig. 23).

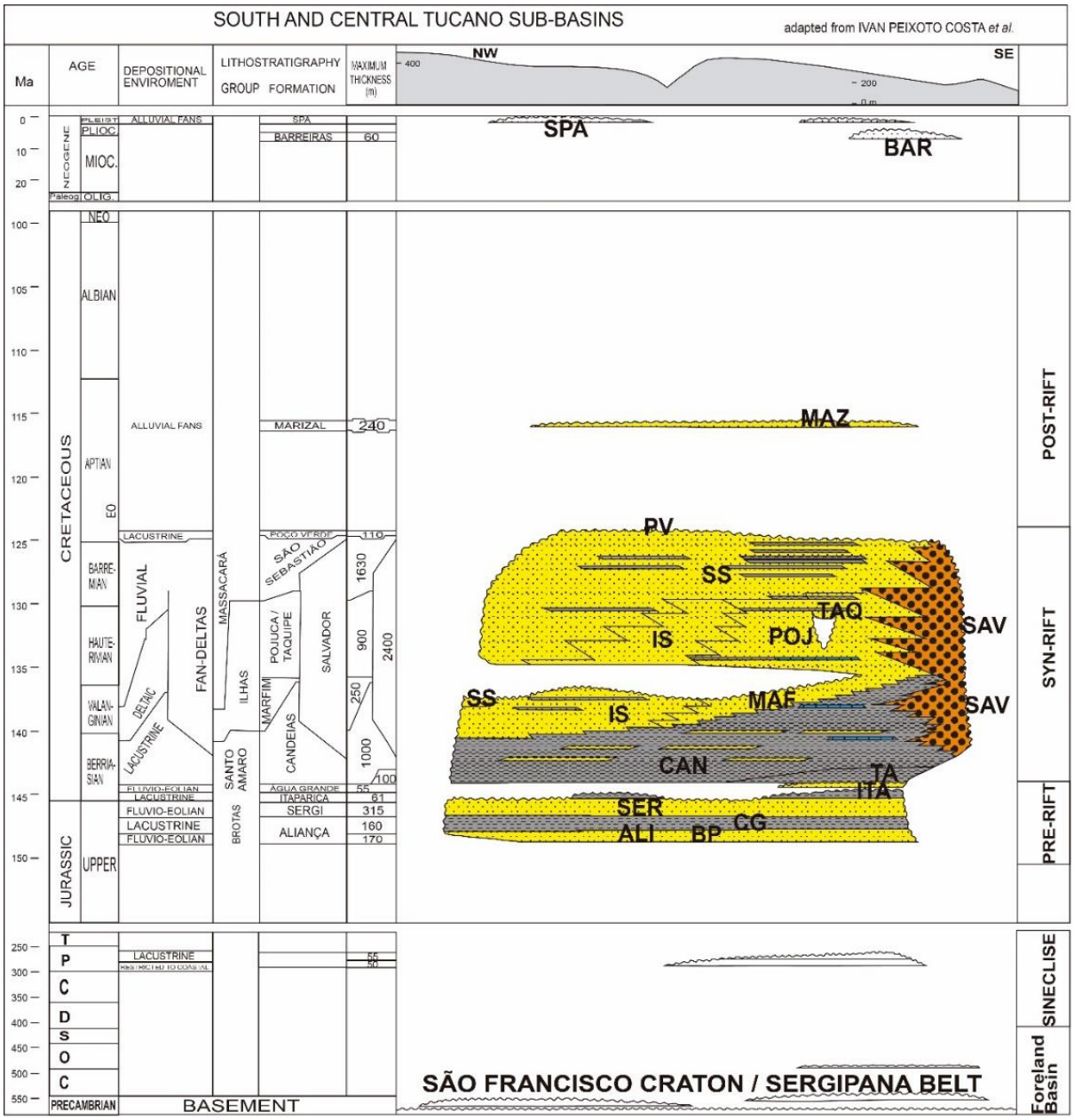

Fig. 23. Central and South Tucano basin chronostratigraphic chart (adapted from Costa et al., 2007).

Pre-rift sequence

In the Tucano Basin, the pre-rift sequence is composed of the Jurassic Brotas Group, including fluvio-eolian and lacustrine successions that were originally not limited by the syn-rift basin-border faults. Its sandstones, including the fluvio-eolian Sergi Formation, form hydrocarbon reservoirs in the Recôncavo Basin to the South, where disposed in syn-rift uplifted fault blocks. Finer-grained lacustrine deposits are included in the underlying Aliança Formation (Scherer and De Ros, 2009).

Syn-rift sequence

In general terms, the syn-rift sequence comprises one major progradational successions deposited from the Berriasian to the Barremian and starting with lacustrine deposits of the Santo Amaro Group, which includes organic-rich hydrocarbon source rocks of the Candeias Formation and isolated deep-water sandstone bodies. Overlying these lacustrine successions and prograding from the north to the south, the Ilhas Group is composed of fine to silty sandstones in a fluvio-deltaic depositional environment (Santos and Reis, 2011). The Barremian fluvial sediments of the São Sebastião Formation overlie the deltaic sediments of the Ilhas Group, being composed of fine to coarse sandstone which are thicker and span a larger time in the North Tucano and Jatobá basin. Laterally to all those syn-rift units, the Salvador Formation comprises the basin-border conglomerates developed next to the major basin-border faults.

Post-rift sequence

The post-rift sequence is represented by the Aptian fluvial successions of the Marizal Formation, deposited on top of a regional angular unconformity with the syn-rift units. The Marizal Formation has been subdivided into two members: the Banzaê Member at the base and the Cícero Dantas Member at the top, bounded by the lacustrine Amargosa Bed (Freitas, 2014). The Marizal Formation overlays most of the Central Tucano basin, locally reaching more than 250 m in thickness. The Marizal Formation was deposited in fluvial systems associated with local alluvial fans. Provenance of basement pebbles and cobbles transported from alluvial fans on the rift border (Figueiredo et al., 2016; Freitas et al., 2017) and the occurrence of deformation bands within the post-rift Banzaê Member of the Marizal Formation studied in this work suggests a late rift pulse or continued rifting until the Aptian.

4.3 The Vaza-Barris Transfer Zone (VBTZ)

The Vaza-Barris Transfer Zone (VBTZ) is a broad 140-km long by 50-km wide NW oriented dextral-normal (high-oblique to dip-slip structures) diffuse fault system, transversal to the major rift border faults (Fig. 24). It accommodates the polarity inversion

between the North and Central Tucano sub-basins, linking the oppositely dipping São Saité, on the western border and dipping southeastward, and Adustina master fault, on the eastern border and dipping northwestwards, (Magnavita and Cupertino, 1988; Milani and Davison, 1988; Magnavita et al., 1994; Szatmari and Milani, 1999; Destro et al., 2003; Gordon et al., 2017) and switching the two faults adjacent depocenters locations from one side of the basin to the other (Fig. 24). The Vaza-Barris transfer zone separates the North and Central Tucano and accommodates the extensional rates difference between the southern and northern rift segments (Magnavita, 1992; Magnavita et al., 1994).

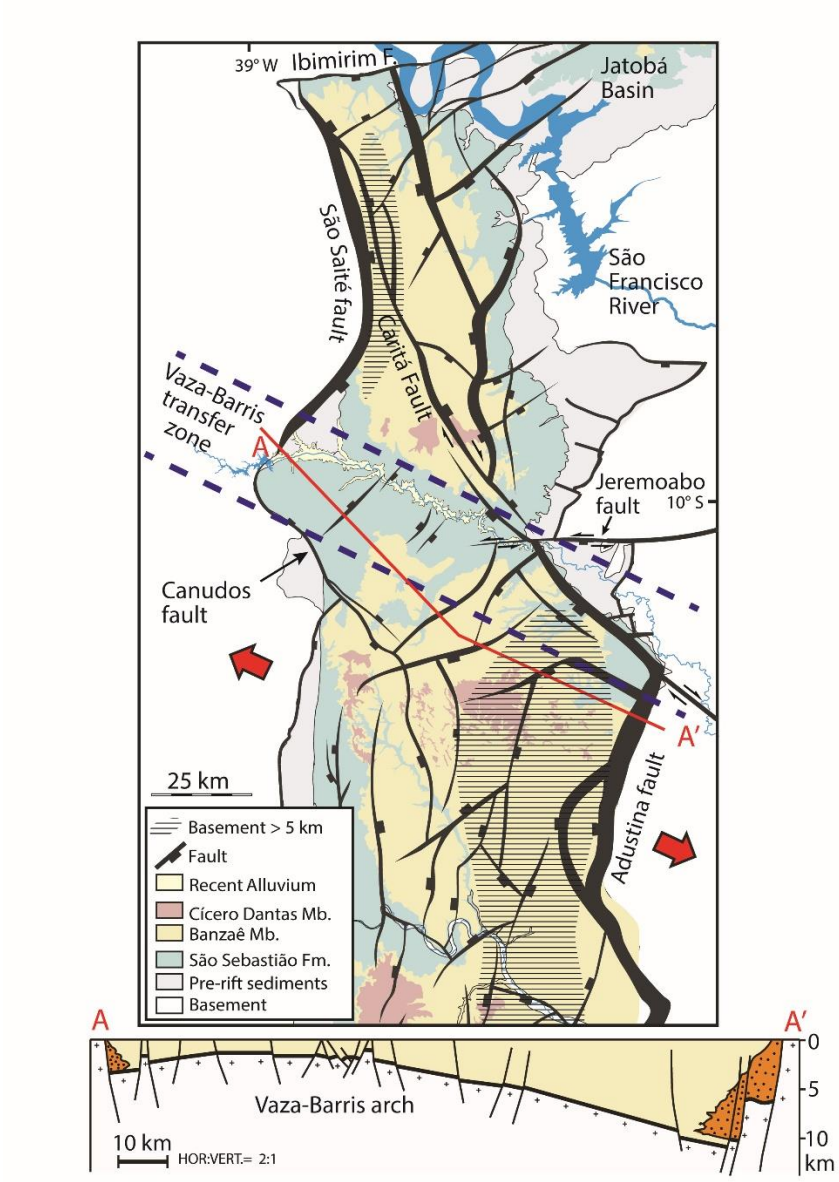

Fig. 24. Geologic map of the Tucano-Jatoba rift system (adapted from Freitas et al., 2017). A cross-section along the Vaza-Barris transfer zone is shown. Based on Magnavita (1992) and Destro (2002).

5. Results

5.1 Spatial and stratigraphic distribution of the subseismic structures

5.1 Spatial distribution

Due to the variations in the kinematic pattern, we divided the study area into five structural subdomains: the western Canudos area (Subdomain 1), central Vaza-Barris transfer zone (2), the Jeremoabo fault (3) and Caritá fault (4) areas on the eastern basin border and the Massacará area (Subdomain 5) south of the transfer zone (Fig. 25).

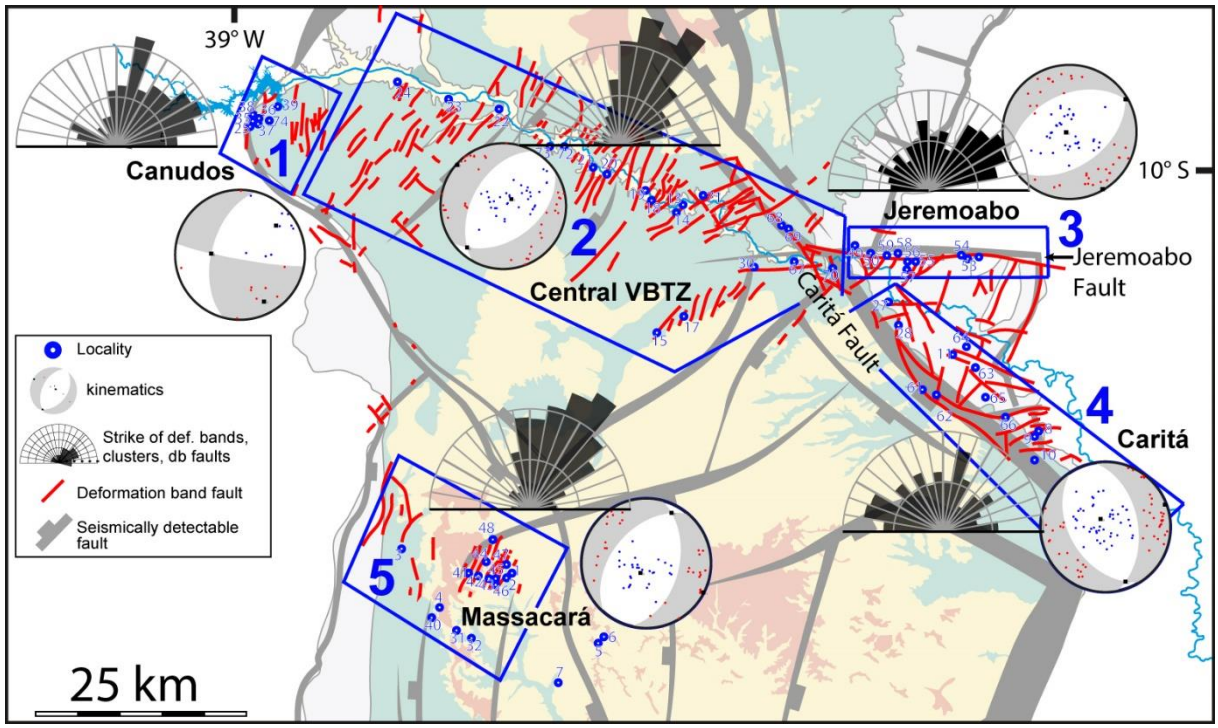

Fig. 25. Structural subdomains with respective kinematic analyses and rose diagrams of deformation bands, clusters and deformation band faults. Based on Magnavita (1992), Destro (2002) and Freitas et al. (2014).

Western basin area – Canudos – syn-rift Ilhas Group (Subdomain 1)

Near the town of Canudos, topographic ridges composed of the Ilhas Group fluvio-deltaic fine sandstones host deformation bands zones more than 30 cm thick. The

kinematics varies from dextral strike-slip structures near the São Saité Fault on the western border to extensional and dextral-extensional oblique structures basinward. The main Riedel structures are the NNE dextral (R) and ENE sinistral (R') trends that are compatible with a regional dextral shear zone, also represented by low rake striations in slip surfaces and rotated horizontal ladder structures with dextral offset, often with more than one generation.

Central Vaza-Barris transfer zone (VBTZ) – syn-rift São Sebastião Formation (2)

The transfer faults along the VBTZ are transversal or oblique to the rift axis, allowing fault kinematic linkage at a high angle between adjacent major basin border faults (Adustina and São Saité Faults). Along the transfer zone, sandstones of the syn-rift São Sebastião Formation host deformation bands conjugate sets, more than 30 cm thick clusters with normal sense rotated ladder structures and metric-scale normal faults. Erosional processes on deformation band clusters conjugate sets can develop geomorphological features known as *tepee* and even more, double *tepee* (Figs. 18c, 19j).

The sandstones within the central VBTZ (subdomain 2) host very steep dip-slip deformation bands and clusters, whit dominated extensional kinematics and dip-slip to high-oblique structures. Local conjugate sets are represented by NNE-oriented dextral (R) and ENE-oriented sinistral (R') trends interpreted as Riedel structures, suggesting NE-SW shortening and NW-SE extension. We locally found occurrences of NW-SE oriented minor strike-slip components (dextral-extensional) parallel to the central transfer zone with low rake striation in slip surfaces, thus suggesting also a NW-SE shortening, but smaller than the extension in the same direction.

Eastern basin border - Jeremoabo Fault –pre-rift Sergi Formation (3)

The road BR-235, east of the town of Jeremoabo, runs approximately parallel to the E-W Jeremoabo Fault and exposes deformation bands within sandstones of the Upper Jurassic Sergi Formation juxtaposed with adjacent Precambrian basement inliers.

Our data show that besides the kinematics complexity indeed observed near its adjacent basement (normal sense, reverse, and strike-slip ladder structures), most of data is compatible with a regional extensional regime. The sandstones host steep deformation band conjugate sets, normal sense ladder structures, more than 15 cm thick clusters and

high rake striation in slip surfaces. Very thick ladder structures, “radiator” rock (Davis, 1999), were also found in this subdomain. Data from at least 17 slip surfaces confirms extension-dominated kinematics, although few local deformation bands show dextral rotation of quartz pebbles within sandstones and low rake lineation in slip surface, thus suggesting strike-slip components. We found just in one locality low angle dipping clusters with rotated ladder structures showing reverse sense kinematics.

Eastern basin border – Caritá Fault – pre-rift Sergi Formation (4)

South of the Jeremoabo subdomain, deformation bands within sandstones of the pre-rift Upper Jurassic Sergi Formation are exposed in elongated ridges located along the seismic-scale NW-oriented Caritá fault. This fault possibly links and mutually interact with the master Adustina Fault and the preexisting basement fabrics. The sandstones host deformation bands, clusters, normal sense rotated ladder structures and high rake striation in slip surfaces, thus confirming extension-dominated kinematics. Local ladder structures show strike-slip components along en-echelon fault segments, thus suggesting a dextral strike-slip kinematics. The subdomain is composed mainly by the NW-trending fault segments but show many very angular fault traces in map view, steep steps with subordinate segments or odd-guiding steps (“zig-zag” pattern), that closely match the tendencies of the basement preexisting structures.

Massacará area – São Sebastião Formation (Subdomain 5)

In this subdomain, localized on the western area, NNE-trending topographic ridges host deformation band clusters and deformation band faults within the São Sebastião Formation that strongly agree with the overall basin extensional direction. The studied deformation bands within the post-rift Banzaê Member of the Marizal Formation also agree with the same overall rift extensional direction.

5.2 Stratigraphic distribution

Separated lower equal hemisphere spherical projections with kinematic analyses were also carried out for each stratigraphic unit (Fig. 26).

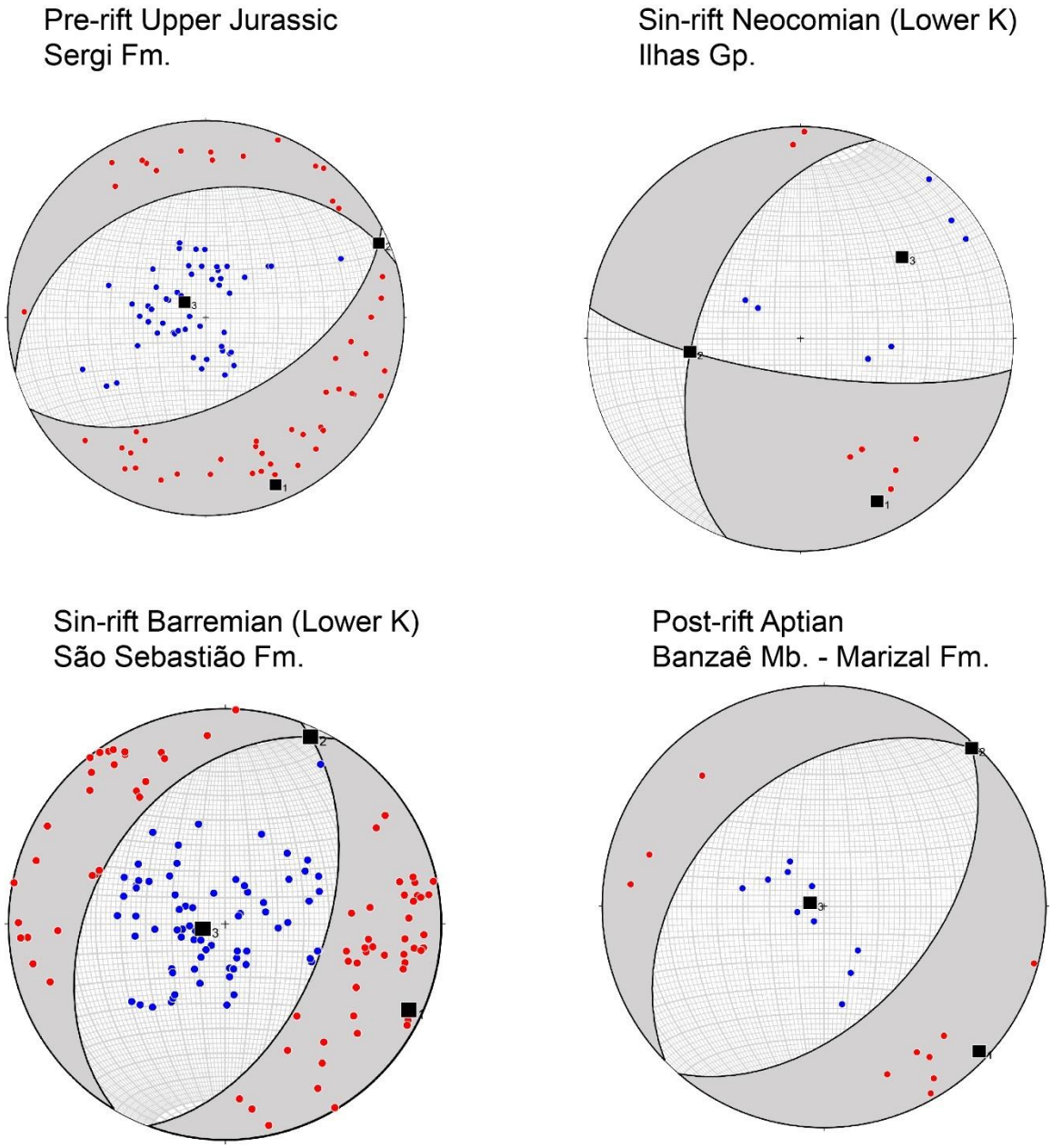

Fig. 26. Lower hemisphere equal area spherical projections with kinematic analyses and strain axes calculated from Linked Bingham analysis separated by stratigraphic unit.

5.2 Permeability reduction estimates: deformation bands and their influence on fluid flow within sandstone reservoirs

Deformation bands and related structures have been shown to influence the permeability structure of reservoir rocks (Fossen and Bale, 2007; Ballas et al., 2015), and an understanding of such structures can therefore be of major importance in many cases. Deformation bands formation typically involve grain slip and rotation and, in many cases, cataclasis (grain fragmentation). Most deformation bands involve reduction of porosity and permeability, particularly those involving cataclasis (Fig. 27).

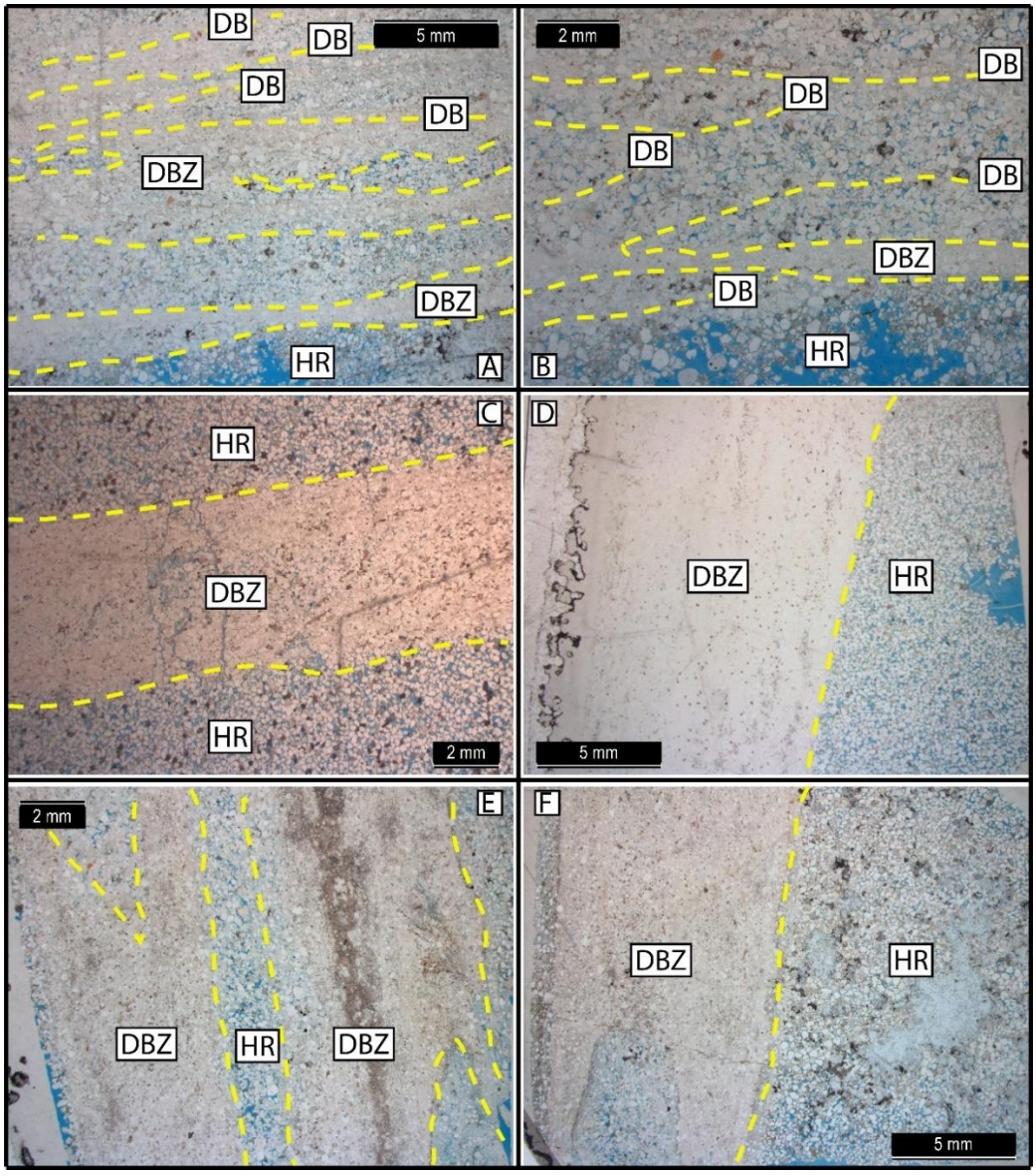

Fig. 27. A-F: Cataclastic deformation bands thin sections within the Colorado Plateau - Utah. HR: Host Rock; DB: Deformation Band; DBZ: Deformation Bands Zone.

When bands have a preferred orientation, they introduce a heterogeneity that can influence the flow of fluids (oil, water, CO2) in a subsurface reservoir (Fig. 28).

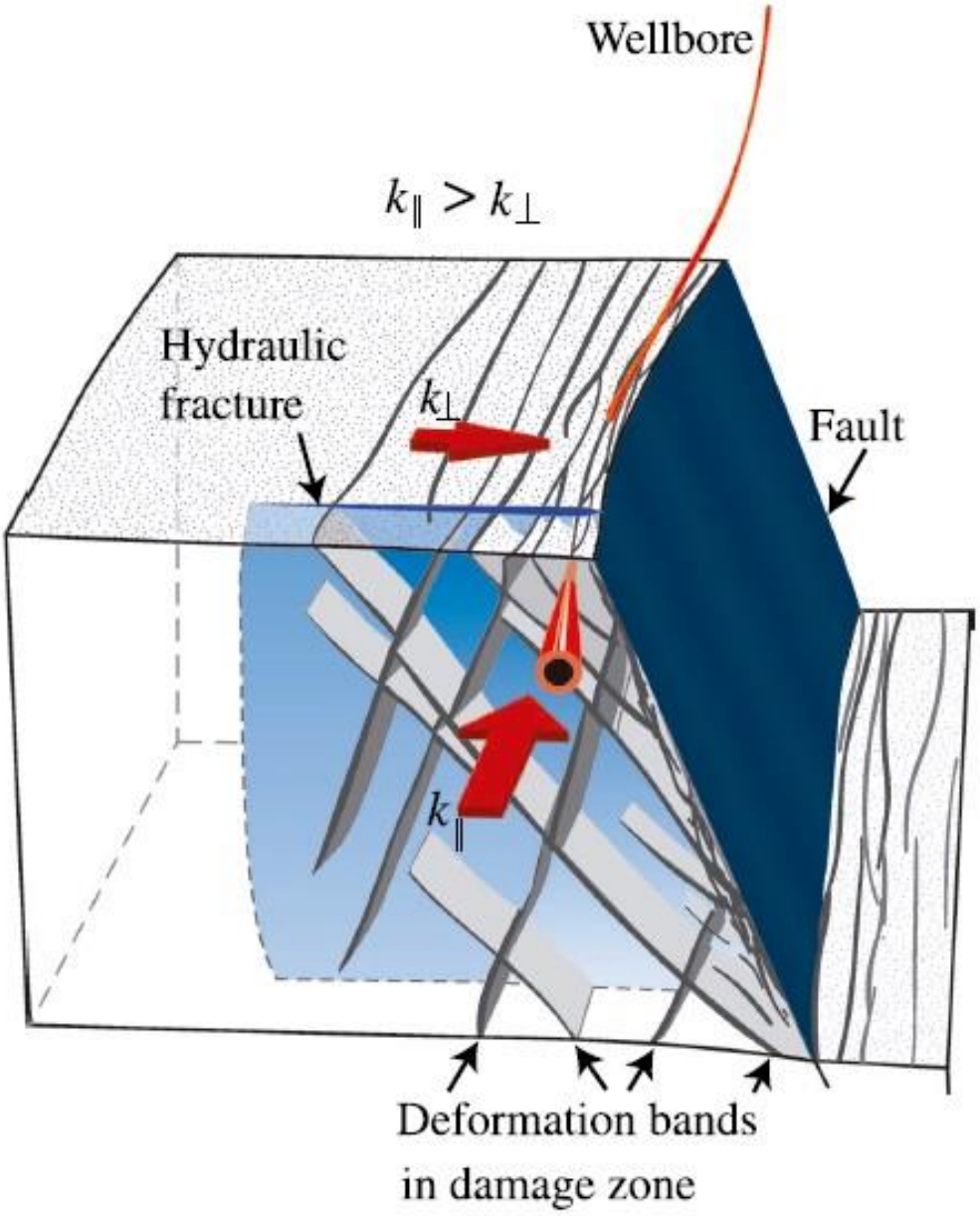

Fig. 28. Fault damage zone and deformation bands arrangement introduce permeability anisotropy, where average permeability parallel to the fault is higher than that perpendicular to the fault (Fossen and Bale, 2007).

In this study, permeability was measured in the field by means of portable air minipermeameter (TinyPerm II). The data measured by the device is then calibrated into permeability values, where the high values of permeability are associated to the host rock while low values are associated to the deformation bands and related structures. Establishing a relation between some of these parameters is useful with respect to prediction of these subseismic structures in reservoirs of this and similar rift systems.

Petrographic description, observation of deformational features and porosity estimates in thin sections were carried out with the aid of the petrographic microscope and/or SEM images (Figs. 29-31).

Due to the influence on fluid flow it is important to observe the preferential orientation of the grains within the deformation bands and that grains are usually fractured due to grain crushing and comminution (cataclasis) in different degrees. The deformation bands also contain survivor grains, well-rounded big grains almost non-deformed.

The deformation bands exhibit both sutured, planar and punctual grains contact. They show open packing with secondary porosity (moldic) due to grain dissolution and infiltrated clay coatings (or even clay minerals, mica and/or lithic fragments). Quartz and feldspar overgrowth are very common. Cementation (silica or carbonate) may take part whereas iron oxide coatings are quite common too. Lithic fragments of mylonitic grains (recrystallized) can also be seen.

The cataclastic deformation bands within the Tucano basin show from 1 to 3.5 orders of magnitude of permeability reduction compared to the host rock, as reported in published literature in other regions (Ballas et al., 2015).

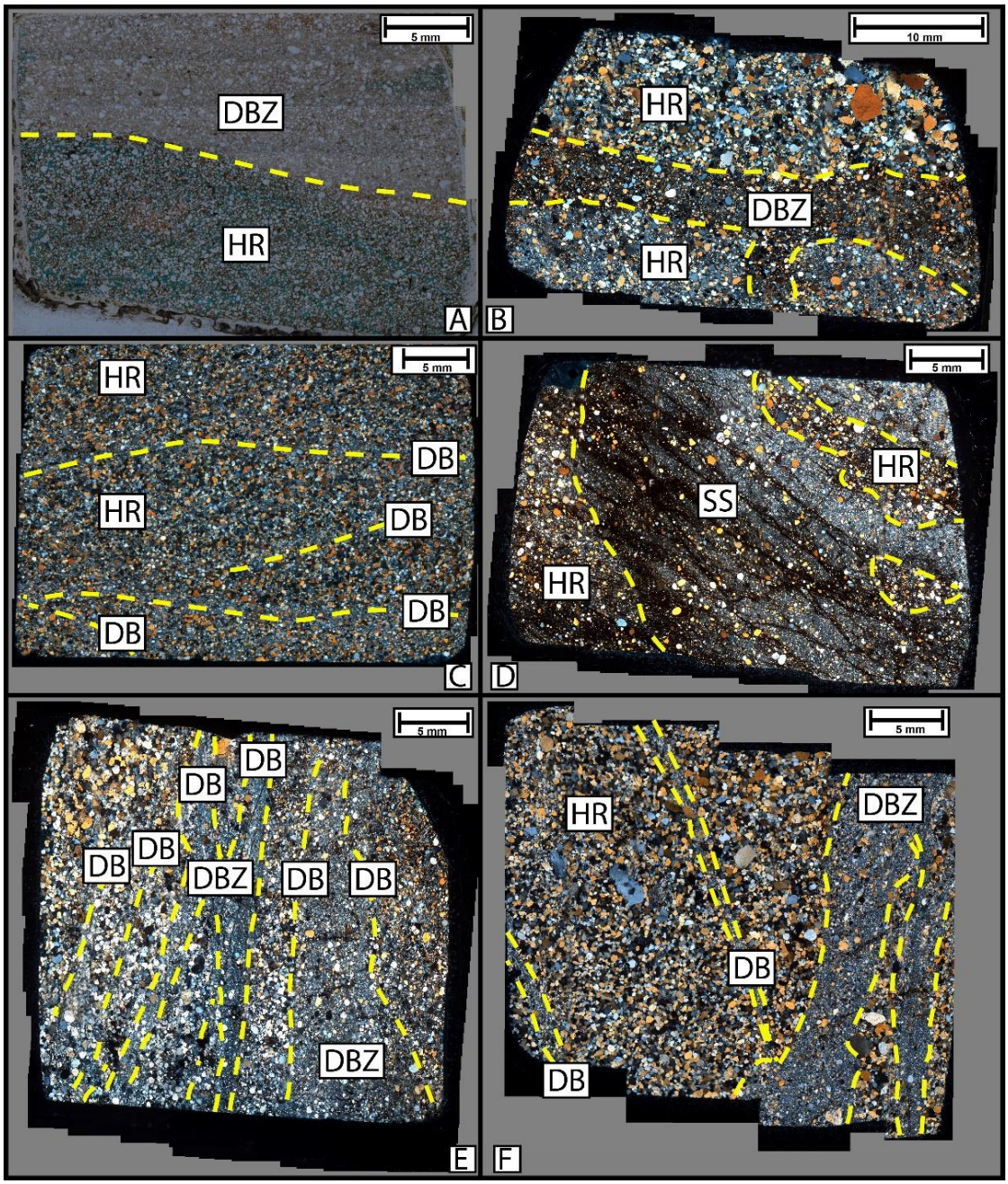

Fig. 29. Cataclastic deformation bands thin sections within the Tucano Basin. HR: host rock; DB: deformation band; DBZ: deformation bands zone; SS: slip surface. **A**: DBZ and HR, syn-rift São Sebastião Fm. – western flexural border near Massacará; **B**: HR and DBZ, pre-rift Upper Jurassic Sergi Fm. – Caritá Fault; **C**: HR with incipient DBs, post-rift Banzaê Mb., Aptian Marizal Fm. **D**: HR and SS (ultracataclasite), pre-rift Upper Jurassic Sergi Fm. – Caritá Fault/Araticum Block. The ultracataclasite (slip surface) shows high porosity contrast between host rock ($16\% < \phi_{HR} < 24\%$) and slip surface ($\phi_{SS} < 0{,}2\%$). **E:** DB and DBZ, pre-rift Upper Jurassic Sergi Fm – Caritá Fault. **F:** HR, DB and DBZ, pre-rift Upper Jurassic Sergi Fm – Caritá Fault.

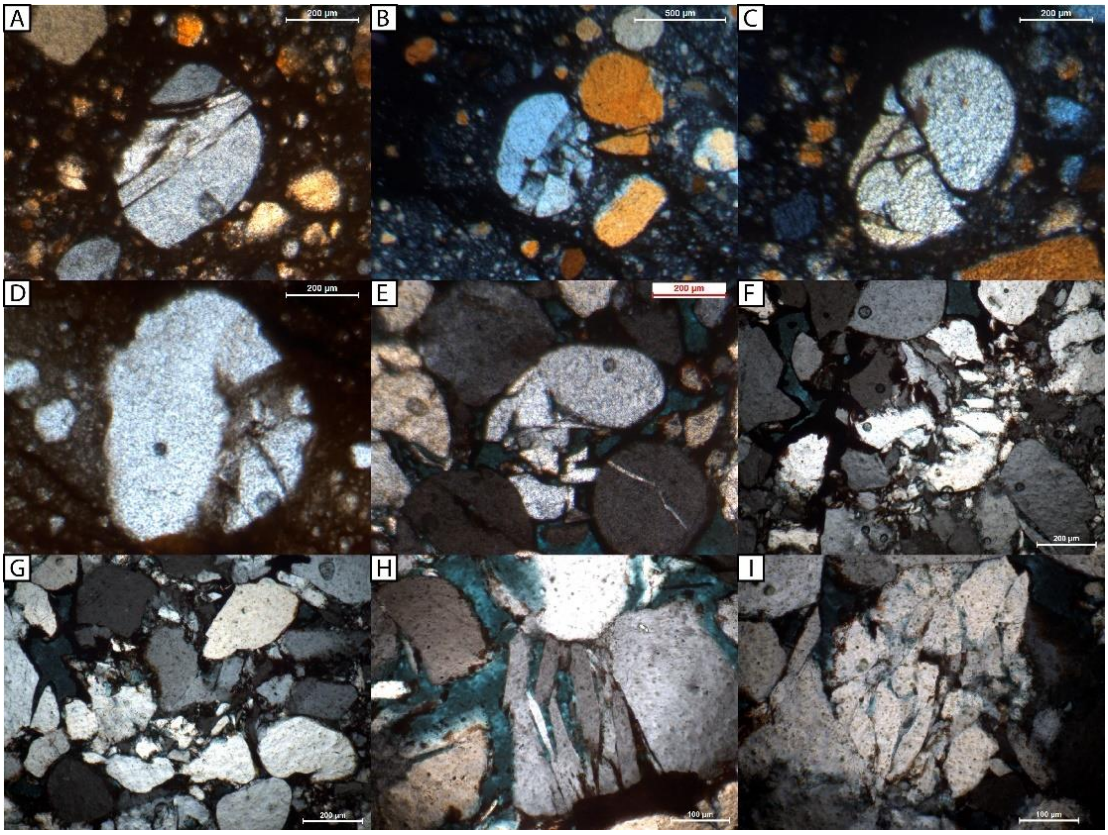

Fig. 30. Fractured grains within deformation bands in the Tucano Basin.

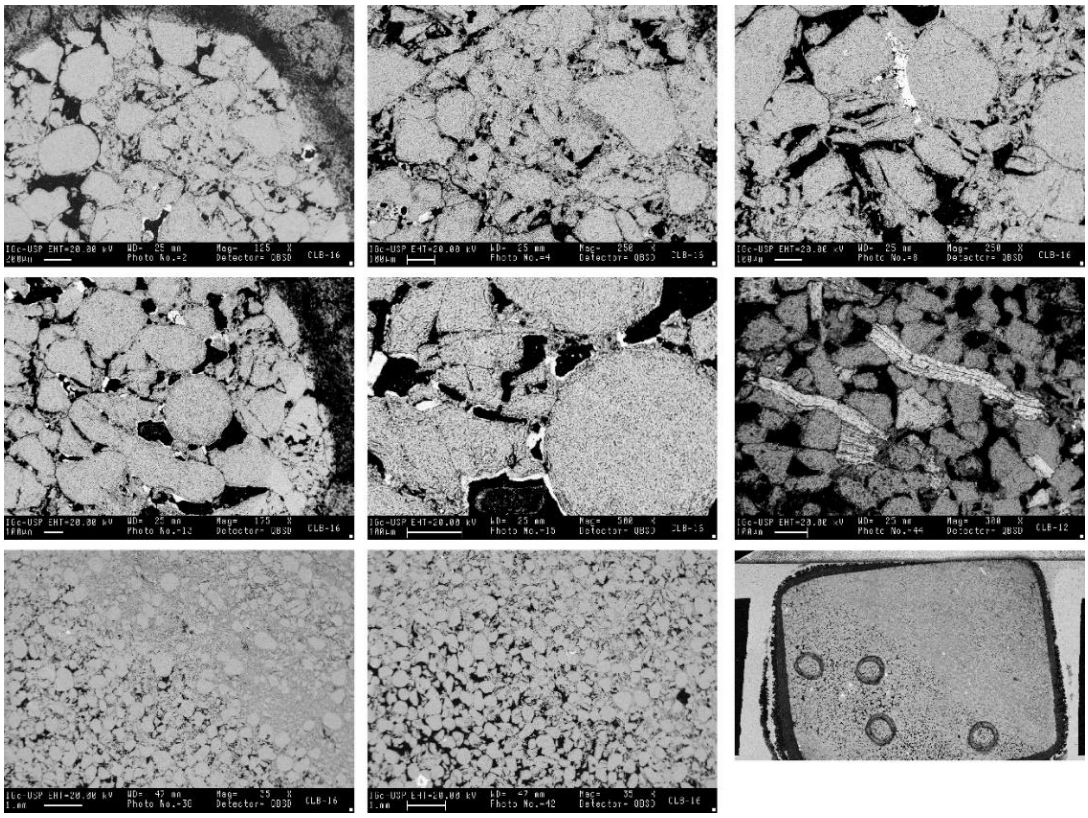

Fig. 31. SEM images showing intragranular fractures and cataclasis (CLB-16).

5.3 Article: *Subseismic deformation in the Vaza-Barris Transfer Zone in the Cretaceous Recôncavo-Tucano-Jatobá rift system, NE Brazil*

Manuscript Details

Manuscript number	SG_2018_197
Title	Subseismic deformation in the Vaza-Barris Transfer Zone in the Cretaceous Recôncavo-Tucano-Jatobá rift system, NE Brazil
Article type	Original article

Abstract

We investigate the subseismic structural expression of the major Vaza-Barris Transfer Zone in the Early Cretaceous Tucano rift basin, NE Brazil based on field observations. Subseismic structures in the Tucano rift fill (porous sandstones) encompass deformation bands, deformation band clusters and deformation band faults. In general, these subseismic structures indicate a ~120° extension direction and document oblique extension across the N-S Tucano Rift, consistent with the movement direction inferred from plate-scale reconstructions. The transfer zone itself is dominated by a large population of NE-SW trending deformation band structures that developed into deformation band faults making at a high angle to the transfer zone. The deformation band faults are quite evenly distributed along the transfer zone, which we attribute to extension related to its arcuate cross-sectional shape (high central part with flanks dipping toward the rift margins). Additional subordinate structures, many of which are oriented parallel to the transfer zone, show strike-slip motion, and indicate that the strain field in the transfer zone also involves a component of NNW-SSE shortening in addition to the main extension along the transfer zone. In terms of subseismic fault prediction, however, the evenly distributed zone-perpendicular structures dominate and would impose restrictions on fluid flow along the zone. This macro-permeability anisotropy should be considered in an injection/production scenario in a transfer zone of the type described here. Although other transfer zones may have different geometries and therefore different subseismic characters, an important observation made here is the close correspondence between first-order geometry (in our case an arch-shaped transfer zone) and subseismic deformation (arch extension). In addition, the observation of deformation bands within the post-rift Banzaê Member of the Marizal Formation studied in this work suggest a late rift pulse or continued rifting until the Aptian.

Keywords	Subseismic structures; Deformation bands; Rift transfer zone; Tucano Basin.

Corresponding Author	Haakon Fossen
Corresponding Author's Institution	University of Bergen
Order of Authors	Cleber Peralta, Haakon Fossen, Renato Paes de Almeida, Bruno Salmoni
Suggested reviewers	Christopher Morley, Martha Withjack, Nivaldo Destro, Fernando Alkmim, Richard Schultz

Subseismic deformation in the Vaza-Barris Transfer Zone in the Cretaceous Recôncavo-Tucano-Jatobá rift system, NE Brazil

Cleber Peralta Gomes Jr. [1], Haakon Fossen [2]*, Renato Paes de Almeida [1], Bruno Salmoni[1]

[1] Instituto de Geociências, Universidade de São Paulo, Rua do Lago, 562, Cidade Universitária, CEP 05508-080 São Paulo, SP, Brazil

[2] Museum of Natural History/Department of Earth Science, University of Bergen, Allégaten 41, N-5007 Bergen, Norway (Haakon.fossen@uib.no)

Highlights:

• Field data confirm that the Tucano Rift is an oblique rift;

• Extension across the Tucano Rift is N120E; Rifting continued at least through the Aptian;

• Subseismic structures in the transfer zone are deformation bands;

• The subseismic structures adds a structural anisotropy to the sandstone reservoir.

Abstract

We investigate the subseismic structural expression of the major Vaza-Barris Transfer Zone in the Early Cretaceous Tucano rift basin, NE Brazil based on field observations. Subseismic structures in the Tucano rift fill (porous sandstones) encompass deformation bands, deformation band clusters and deformation band faults. In general, these subseismic structures indicate a ~120° extension direction and document oblique extension across the N-S Tucano Rift, consistent with the movement direction inferred from plate-scale reconstructions. The transfer zone itself is dominated by a large population of NE-SW trending deformation band structures that developed into deformation band faults making at a high angle to the transfer zone. The deformation band faults are quite evenly distributed along the transfer zone, which we attribute to extension related to its arcuate cross-sectional shape (high central part with flanks dipping toward the rift margins). Additional subordinate structures, many of which are oriented parallel to the transfer zone, show strike-slip motion, and indicate that the strain field in the transfer zone also involves a component of NNW-SSE shortening in addition to the main extension along the transfer zone. In terms of subseismic fault prediction, however,

the evenly distributed zone-perpendicular structures dominate and would impose restrictions on fluid flow along the zone. This macro-permeability anisotropy should be considered in an injection/production scenario in a transfer zone of the type described here. Although other transfer zones may have different geometries and therefore different subseismic characters, an important observation made here is the close correspondence between first-order geometry (in our case an arch-shaped transfer zone) and subseismic deformation (arch extension). In addition, the observation of deformation bands within the post-rift Banzaê Member of the Marizal Formation studied in this work suggest a late rift pulse or continued rifting until the Aptian.

Keywords: Subseismic structures; Deformation bands; Rift transfer zone; Tucano Basin.

1. Introduction

Transfer zones are integral components of continental rifts, separating first-order compartments of contrasting structural expression and connecting basin-bounding master faults (Gibbs, 1984; Rosendahl et al., 1986). Several geometrically different types of transfer zones have been described in the literature (Rosendahl et al., 1986; Morley, 1990), and a particularly common type is the conjugate overlapping type (Morley, 1990), where two oppositely dipping master faults and their associated depocenters switch locations from one side of the basin to the other across the transfer zone.

The structure of rift transfer zones is known from field observations (Younes and McClay 2002; Mack and Seager, 1995), seismic data (Scott and Rosendahl, 1989), physical (Schliche and Withjack, 2009) and numerical (Allken et al., 2013) modeling. However, these studies mostly discuss large-scale aspects of such zones. Little or no attention has been paid to subseismic structures (deformation bands, clusters or deformation band zones, slip surfaces and subseismic faults) in transfer zones, which are of particular interest with respect to hydrocarbon production and CO_2 sequestration.

In this work we investigate the structural expression along a first-order rift transfer zone known as the Vaza-Barris Transfer Zone in the Cretaceous Recôncavo-Tucano-Jatobá rift system (Fig. 1) with the purpose of gaining information about subseismic structures; their nature, distribution and orientation, and the strain regime that they represent. The Tucano basin fill is dominated by porous sandstones in which faults developed through a precursory history of deformation band formation (Chemalle Jr. et

al., 1994; Roque and Chemale Jr., 1994; Ferreira and Da Silva, 2010; De Araújo Netto et al., 2012), including the formation of conjugate sets of bands, deformation band zones and ladder structures. These structures record local strain and are thus used in this work to characterize strain in the transfer zone. Comparison with similar subseismic rift structures away from the transfer zone allows us to evaluate to what extent the rift transfer zone differs from the rift structure in general at the subseismic scale (structures with offset < 20-30 m in the study area).

2. Geologic Setting

2.1 The Recôncavo-Tucano-Jatobá Rift System

The mostly N-S trending Recôncavo-Tucano-Jatobá rift system (Fig. 1) is a failed intracontinental rift formed during the Gondwana break-up as a prelude to the opening of South Atlantic in the Late Jurassic to Early Cretaceous (Szatmari et al., 1985, 1987; Magnavita and Cupertino, 1987; Milani and Davidson, 1988; Magnavita, 1992; Magnavita et al., 1994; Szatmari and Milani, 1999; Gordon et al., 2017). It consists of three main rifts or rift segments, with the N-S trending Tucano Rift as the major central component. The Recôncavo-Tucano-Jatobá rift system is a well-known example of a rift system whose location and orientation is strongly influenced by preexisting basement structures. In what is known as the south and central Tucano basin (or Tucano Rift) (Fig. 1), the rift closely follows the N-S trending pre-Brasiliano fabric in the São Francisco craton, and maintains this orientation northward until abruptly changing its orientation into the ENE-WSW trending Jatobá Basin, which seems to be controlled by the steep basement shear zones of the Borborema Province, notably the Pernambuco shear zone (Fig. 1) (Milani and Davison, 1988).

The Tucano Rift is a 400 km long and 50-100 km wide part of the Recôncavo-Tucano-Jatobá rift system. Structurally it is divided into two oppositely facing half-grabens, separated by the Vaza-Barris Transfer Zone that crosses the rift obliquely at around latitude 10°S, separating the North Tucano basin from the Central and South Tucano basins (Magnavita et al., 1994). This transfer zone is located where the rift crosses the NW-SE trending Brasiliano Sergipe belt (Fig. 1). Several major rift faults or fault segments in this area parallel the Sergipe basement trend and are believed to be controlled by the Sergipe basement structure (Milani and Davison, 1988; Magnavita et al., 1994;

Destro et al., 2002). The main depocenters in the Tucano Rift display up to 15 km of sedimentary strata (Fig. 1) with only limited amounts of volcanic rocks.

2.2 Stratigraphy

The Tucano basin stratigraphy has been divided into pre, syn and post-rift sequences (Fig. 2). The studied pre-rift unit is represented by the Late Jurassic Sergi Formation, the syn-rift by the Ilhas Group and the São Sebastião Formation and, on top, the post-rift sequence is represented by the Banzaê Member of the Marizal Formation.

The pre-rift Upper Jurassic Sergi Fm. crops out along the eastern border of the Central Tucano basin, along the Caritá and Jeremoabo faults (Figs. 2a and 2b). It is typically composed of fine to conglomeratic cross-stratified sandstones bearing fossil wood. These are interpreted to represent sandy braided fluvial and ephemeral lake deposits formed under semiarid climate (Scherer and De Ros, 2009).

On the western basin border of the study area, the syn-rift sequence comprises mainly the Barremian fluvial sediments of the São Sebastião Formation, overlaying deltaic sediments of the Ilhas Group. The Ilhas Group is composed of fine to silty sandstones deposited in a fluvio-deltaic depositional environment (Santos and Reis, 2011). The São Sebastião Formation can be recognized by its reddish fine to coarse sandstones near the rift borders and along the Vaza-Barris Transfer Zone. They are interpreted to have been deposited by braided sandy rivers with large bar units or large compound dunes and downstream accretion compound bars (Figueiredo, 2013). The architectural elements suggest deep fluvial channels in the region.

The post-rift sequence is separated from the underlying units by a regional unconformity and is represented by the Aptian sedimentary succession of the Marizal Formation. This formation has been subdivided into the Banzaê Member at the base and the overlaying Cícero Dantas Member (Freitas, 2014). The Marizal Formation caps most of the Central Tucano basin, being composed of sandstones and subordinate conglomerates developing mesas and plateaus with incised canyons. The Marizal Formation was deposited in fluvial systems associated with local alluvial fans. Provenance of basement pebbles and cobbles transported from alluvial fans on the rift border (Figueiredo, 2016; Freitas, 2017) and the deformation bands within sandstones of the Banzaê Member of the Marizal Formation studied in this work suggest that rifting occurred also after deposition of this Aptian unit.

2.3 The Vaza-Barris Transfer Zone (VBTZ)

The Vaza-Barris Transfer Zone (VBTZ) (Magnavita and Cupertino, 1988; Milani and Davison, 1988; Chemalle Jr. et al., 1994; Magnavita et al., 1994; Szatmari and Milani, 1999; Destro, 2002; Gordon et al., 2017) is a ~125 km long and ~50 km wide WNW-ESE trending basement high that stand out as a positive gravity anomaly in Figure 1b and separates the North Tucano basin from the Central Tucano basin to the south (Figs. 1 and 3). It accommodates the polarity inversion between the east-facing North Tucano basin and the west-facing Central Tucano basin, linking the oppositely dipping São Saité and Adustina master faults (Fig. 3). Structurally it not only forms an oblique basin high, which is a characteristic feature of many transfer or step-over zones (Rosendahl et al., 1986; Fossen et al., 2010), but also displays an arch-shaped geometry in cross-section along its length (the Vaza-Barris arch; e.g., Milani and Davison, 1988), as shown in Fig. 3. The southern master fault, (Adustina fault; Fig. 3) bends abruptly into a NW-SE orientation as it enters the transfer zone. An apparent extension of its trend is represented by two oppositely dipping faults, both apparently referred to as the Caritá fault in the literature and are thus better referred to as the Caritá fault zone. This fault zone parallels the trend of the underlying Sergipana belt, which is slightly oblique to the average trend of the transfer zone (Fig. 3). The master fault of the north basin (São Saité fault) looses most of its displacement as it enters the transfer zone on the west side, but appears to be linked to a smaller NW-SE trending fault (named Canudos fault in Fig. 3). The Vaza-Barris Transfer Zone is largely confined by these faults, although with a slightly more WNW-ESE orientation. Internally the transfer zone shows a lower density of seismically resolvable faults, particularly in its central and western part.

The existing fault map and seismic resolution

The faults shown in Figure 3 are well constrained by seismic data acquired by Petrobras and presented by Aragão and Peraro (1994). They are mapped at the top of the pre-rift Sergi Formation level and extrapolated to the surface, with a fault resolution of a few tens of meters (Destro, pers. comm., 2018). The heaves (horizontal separation) shown on the map therefore represent the heaves at top Sergi Formation level. Hence, subseismic structures in the Tucano Rift would be any structure with offset < 20-30 m.

3. Structures and structural analysis

Structural mapping revealed the extensive presence of deformation bands, deformation band clusters and faulted deformation band zones (deformation band faults), as previously noted by Destro et al., (2002, 2003) (Fig. 4). A description of these structures, their distribution, geometry and orientations is given below, followed by a kinematic analysis.

3.1 Deformation bands

Deformation bands (Fossen et al., 2007) are widespread in the basin, and stand out in the field as more resistant to weathering than their host rock, as is typical for cataclastic bands (Fig. 4a). Each single band shows an offset up to a few cm, while zones of several bands show offsets that correspond to the cumulative offset of individual strands. Microscopically the bands show abundant evidence of grain size reduction, where the finer-grained material within the bands is more angular than the grains in the host rock, i.e. features characteristic of cataclasis (Fig. 5). The degree of cataclasis increases from almost none in the immediately surrounding host rock to ultracataclasites in the most strongly deformed central parts of well-developed bands (Fig. 5 – D: high porosity reduction from host rock with up to 24% porosity to slip surface with porosity < 0.2%). The cataclastic deformation bands within the Tucano Rift show from 1 to 3.5 orders of magnitude of permeability reduction as compared to the host rock, where clusters and slip surfaces are the least permeable structures (Fig. 6). This is similar to published data from different localities worldwide (Ballas et al., 2015).

In general the bands are very similar to classical extensional cataclastic deformation bands described from Jurassic sandstones in southern Utah and the Nubian sandstone in Sinai in terms of deformation mechanism, geometry and their tendency to link up with each other both the vertically and horizontally to form zones and clusters (Aydin and Johnson, 1983; Fossen and Hesthammer, 1997; Rotevatn et al., 2008). Conjugate sets are also common, and both sets of single bands and thin clusters form conjugate sets that mutually offset each other (Fig. 4g). The fact that the extensional bands show strong cataclasis suggests a minimum burial depth of ~1 km, possibly several kilometers (Fossen et al., 2007, 2017).

3.2 Deformation band clusters and zones

Deformation bands commonly occur together in clusters consisting of a few to hundreds of bands (Fig. 4b, d). These clusters are very tight, with band material commonly constituting more than 50% of the total rock volume. Several closely spaced clusters can constitute a wider deformation band (shear) zone that normally shows one or more slip surfaces (see below). The clusters show more or less symmetric anastomosing patterns of intertwined deformation bands in sections perpendicular to the displacement direction (Fig. 4b). A very different asymmetric arrangement is typically seen in zone-perpendicular sections containing the displacement vector (i.e., the vertical section for normal-sense and reverse-sense zones; Fig. 4d). This section typically exhibits a set of long and steeply dipping bands and a multitude of shorter bands at a high angle to the first set. The second set is commonly bound by the first set. This arrangement is referred to as ladder structures (Davis, 1999; Schultz and Balasko, 2003) and is further discussed below in terms of kinematics. The ladder structures can form conjugate sets and in extreme cases reach thicknesses of several meters, in which case the term radiator rock has been suggested (Davis, 1999) (Fig. 4e).

When considering the surface of cluster zones, they commonly show a corrugated surface with a geometric lineation pointing down-dip for normal and reverse zones and horizontally for strike-slip zones (Fig. 4c) (Fossen and Hesthammer 1997; Fossen 2018). The corrugation pattern is not directly related to slip but reflects the shape of the anastomosing deformation bands in three dimensions.

3.3 Deformation band faults

Meter- to tens of meter-thick zones of deformation bands usually display one or more through-going slip surfaces with a sub-planar geometry and well-developed slickenlines (Fig. 4f). The slip surfaces are composed of a mm-thick zone of ultracataclasite, and show meters or tens of meters of displacement, i.e. much more than the clusters or zones of deformation bands themselves, but mostly less than the 20-30 m vertical resolution of the seismic data. Deformation band zones with major slip surfaces, here termed deformation band faults, form characteristic positive features (ridges) in the terrain that can be identified from remote sensing images in well-exposed areas. Both field and remote-sensing data indicate a typical spacing of these first-order deformation

band zones of 0.5-2 km (see Section 4). Deformation band faults typically contain several hundreds of deformation bands (as measured perpendicular to the zone).

3.4 Extracting stress, strain and kinematics: methodology

Most deformation bands are shear localization features that form at an angle to the maximum principal stress (σ_1) or shortening direction that is found to vary from 18-34° for bands formed in the extensional regime (Fossen et al., 2017). Hence conjugate sets bisected by the shortening direction constrain the principal stress or strain directions (Fig. 7a-b).

In addition to conjugate sets, we use the different geometries observed in different sections of deformation band zones: Anastomosing bands characterize the section perpendicular to the shear direction, while a Riedel-shear type arrangement known as ladder structures typically appear in sections perpendicular to the zone and parallel to the shear direction (Figs. 4d and 7a, e). Ladder structures and the asymmetric arrangements of long and short elements (R and R', respectively) reveal the sense of shear of deformation band zones, as indicated in Fig. 7a, c, d, and e. The long elements are slightly oblique to the zone with offsets synthetic to that of the main zone, and are of Riedel-type (R). The connecting antithetic elements have the orientation and kinematics of anti-riedels (R'). R' structures seem to rotate during shearing, and younger sets may offset earlier R' elements. They may also obtain a slightly sigmoidal shape due to this rotation by distributed shear (Katz and Weinberger, 2005).

For strike slip zones, the ladders are observed in the horizontal section, while for normal (Fig. 7) and reverse (Fig. 5d) structures, they appear in the vertical section. Ladder structures are extremely common in the Tucano Basin and have proved very useful for kinematic analysis, particularly where sense of displacement on fault slip planes is ambiguous.

Fault slip analysis was performed on slip data from slip surfaces. The presence of striations is a distinguishing criterion for separating slip surfaces from deformation bands, together with their very fine-grained ultracataclastic fault rock that is less than one millimeter thick in most cases. Sense of slip can be ambiguous from the slip surfaces themselves, but ladder structures in the walls provided reliable and consistent slip sense criteria. Limited occurrence of slip surfaces is a limiting factor in the kinematic analysis of the data, and some grouping of data from neighboring localities has been necessary.

The method used is that described by Marrett and Allmendinger (1990) and both Orient (Vollmer, 2017) and FaultKin (Allmendinger, 2017) softwares were used in the calculations of P (shortening) and T (extension) axes and quadrants.

At this point the long-standing question whether stress or strain is recorded appears: clearly the deformation structures represent displacements and strain, hence strain axes are recorded. However, because of the relatively small strains involved, the principal strain axes ($X \geq Y \geq Z$) may be interpreted to represent principal stress directions ($\sigma_1 \geq \sigma_2 \geq \sigma_3$), particularly for conjugate sets with small offsets and negligible block rotations (Fig. 7). For fault slip analysis, however, care needs to be exercised when making this assumption (Twiss and Unruh, 1998; Marrett and Peacock, 1999), and we generally prefer to refer to strain axes in this work.

4. Results

4.1 General structural picture

Deformation bands show a predominantly (N)NE-(S)SW orientation, with a pole maximum at 118/06 (from Bingham analysis; Fig. 8a), consistent with ~N118E extension across the Tucano Rift. Subseismic deformation band faults show the same general pattern (red lines in Fig. 9), with a subpopulation oriented parallel to the transfer zone, i.e. WNW-ESE. The latter trend is found within the Vaza-Barris Transfer Zone, and is not observed in the area south of the transfer zone. In the following we will refer to five structural subdomains: the western Canudos area (Subdomain 1), the central Vaza-Barris Transfer Zone (2), the Jeremoabo fault (3) and Caritá fault (4) areas on the eastern basin border, and the Massacará area (Subdomain 5) south of the transfer zone (Fig. 10).

4.2 Conjugate sets of bands

Conjugate sets of bands and clusters (Fig. 8b) define the orientations of the principal strain axes as shown in Figure 7. In simple cases only two conjugate sets occur, and the three strain axes are easily defined. This is the case with plots 2, 4, 7, and 8 in Figure 9a. Some of these (2 and 8) clearly reflect the general WNW-ESE extension suggested by the majority of deformation bands (Fig. 8a, b) and deformation band faults (Fig. 8d, e). Plot 7 shows NNE-SSW extension, perpendicular to the local fault

orientation. In contrast, Plot 4 indicates a strike-slip regime, with NE-SW directed horizontal shortening (Z) and NW-SE extension (X). A similar strain field is indicated by NE-trending conjugate sets in Plot 3, which also shows a set consistent with NE-SW extension (Fig. 9a). These two sets in Plot 3 are difficult to explain in a single strain field and are interpreted to represent a change in strain field during rifting. Plots 6 and 5, however, show two double sets of conjugate bands that represent horizontal stretching in all directions (orthorombic systems), i.e. X being close to Y. Whether this represents a true flattening deformation history or a temporal change in extension direction in these areas is not clear from the field relations. Finally, there is the polymodal expression of Plot 1 that also indicates finite extension in all directions in the horizontal plane, plus a kinematically incompatible double set (red great circles in the plot in Fig. 9a) consistent with a strike-slip regime with NE-SW shortening. It is tempting to relate these variations in strain axes orientations to temporal changes in the extension direction along the border fault at the location of the transfer zone.

4.3 Fault slip kinematic analysis

Kinematic data were collected from striated slip surfaces from 74 different localities. Because of scarcity of data, these were combined into 42 localities for detailed analysis. Considering all data together, it is impossible to fit them into one strain field. The strain field that can explain most (70%) of the data was calculated, and suggest a regional extensional regime with extension towards ~120 (ESE-WNW) (Fig. 8f). This is consistent with the general extension direction inferred from the general structural trend of deformation bands (see previous section). The remaining 30% of the data were then treated separately, yielding a secondary strain field of vertical faulting (Fig. 8g), and a tertiary strike-slip regime (Fig. 8h). The latter is consistent with NW-SE extension and NE-SW shortening, with a vertical intermediate strain axis.

Breaking down the data to 42 localities distributed within the area gives a better impression of the spatial variation in strain axes orientation. This dataset, presented in Figs. 9b and 11, shows that evidence of strike-slip kinematics is found in many localities within the transfer zone, but not in the Central Tucano basin south of the transfer zone, where a WNW-ESE extensional regime completely dominates. The strike-slip regime is relatively consistent along the transfer zone, with NE-SW shortening and NW-SE extension. This is also the regime reported by Destro (2003) from the Jeremoabo fault area in the eastern part of the transfer zone.

4.4 Distribution

The majority of deformation bands and related subseismic slip surfaces are NNE-SSW oriented extensional structures, agreeing with overall WNW-ESE directed rift basin extension (Fig. 8). However, there are variations close to major faults, notably along the NW-SE trending Caritá fault (Subdomain 4) and in part along the Jeremoabo fault (Subdomain 3). The maps (Figs. 9 and 10) give the impression that the subseismic deformation band faults are quite regularly spaced and distributed across the transfer zone (Subdomain 2 in Fig. 10). Their density in the WNW-ESE (extension) direction is at least 0.5-1/km, as estimated along the river transect. In other areas the poor degree of exposure of the pre- and synrift sequence complicates such estimates over long distances, but the map shows that the distribution looks quite uniform. This also goes for the relatively small Subregion 5 south of the transfer zone. Each deformation band fault is associated with many hundreds of bands that together constitute the fault core and damage zone to these faults, hence the band density is more than 2-3 orders of magnitude higher than the fault density (in the order of 1000 bands/km).

5. Discussion

This work has demonstrated an abundance of subseismic structures within the Vaza-Barris Transfer Zone in the Recôncavo-Tucano-Jatobá rift system. The structures are classical deformation band structures and deformation band faults typical of deformed porous sandstones, and their orientation, and distribution have several interesting implications, as discussed below.

Extension direction across the Recôncavo-Tucano-Jatobá rift system

The extension direction during the evolution of the rift system has been debated in the past, as the large range in orientation of larger faults can be interpreted in different ways. For instance, Cohen (1985) argued that the fault pattern interpreted from seismic data suggests that the rift system opened by E-W (i.e., orthogonal) stretching. On the contrary, Milani and Davison (1988) argued for a WNW-SSE extension direction based on their interpretation of the fault pattern, consistent with more regional palinspastic considerations by Szatmari et al. (1985, 1987). Our data provide additional constraints on

the extension direction, with the advantage of involving not only the orientation of shear bands and faults, but also kinematics (shear or slip direction). Hence, the extension direction can be better constrained.

As documented above, the majority of the subseismic structures mapped in this work are oriented NE-SW, and the kinematic data clearly shows a predominance of extension vector (X) to be oriented at ~120°. This extension direction is found within the transfer zone as well as in the Central Tucano basin (Subregion 5 in Fig. 10). Hence our data support the interpretation by Milani and Davison (1988) of oblique rifting. Further, the 120° extension direction documented here conforms perfectly with the local kinematic pattern predicted from plate reconstruction by Heine et al. (2013), where Brazil rotates clockwise relative to the African side of the rift system (Fig. 12). Magnavita (1992) suggested an earliest Cretaceous E-W extension followed by NW-SE extension in the late Barremian and early Aptian time. We find no evidence for early E-W extension in our subseismic data base. Deformation band structures form during any stage of rifting, including the earliest stages (e.g., Fossen et al., 2007), and we would expect them to record such a change in extension direction.

There is however a subordinate set of NW-SE trending deformation band structures that are somewhat underrepresented in the rose diagrams of Fig. 10, because most of the observations were done along the WNW-trending Vaza Barris river valley. This subordinate set of deformation band faults are subparallel to the main faults mapped from seismic data, i.e. the Caritá fault and a parallel fault to the south that is here named Canudos fault (Fig. 3), and typically display strike-slip dominated movement. Hence, while the trend of the seismically resolvable faults in the transfer zone are represented among the subseismic faults and deformation bands, the main population of subseismic structures have an orientation that is different from that of larger faults. Kinematically these and related deviating structures indicate a component of NE-SW shortening and are interpreted as being due to complications along the transfer zone.

Distribution of subseismic structures

A particularly interesting characteristic feature of the subseismic deformation band faults in the transfer zone is their relatively even distribution. Deformation bands are concentrated around the slip surfaces as damage zones, but the distribution of the latter (deformation band faults of mostly subseismic size) is extraordinarily even at around

1/km (see red lines in Fig. 10). In general, this clustering of deformation band structures into zones and deformtaion band faults is typical for the extensional (normal fault) regime, and different from the contractional regime where bands tend to be much more distributed (Soliva et al., 2016). The deformation band *faults*, however, are quite evenly distributed in the transfer zone. In general, the distribution of subseismic deformation depends on the local boundary conditions (Fossen and Rotevatn, 2012). For example, deformation band stuctures (either as bands or deformation band faults) are generally well distributed in extensional relay ramps (e.g., Rotevatn and Fossen, 2007) and in the steep limb of large fault propagation folds (monoclines) (Zuluaga et al., 2014; Fossen et al., 2017). In the San Rafael monocline, Utah, the spacing between small deformation band clusters/faults was observed to be a few meters in the steep dip part of the monocline. The cross-section along the Vaza-Barris Transfer Zone shows that the zone defines a major arch in the WNW-ESE direction (Fig. 3, profile), and we suggest that the formation of this arch may have involved enough stretching along the arch to cause or help create the even distribution of deformation band faults. The spacing is much larger than for the San Rafael Monocline example described by Zuluaga et al. (2014), but that moncline involves much higher strains (higher dips and dip gradients) for a thinner sandstone unit. Our interpretation is that since strain is distributed along the Vaza-Barris arch, large faults that cross-cut and offset the arch did not develop. In contrast, strain did localize into larger faults in the main rift basins to the north and south.

A relevant question in this context is whether the distribution is different outside of the Vaza-Barris Transfer Zone. Unfortunately, the level of exposure and extensive cover by postrift sediments make it difficult to evaluate the density of structures away from the transfer zone. In part of Subdomain 5, south of the transfer zone, similar densities are observed, but in a location near a larger ENE-trending fault. In other places there seems to be fewer structures. We consider the fairly even distribution of subseismic structures in the Vaza-Barris Transfer Zone along with a smaller amount of larger faults to be a characteristic feature of this transfer zone, and probably also of many other rift transfer zones.

Strain regime

The overall deformation in the Vaza-Barris Transfer Zone as revealed by slip surface kinematic data (Figs. 9b and 10) show a dominance of NE-SW stretching

(extensional regime), although with some variation in terms of extension direction and with some indications of 3D strain. In addition, a strike-slip regime is identified in several locations, with a remarkably uniform expression of NE-SW shortening (Z) and NW-SE extension (X) (Figs. 9b, 10 and 11). This regime, which constitutes a relatively small proportion of the entire data set (Figs. 8h and 11), is consistent with that described by Destro (2003) from the Jeremoabo fault area, and dextral strike-slip on the Caritá fault. However, the amount of extension in the NW-SE (X) direction is clearly much larger than the amount of shortening in the NE-SW direction (Z); hence the strain regime is transtensional. This observation may be related to the preexisting basement structure and its influence the location and orientation of the NW-SE trending major faults that diagonally crosscut the rift (notably the Caritá and Canudos faults; Fig. 4). These faults strike parallel to some of the basement structures in the Neoproterozoic Sergipana orogenic belt, notably the structure marked as the Itaporanga fault zone in Fig. 1 (Destro, 2003). A dextral component on this trend and sinistral slip on the Jeremoabo fault trend fit the strain field found for the Vaza-Barris Transfer Zone (Fig. 4). Clearly, the location and orientation of the Sergipana belt must have controlled the location of the Vaza-Barris Transfer Zone and the NW-SE trending faults in this area. However, the majority of subseismic structures appear to be controlled by the rift extension and the bending of the Vaza-Barris arch, striking N(N)W-S(S)E, as shown by the red lines in Figs. 9 and 10.

Implications for fluid flow

Deformation bands and subseismic deformation band faults in extensional setting generally are not able to trap significant amounts of hydrocarbons, but can introduce a macropermeability anisotropy in reservoirs (Fossen and Bale, 2007; Ballas et al., 2015). Hence, the strongly preferred orientation of the deformation bands and deformation band faults in the Vaza-Barris Transfer Zone introduces a quite significant km-scale anisotropy, with restricted flow in the 120° direction NW-SE) and relatively easy flow in the direction perpendicular to the transfer zone. In a hydrocarbon injection/production situation, this anisotropy should be taken into consideration during well planning, given the high density of subseismic structures documented in this work: drilling perpendicular to these structures (parallel to the transfer zone) would be beneficial for most purposes.

Rifting continued into the "postrift" era

The occurrence of deformation bands and local slip surfaces in what has been considered the post-rift sequence of the rift system (the Banzaê Member of the Marizal Formation) shows that rifting affected Aptian deposits. Whether this was the end of continuous rifting or a late pulse is unknown, but the NW-SE extension direction during this late stage rifting was identical to that of the main rift phase. Hence we conclude that the regional stress field responsible for the rift evolution was still in place in or after the Aptian.

6. Conclusions

We have investigated the subseismic deformation of the Vaza-Barris rift transfer zone in the Cretaceous Recôncavo-Tucano-Jatobá rift system, and found the following characteristics:

-Abundant subseismic structures in the form of deformation bands, deformation band clusters and fully developed deformation band faults.

-Large population of parallel orientation and even distribution of the subseismic deformation band faults perpendicular to the transfer zone. Subordinate transfer zone-parallel structures are less common.

-Subseismic structures are consistent with NW-SE extension along the transfer zone (120°), which we relate to its arcuate shape in cross-section (the Vaza-Barris arch).

-This stretching direction is also found south of the transfer zone, and is considered document oblique rifting in a direction consistent with Early Cetaceous plate reconstructions (e.g., Heine et al., 2003).

-Rift-related structures consistent with the main rift strain field are also recorded in what is considered the Aptian post-rift sequence (Marizal Formation), thus extending the history of rifting at least until the Aptian.

-In a petroleum exploration and production perspective, a transfer zone of the type investigated here represents a basin-scale structural high that could potentially host hydrocarbons, and management of production from such a zone should take the macropermeability anisotropy imposed by the deformation bands and deformation band faults into consideration.

Acknowledgments

This work was made possible through FAPESP grants 2016/03091-5 and 2015/23572-5) and a Petrobras master's degree scholarship (FUSP – PFRH) to the first author.

Figures Article

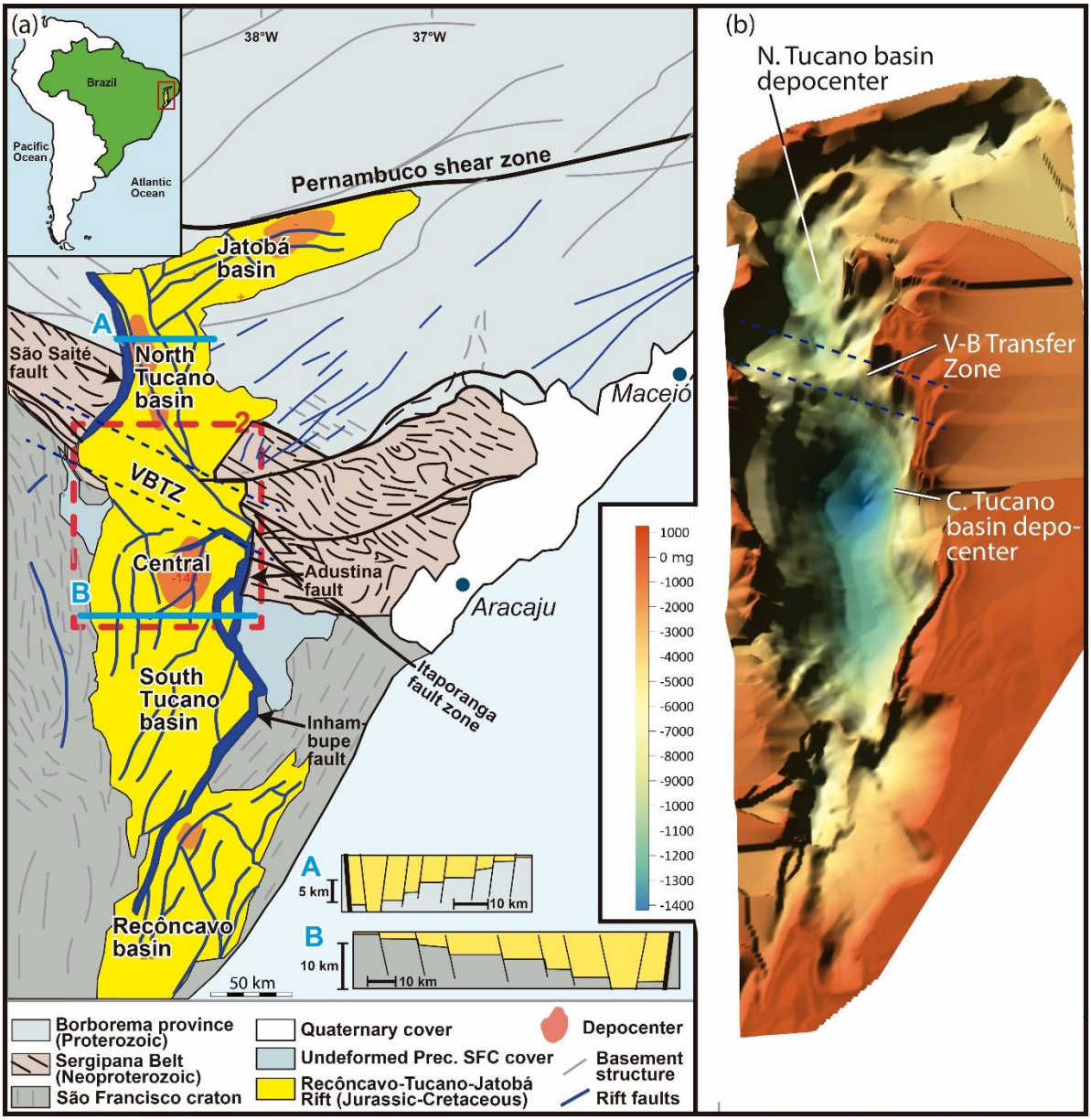

Fig. 1. (a) Recôncavo-Tucano-Jatobá rift system. Based on Magnavita (1992), Szatmari and Milani (1999) and Gordon et al. (2017). Study area indicated (red dashed square). Profiles illustrate the change in polarity across the transfer zone. (b) Gravimetric model of the rift system, illustrating the deep Central Tucano basin and the shallow Vaza-Barris (V-B) transfer zone separating it from the North Tucano basin depocenter. Gravimetric data from Magnavita (1992).

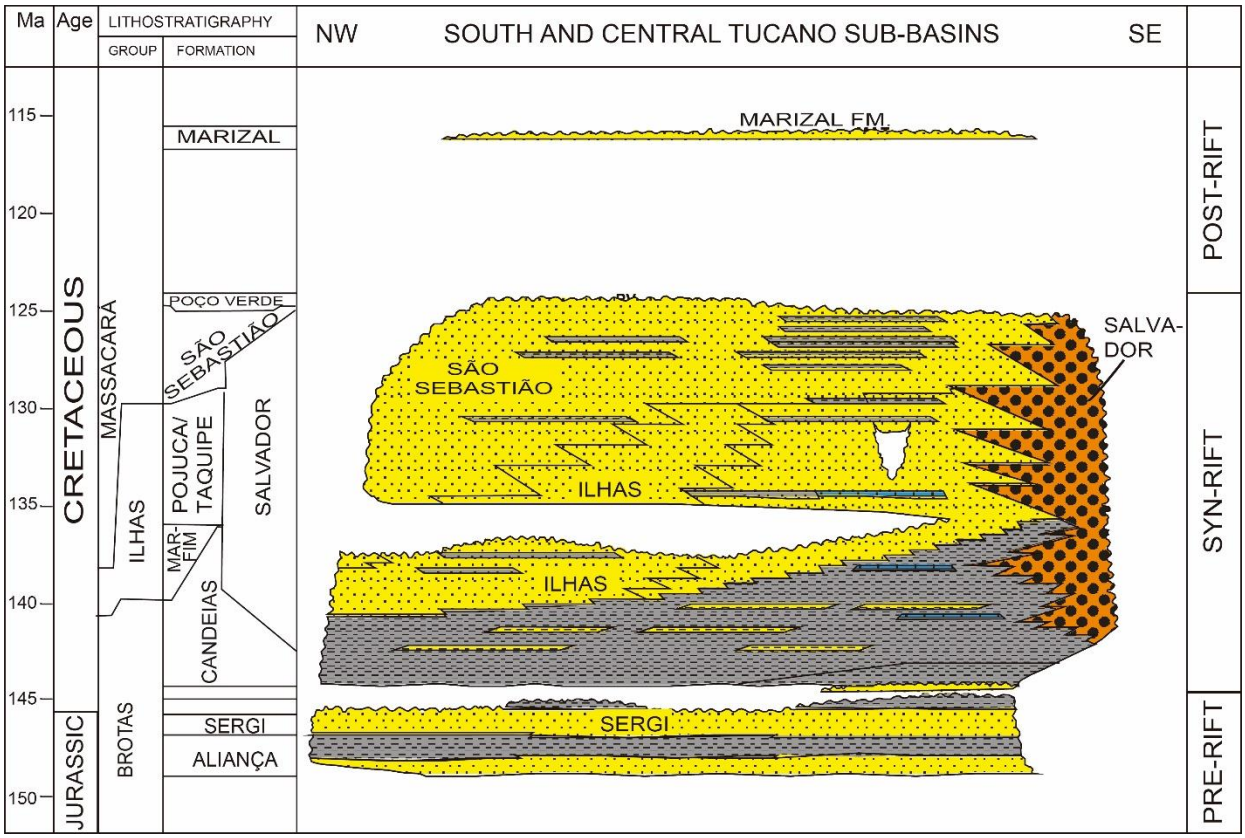

Fig. 2. Central and South Tucano basin chronostratigraphic chart. From Costa et al. (2007).

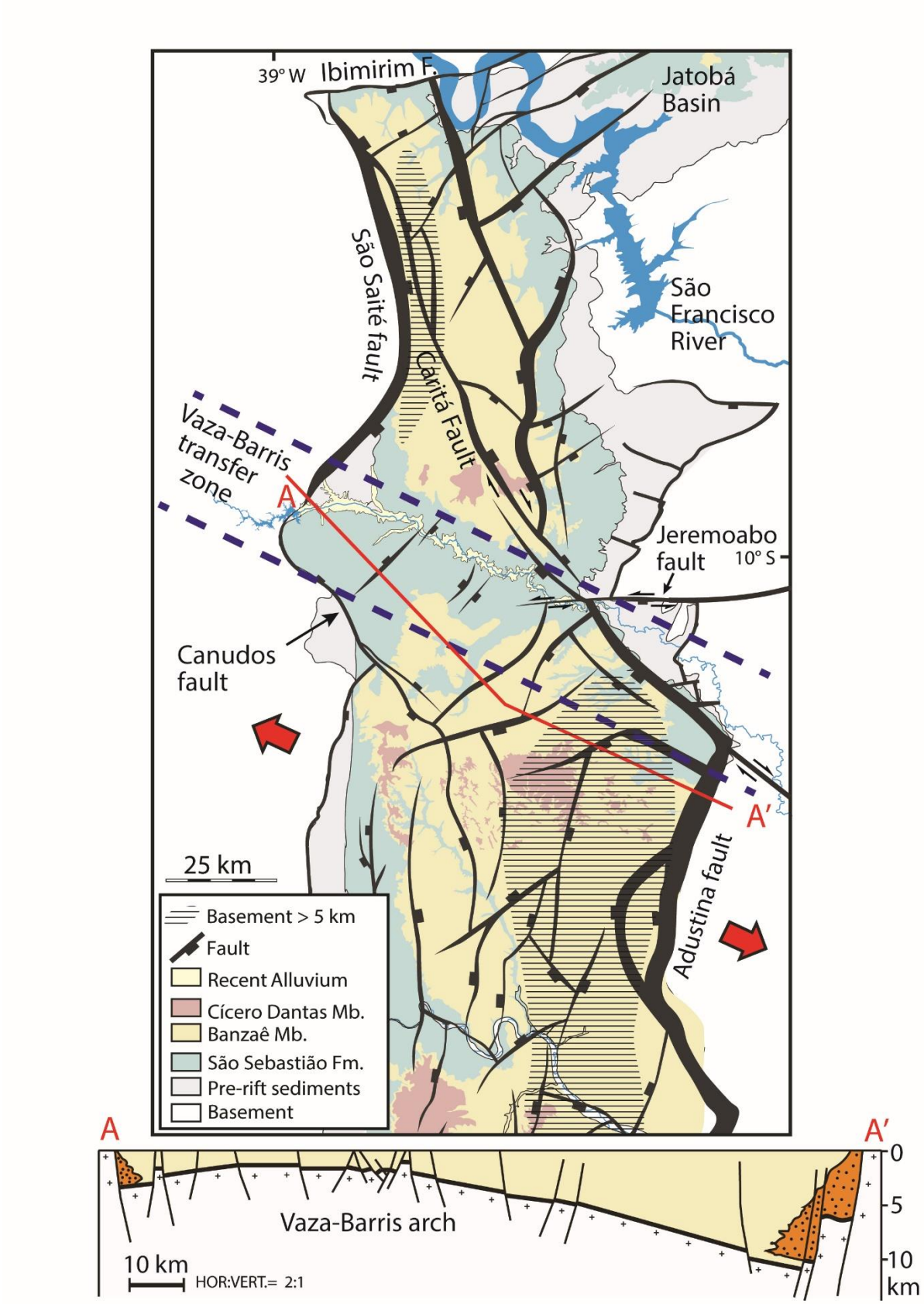

Fig. 3 Geologic map of the Tucano-Jatobá rift system. A cross-section along the Vaza-Barris transfer zone is shown. Fault pattern from Destro (2002), based on Aragão (1994) and Aragão & Peraro (1994).

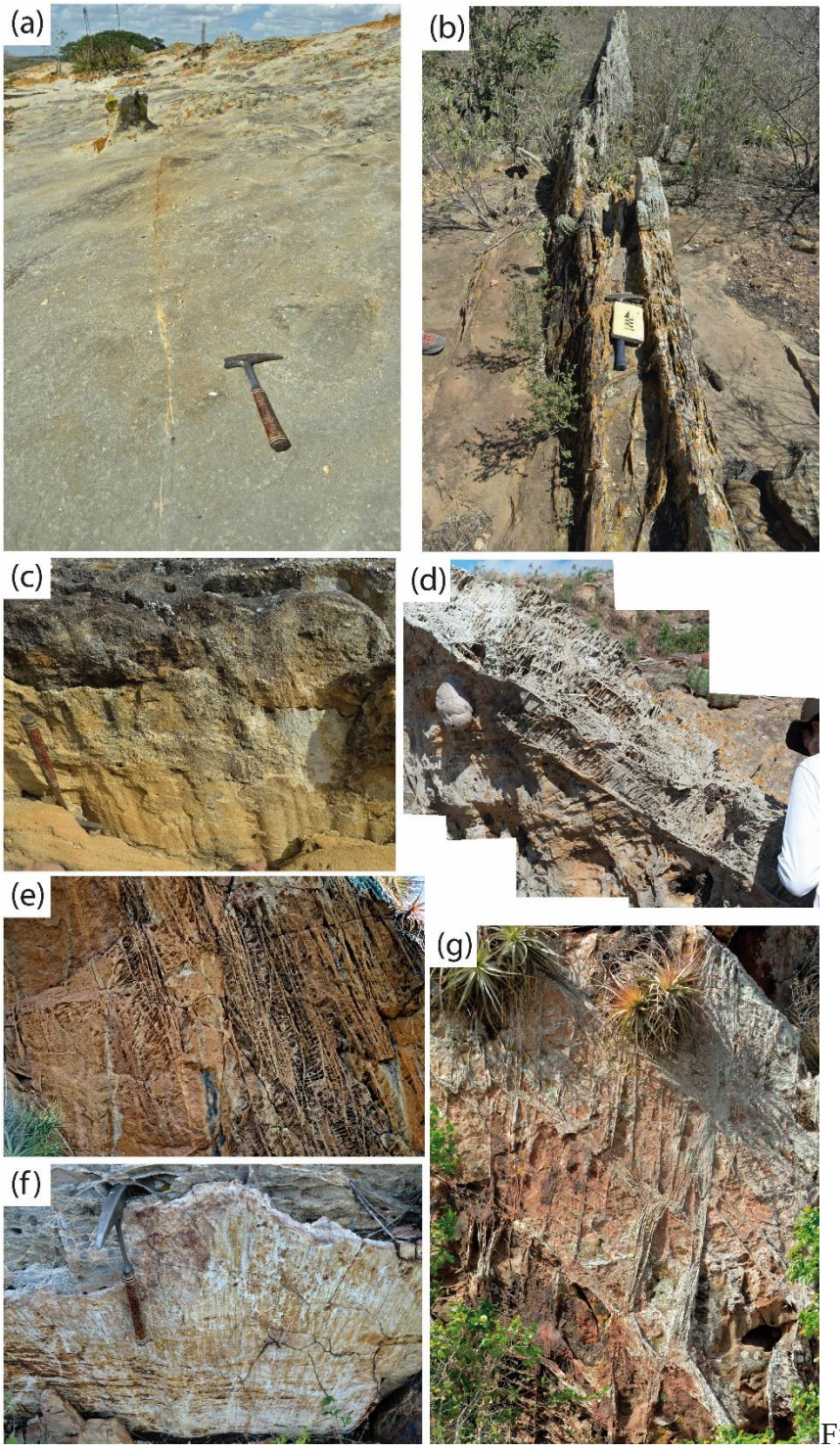

Fig. 4 (a) Single deformation band, showing evidence of linkage along strike. (b) Typical deformation band cluster as viewed at a high angle to the shear direction. (c) Corrugations created by curved deformation band. The corrugation axis (geometric lineation) is parallel to striae on slip surfaces in the area. (d) Well-developed ladder structure, showing reverse-oblique offset. (e) Radiator rock (very thick ladder structure), normal sense of shear. (f) Slip surface in deformation band zone (deformation band fault). g) Mutually crosscutting conjugate sets of bands.

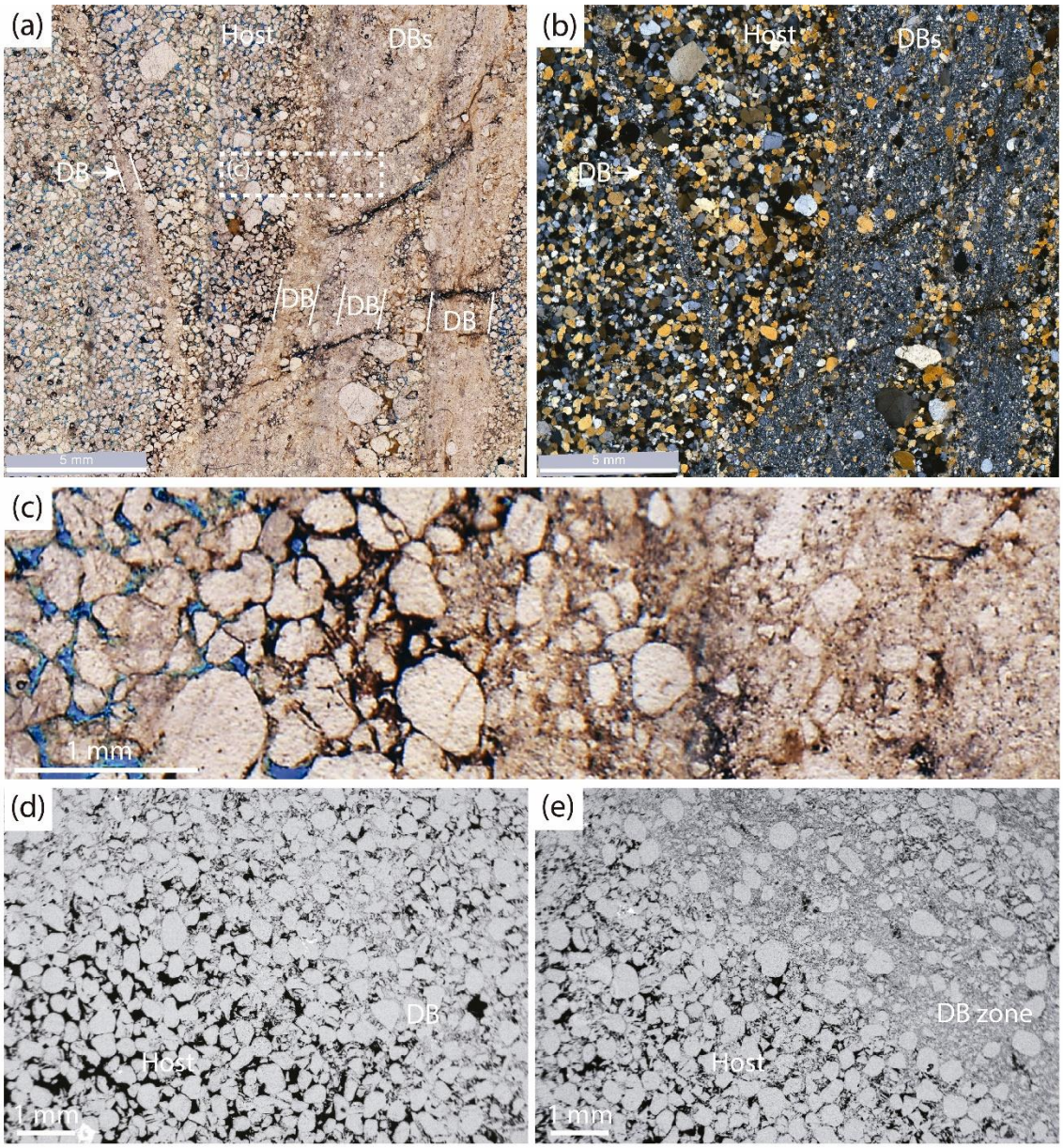

Fig. 5. Microscale appearance of deformation bands from the Sergi Fm., as seen through the optical micro-scope (a-c) and Scanning Electron Microscope (d-e). (a-b) Parallel and crossed nicols, respectively, showing single deformation band (DB) and a zone of several bands on the right. (c) is a magnified part as shown in (a). Note significant loss of porosity and reduction in grain size, as also seen in the SEM images (d-e).

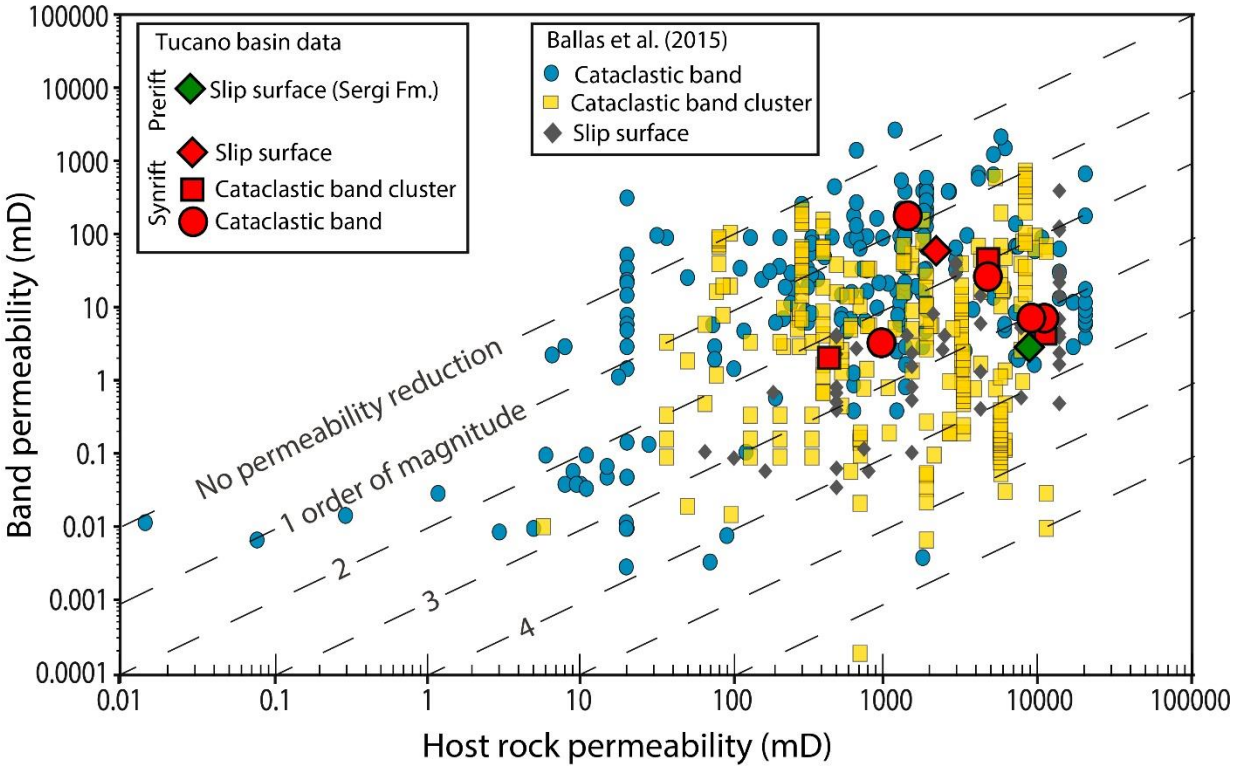

Fig 6. Permeability data from the Tucano basin deformation structures (TinyPerm II portable air permeameter measurements performed in the field) plotted together with global data presented by Ballas et al. (2015).

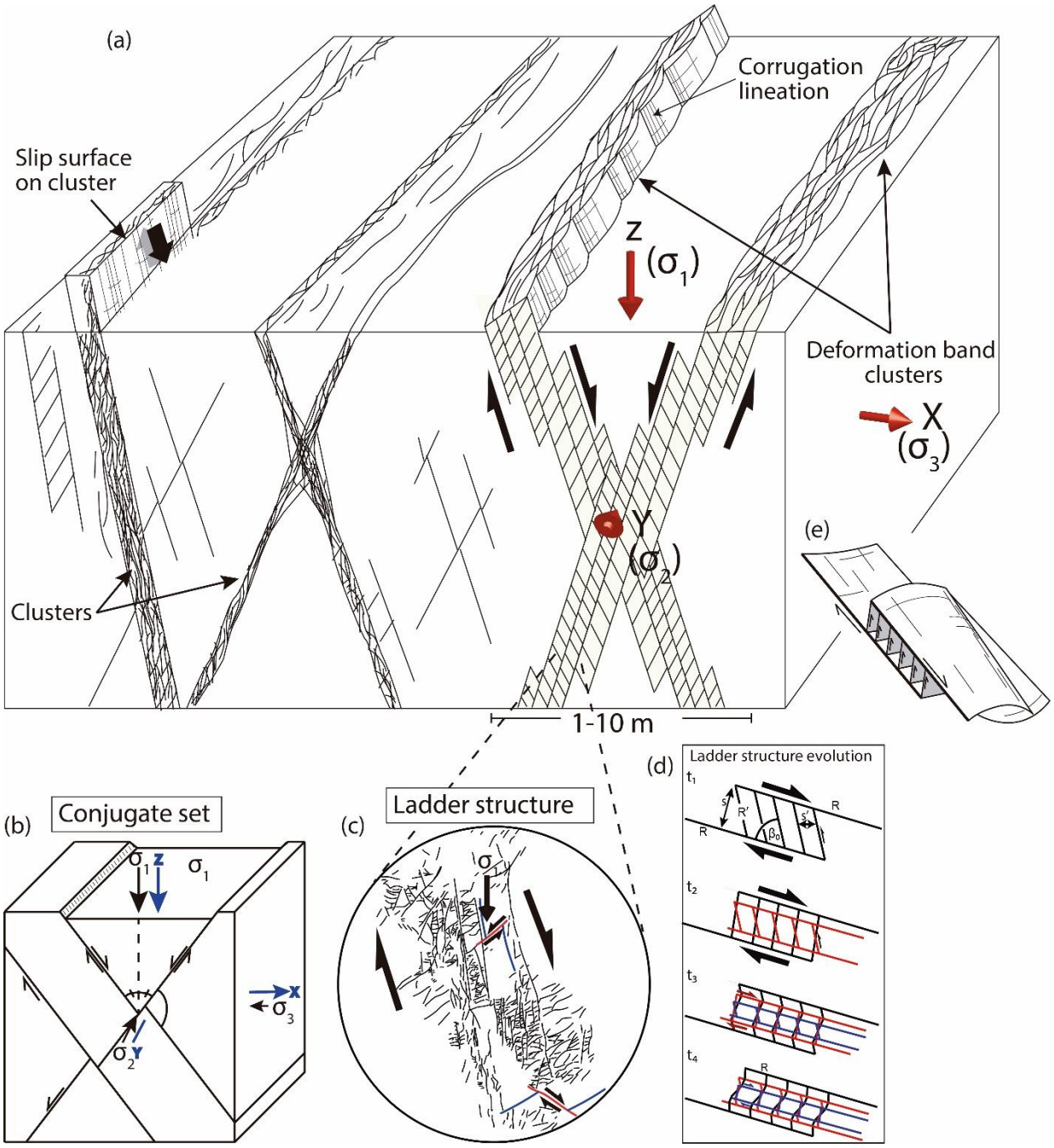

Fig. 7. (a) Block diagram showing normal-sense deformation band faults damage zone (upper left) and conjugate ladder sets (upper right) (modified from Fossen, 2018). Geometries are similar for strike-slip zones but must be rotated 90°around the X axis. (b) Deformation band conjugate sets (bottom left). (c) Ladder structure, redrawn from field photo. (d) Evolution of ladder structures (modified from Katz et al., 2005). (e) 3D geometry of ladder structure (modified from Schultz and Balasko, 2003). Both principal stresses (s1>s2>s3) and strains (X>Y>Z) are shown.

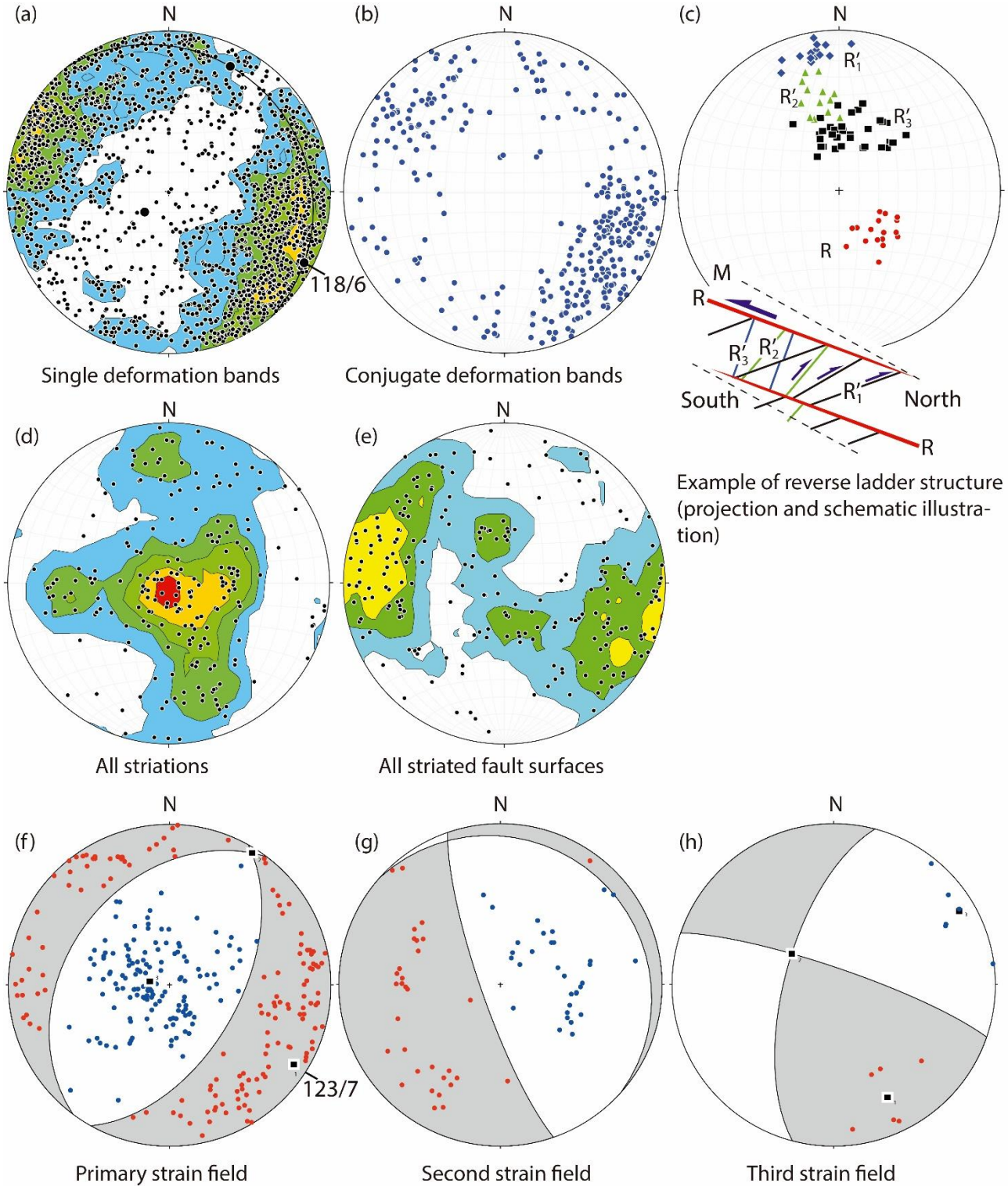

Fig 8. Orientation data from the entire study area. (a) Deformation bands, (b) conjugate deformation bands, (c) example of data from reverse ladder structure (measurements and principal sketch), (d) Striations (lineations), (e) slip surfaces with striations, (f-e) P and T axes from all data, separated into primary, secondary and tertiary strain fields. See text for discussion.

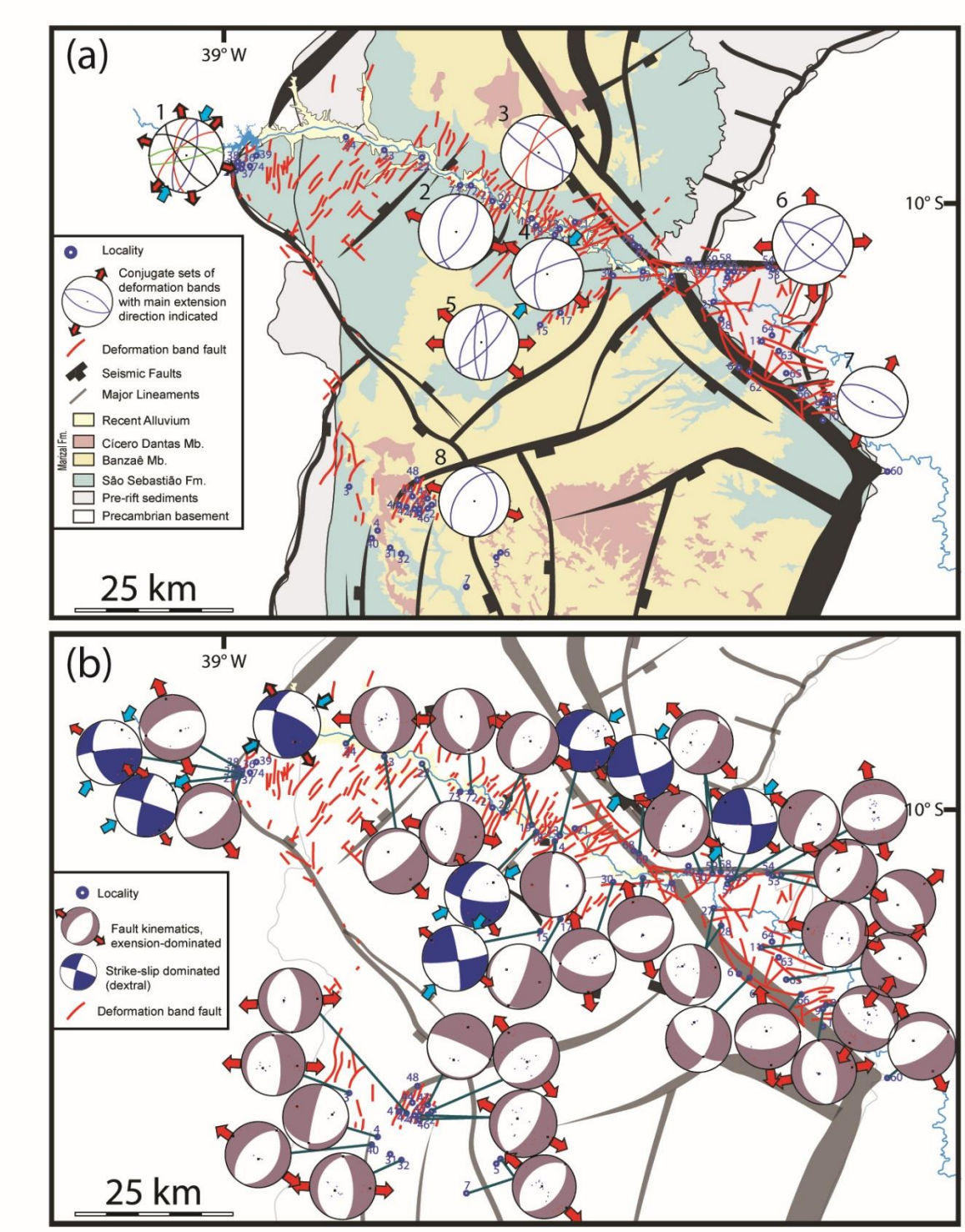

Fig. 9. a) Kinematics reflected by conjugate sets of deformation bands and deformation band clusters (lower hemisphere equal area spherical projections). b) Kinematics from fault-slip data. Red arrows indicate horizontal extension directions where definable. Blue arrows are shortening directions. Strike-slip solutions are marked in deep blue color.

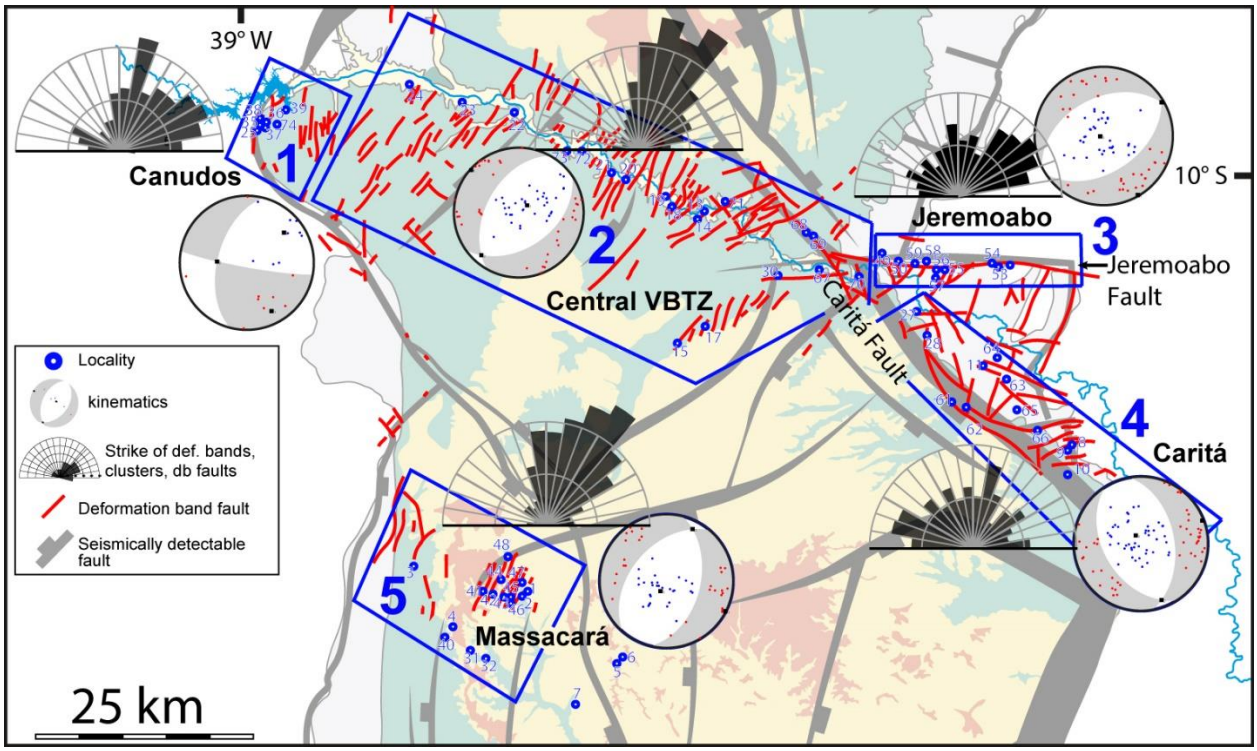

Fig. 10. Subdomains discussed in the text, deformation band fault orientations and best fit kinematic P-T diagrams for each subdomain. Rose diagrams show the trend of deformation bands, band clusters and defor-mation band faults. Deformation band fault orientations are in part from Magnavita (1992).

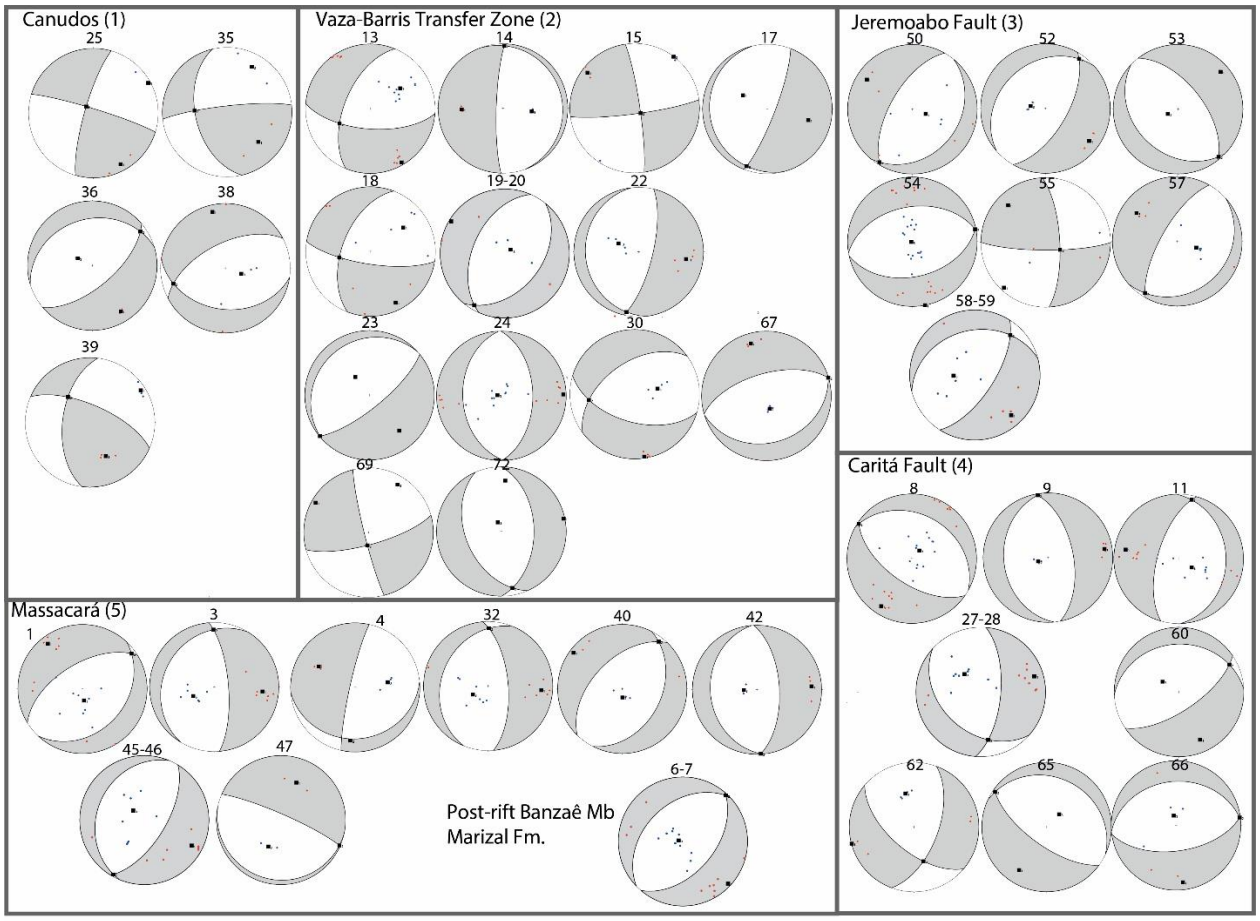

Fig. 11. Strain fields calculated from fault slip data for different subdomains and localities. Their distribution is shown in Fig. 9b.

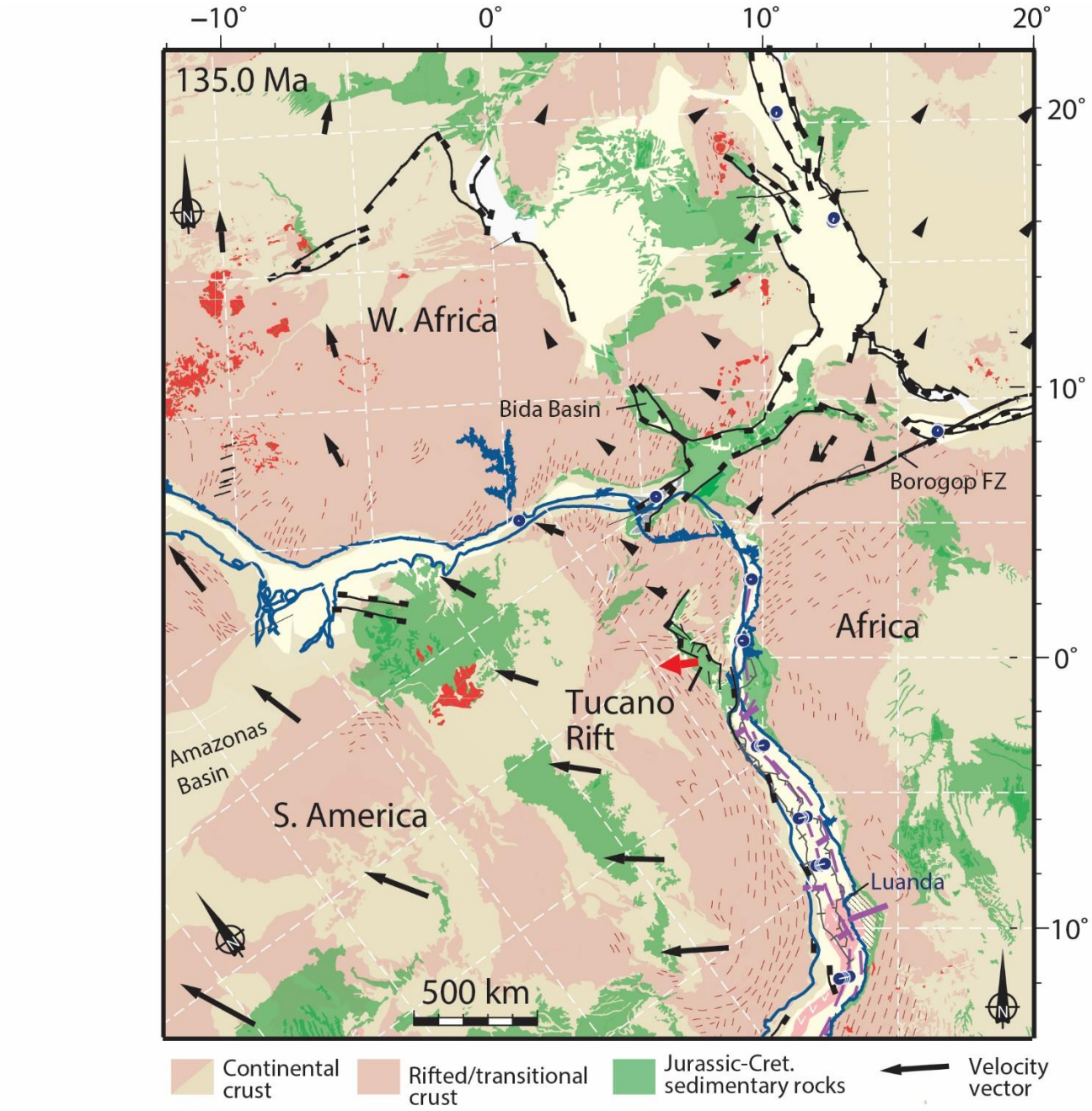

Fig. 12. The Tucano Rift in a kinematic context, modified from Heine et al. (2013). Black arrows indicate mo-tion (velocity vectors) relative to a fixed southern Africa. Brazil is rotating clockwise according to this model, and the extension direction documented in this work from subseismic structures (120°, indicated by a red arrow at Tucano Rift) fits perfectly well with this model.

6. Synthesis

B*asement heritage of Precambrian basement structure on rift basin development*

A long-standing question in the formation of rift basins is the role of pre-existing brittle and ductile structures in underlying basement. In other words, to what extent do basement structures and fabrics influence or control the location, distribution, orientation and growth of rift-related normal faults, and thereby the overall rift geometry and petroleum distribution. Reactivation of the Neoproterozoic Sergipe belt basement structures by the Vaza-Barris Transfer Zone and the Caritá Fault might have influenced the development of transfer faults during rifting such as the Jeremoabo Fault (Magnavita et al., 1994; Destro et al., 2003). Preexisting basement structures can have rather profound influence on the location and geometry of rift-related faults, although the actual effect will depend on the orientation, dip, strength, continuity and size of the preexisting structure. Tectonic faults can be oriented parallel to the rift axis but show many steep steps with subordinate segments or odd-guiding steps that closely match the tendencies of the basement lineaments. This produces very angular fault traces in map view (‘zig-zag’ pattern) that can be attributed to the reactivation of the basement during the connection of fault segments.

Deformation bands in a major rift transfer zone

The analysis of deformation bands in different areas of the Tucano basin enables the comparison between orientation and kinematic patterns within the Vaza-Barris Transfer Zone and away from it. The great dominance of north to north-east striking high angle clusters showing normal-slip sense agrees with the overall structure of the rift, revealing that the majority of the subseismic structures are compatible with the regional stress field responsible for the basin formation. Moreover, the orientation of the deformation bands indicates that, even in a context with a complex pattern of syn-rift faults reactivating inherited basement structures of varied orientation, the subseismic structures tend to be frequently related to the main normal faults orthogonal to the extension direction.

This pattern can be found both in outcrops on top of the major Vaza-Barris Transfer Zone (VBTZ) and away from it. Subordinate strike-slip deformation bands are found only along the transfer zone and at the basin-borders, possibly recording local stresses related to fault tips and transfer faults. Different orientation of subseismic structures is dominant only in pre-rift successions to the east of the area, possibly related to different regional stress fields.

Our new data shows conjugate sets, quadrimodal (rhombic) and polymodal faulting forming and slipping simultaneously (Reches, 1983; Krantz, 1988; Healy et al., 2015), which may introduce 3D strain complicated patterns from truly triaxial stresses.

Transfer zone subseismic structures dip

The Vaza-Barris Transfer Zone (VBTZ) shows predominance of steep (60°-80° dip angle) subseismic structures (i.e. deformation bands, clusters, slip surfaces and deformation band faults), conjugate sets with an average dihedral angle of 40°, normal-slip sense ladder structures and high rake (dip-slip to high-oblique) striation in slip surfaces, along the transfer zone and its surroundings. The transfer zone itself exhibits an arcuate shape with a less efficient mechanism to accommodate extension and displacement between overlap major fault-bounded rift borders. Minimum horizontal displacement occurs as structures are very steep, often vertical, agreeing with the overall shallower basin depth and therefore smaller beta stretching factor.

Implications for fluid flow

Due to cataclasis, these subseismic structures reduce the permeability from undeformed host rock along within the transfer zone, having influence on fluid flow within reservoir rocks and introducing a macro permeability anisotropy, in orders of magnitude similar to other published data (Ballas et al., 2015). Possibly due to overburden and precursory deformational history, the permeability hence is even lower within younger units.

Limitations related to the current study

The investigated data is limited by the degree of exposure of subseismic structures and because most part of the basin is covered by the so-called post-rift sediments of the Banzaê Member of the Marizal Formation.

Suggestions for future work

As a continuation of this work, it is suggested more fieldwork to measure permeability data in all the investigated units aiming to increase the sampling density compared to other published data. This will reveal the potential influence on fluid flow in reservoir production situations along major rift transfer zones.

In addition, more structural data will allow to refine the structural geological mapping of these subseismic structures. Each structure investigated should be separated by type and methodology used, taking notes of every useful information.

Finally, thermochronological studies would help in addition to investigate the age, thermal history, burial depth, subsidence curve and define periods of higher tectonic activity.

7. References

Allen, P.A. & Allen, J.R., 2005. Basin analysis – principles and applications. Blackwell Scientific.

Allken, V., Huismans, R.S., Fossen, H., Thieulot, C., 2013. 3D numerical modelling of graben interaction and linkage: A case study of the Canyonlands grabens, Utah. Basin Research 25, 436–449. https://doi.org/10.1111/bre.12010

Allmendinger, 2017. FaultKin 7. http://www.geo.cornell.edu/geology/faculty/RWA/programs/faultkin.html

Allmendinger, 2017. Stereonet 10.

http://www.geo.cornell.edu/geology/faculty/RWA/programs/stereonet.html

Aragão, M.A.N.F., 1994. Arquitetura, estilos tectônicos e evolução da Bacia do Recôncavo, Brasil, in Dias-Brito, D., et al., eds., Boletim do Terceiro Simpósio sobre o Cretáceo do Brasil: Rio Claro, Brazil, Universidade Estadual Paulista 3, p. 161-164.

Aragão, M.A.N.F., Peraro, A. A., 1994. Elementos estruturais do rifte Tucano-Jatobá, in Dias-Brito, D., et al., eds., Boletim do Terceiro Simpósio sobre o Cretáceo do Brasil: Rio Claro, Brazil, Universidade Estadual Paulista, p. 161-164.

Aydin, A., Johnson, A.M., 1983. Analysis of faulting in porous sandstones. Journal of Structural Geology, 5, p.19-31.

Ballas, G., Fossen, H., Soliva, R., 2015. Factors controlling permeability of cataclastic deformation bands and faults in porous sandstone reservoirs. Journal of Structural Geology 76, 1-21. doi:http://dx.doi.org/10.1016/j.jsg.2015.03.013

Bosworth, W., 1985. Geometry of propagating continental rifts. Nature 316, 625–627. https://doi.org/10.1038/316625a0

Chemalle Jr. et al., 1994. Análise das Principais Feições Estruturais Nas Subbacias do Tucano Sul e Central - Bahia., Geociências (São Paulo), Rio Claro, v. 13, n. 2, p. 405-419, 1994.

Cohen, C., 1985. Role of fault rejuvenation in hydrogen accumulation and structural evolution of Reconcavo Basin, Northeast Brazil. Am. Assoc. Pet. Geol. Bull. 64, 65-76.

Costa, I.P., Milhomem, P. da S., Bueno, G.V., Silva, H.S.R.L. e, Kosin, M.D., 2007. Boletim de Geociências da Petrobras 15, 433-443.

Davis, G. H., 1999. Structural Geology of the Colorado Plateau Region of Southern Utah, with Special Emphasis on Deformation Bands. Geological Society of America Special Paper 342.

De Araújo Netto, J.M., Da Silva, F.C.A., De Sá, E.F.J., 2012. Caracterização meso e microscópica de bandas de deformação em arenitos porosos: um exemplo nas tectonossequências Paleozóica, Pré- e Sin-rifte da Bacia do Araripe, Nordeste do Brasil. Geologia USP - Serie Cientifica 12, 83–98. https://doi.org/10.5327/Z1519-874X2012000100007

Della Piazza, H., Muhlmann, H., 1963. Geologia do Vale do Rio Vasa Barris - área de Cocorobó a Jeremoabo. PETROBRÁS Int. Rep. No. 108-1777, Salvador, 70 p.

Destro, N., 2002. Falhas de Alívio e de Transferência: O Significado Tectônico e Econômico no Rifte Recôncavo-Tucano-Jatobá, NE Brasil. Universidade Federal de Ouro Preto.

Destro, N., Alkmim, F.F., Magnavita, L.P., Szatmari, P., Stern, R.J., 2003. The Jeremoabo transpressional transfer fault, Recôncavo-Tucano Rift, NE Brazil. Journal of Structural Geology 25, 1263–1279. https://doi.org/10.1016/S0191-8141(02)00164-5

Dixey, F., 1926. The nyasaland section of the great rift valley. The Geographical Journal, 68:117-137.

Dixey, F., 1938. The nyasa-shire rift. The Geographical Journal, 91:51-56.

Dos Santos Scherer, C.M., De Ros, L.F., 2009. Heterogeneidades dos reservatórios flúvio-eólicos da Formação Sergi na Bacia do Recôncavo. Boletim de Geociencias Da Petrobras 17, 249–271.

Einsele, G., 2000. Sedimentary Basins. Evolution, Facies and Sediment Budget. Springer.

Ferreira, T.S., Da Silva, F.C.A., 2010. Bandas de deformação em arenitos porosos: Estudo de casos em bacias do nordeste do Brasil. Boletim de Geociências Da Petrobras 18, 207–231.

Figueiredo, F.T., 2013. Proveniência e arquitetura de depósitos fluviais das Sub-Bacias Tucano Central e Norte, Cretáceo (BA). Universidade de São Paulo.

Figueiredo, F.T., Almeida, R.P., Freitas, B.T., Marconato, A., Carrera, S.C., Turra, B.B., 2016. Basin Research 28, 433-445. doi: 10.1111/bre.12115

Fossen, H., Johansen, T.E.S., Hesthammer, J., Rotevatn, A., 2005. Fault interaction in porous sandstone and implications for reservoir management; examples form southern Utah. AAPG Bulletin, 89, 12, 1593-1606. Doi: 10.1306/07290505041

Fossen, H., 2010. Deformation bands formed during soft-sediment deformation: Observations from SE Utah. Marine and Petroleum Geology 27, 215-222. doi:10.1016/j.marpetgeo.2009.06.005

Fossen, H., 2018. Geologia estrutural. Oficina de textos, 2nd edition.

Fossen, H., Bale, A., 2007. Deformation bands and their influence on fluid flow. AAPG Bulletin, 91, 1685-1700. doi:10.1306/07300706146.

Fossen, H., Hesthammer, J., 1997. Geometric analysis and scaling relations of deformation bands in porous sandstone. Journal of Structural Geology 19, 1479-1493.

Fossen, H., Rotevatn, A. 2012. Characterization of deformation bands associated with normal and reverse stress states in the Navajo Sandstone, Utah: Discussion. AAPG Bulletin 96, 869-876. doi:10.1306/09221110173

Fossen, H., Rotevatn, A., 2016a. Fault linkage and relay structures in extensional settings-A review. Earth-Science Reviews 154, 14–28. doi:https://doi.org/10.1016/j.earscirev.2015.11.014

Fossen, H., Howell, J.A. & Eide, C.H., 2016b. Deposition and deformation of clastic sediments on the Colorado Plateau: a field guide. Unpublished field guide, University of Bergen, 116 pp.

Fossen, H., Schultz, R.A., Shipton, Z.K., Mair, K., 2007. Deformation bands in sandstone: a review. Journal of the Geological Society, London, 164, 755-769.

Fossen H., Soliva, R., Ballas, G., Trzaskos, B., Cavalcante, C., Schultz, R.A., 2017. Geological Society, London, Special Publications, 459. doi:https://doi.org/10.1144/SP459.4.

Freitas, B.T., 2014. A Formação Marizal (Aptiano) na Bacia do Tucano (BA): Contribuições à análise da arquitetura de depósitos fluviais e implicações paleobiogeográficas. PhD thesis, Universidade de São Paulo.

Freitas, B.T., Almeida, R.P., Carrera, S.C., Figueiredo, F.T., Turra, B.B., Varejão, F.G., Assine, M.L., 2017. Aptian sedimentation in the Recôncavo-Tucano-Jatobá Rift System and its tectonic and paleogeographic significance. Journal of South American Earth Sciences 80, 460–481. doi:https://doi.org/10.1016/j.jsames.2017.10.001

Gawthorpe, R.L., Leeder, M.R., 2000. Tectono-sedimentary evolution of active extensional basins. Basin Research, 12, 195-218.

Gibbs, A.D., 1984. Structural evolution of extensional basin margins. Journal of the Geological Society 141, 609–620. https://doi.org/10.1144/gsjgs.141.4.0609

Gordon, A., Destro, N., Heilbron, M., 2017. São Francisco Craton, Eastern Brazil. 171–185. doi:https://doi.org/10.1007/978-3-319-01715-0

Gregory, J.W., 1894a,b. Contributions to the physical geography of british east Africa. The Geographical Journal, 4:289-315, 4:505-514.

Gregory, J.W., 1920a,b. The African rift valleys. The Geographical Journal, 56:13-41, 56:327-328.

Healy, D., Blenkinsop, T.G., Timms, N.E., Meredith, P.G., Mitchell, T.M., Cooke, M.L., 2015. Polymodal faulting: Time for a new angle on shear failure. Journal of Structural Geology 80, 57–71. doi: https://doi.org/10.1016/j.jsg.2015.08.013

Huismans, R., Beaumont, C., 2011. Depth-dependent extension, two-stage breakup and cratonics underplating at rifted margins. Nature, 473, 74-79. doi: 10.1038/nature09988

Katz, Y., Weinberger, R., 2005. Strain localization in sandstone during embryonic stages of shear-zone evolution. Terra Nova 17, 311–316. doi;https://doi.org/10.1111/j.1365-3121.2005.00615.x

Krantz, R.W., 1988. Multiple fault sets and three-dimensional strain: Theory and application. Journal of Structural Geology 10, 225–237. doi:https://doi.org/10.1016/0191-8141(88)90056-9

Lister, G.S., Etheridge, M.A., Symonds, P.A., 1986. Detachment faulting and the evolution of passive continental margins. Geology, 14, 246-250.

Mack, G.H., Seager, W.R., 1995. Transfer zones in the southern Rio Grande rift. Journal of the Geological Society 152, 551–560. doi:https://doi.org/10.1144/gsjgs.152.3.0551

Magnavita, L.P., 1992. Geometry and kinematics of the Recôncavo-Tucano-Jatobá Rift, NE Brazil. PhD Thesis, University of Oxford, 493 p.

Magnavita, L.P., Cupertino, J.A., 1987. Concepção atual sobre as bacias do Tucano e Jatobá, Nordeste do Brasil. Boletim de Geociências da Petrobras, 1, 119-134.

Magnavita, L.P., Cupertino, J.A., 1988. A new approach to the geological configuration of the Lower Cretaceous Tucano and Jatobá basins, northeastern Brazil. Revista Brasileira de Geociências 18, 222-230.

Magnavita, L.P., Davison, I., Kusznir, N.J., 1994. Rifting, erosion, and uplift history of the Recôncavo- Tucano-Jatobá Rift, northeast Brazil. Tectonics 13, 367–388. doi:https://doi.org/10.1029/93TC02941

Marrett, R., Allmendinger, R. W., 1990. Kinematic analysis of fault-slip data. Journal of Structural Geology 12, 973-986.

Marrett, R., Peacock, D.C.P., 1999. Strain and stress. Journal of Structural Geology 21, 1057-1063.

McKenzie, D.P., 1978. Some remarks on the development of sedimentary basins: Earth and Planetary Science Letters, 40, 25-32.

Milani, E.J., Davison, I., 1988. Basement control and transfer tectonics in the Recôncavo-Tucano-Jatobá rift, Northeast Brazil. Tectonophysics 154, 41–70. https://doi.org/10.1016/0040-1951(88)90227-2

Morley, C.K., Nelson, R.A., Patton, T.L., Munn, S.G., 1990. Transfer zones in the East African Rift System and their relevance to hydrocarbon exploration in rifts. AAPG Bulletin 74, 1234-1253.

Moustafa, A.R., 1997. Controls on the development and evolution of transfer zones: the influence of basement structure and sedimentary thickness in the Suez rift and Red Sea. Journal of Structural Geology 19, 755–768. doi:https://doi.org/10.1016/S0191-8141(97)00007-2

Olsen, K.H. & Morgan, P., 1995. Progress in understanding continental Rifts. In: Olsen, K.H., (Ed.), Continental Rifts: Evolution, Structure, Tectonic, p.3-26. Elsevier.

Prosser, S., 1993. Rift-related linked depositional systems and their seismic expression. Geological Society, London, Special Publicaitons, 71, 35-66.

Reches, Z., 1983. Faulting of rocks in three-dimensional strain fields II. Theoretical analysis. Tectonophysics 95, 133–156. doi:https://doi.org/10.1016/0040-1951(83)90264-0

Riedel, W., 1929. Zur Mechanik Geologischer Brucherscheinungen. Zentral-blatt fur Mineralogie, Geologie und Paleontologie B, 354-368.

Roque, N.C., Chemale Jr., F., 1994. Mecanismo de Falhamento nos arenitos da Bacia do Tucano, Bahia. Geociências (São Paulo), Rio Claro, 1994.

Rosendahl, B.R., Reynolds, D.J., Lorber, P.M., Burgess, C.F., Mcgill, J., Scott, D., Lambiase, J.J., Derksen, S.J., 1986. Structural expressions of rifting: lessons from Lake Tanganyika, Africa. Sedimentation in the African Rifts, Geological Society Special Publication 25, 29–43.

Rosendahl, B.R., 1987. Architecture of continental rifts with special reference to East Africa. Annual Review of Earth and Planetary Science, 15, 445-503.

Rotevatn, A., Torabi, A., Fossen, H., Braathen, A., 2008. Slipped deformation bands: A new type of cataclastic deformation bands in Western Sinai, Suez rift, Egypt. Journal of Structural Geology, 30, 1317-1331.

Santos, C.; Reis, C., 2011. Geologia e Recursos Minerais das folhas Caimbé – SC.24-Z-A-I e Jeremoabo – SC.24-Z-A-II.

Scherer, C.M.S., De Ros, L.F., 2009. Heterogeneidades dos reservatórios flúvio-eólicos da Formação Sergi na Bacia do Recôncavo. Boletim de Geociências da Petrobras 17, n. 2, p. 249-271.

Schliche, R.W., Withjack, M.O., 2009. Origin of fault domains and fault-domain boundaries (transfer zones and accommodation zones) in extensional provinces: Result of random nucleation and self-organized fault growth. Journal of Structural Geology, 31, 910-925. doi:10.1016/j.jsg.2008.09.005

Schueller, S., Braathen, A., Fossen, H., Tveranger, J, 2013. Spatial distribution of deformation bands in damage zones of extensional faults in porous sandstones: Statistical analysis of field data. Journal of Structural Geology, 52, 148-162. http://dx.doi.org/10.1016/j.jsg.2013.03.013

Schultz, R.A., Balasko, C.M., 2003. Growth of deformation bands into echelon and ladder geometries. Geophysical Research Letters 30, n/a-n/a. https://doi.org/10.1029/2003GL018449

Schultz, R.A., Fossen, H., 2002. Displacement-length scaling in three dimensions: the importance of aspect ratio and application to deformation bands. Journal of Structural Geology, 24, 1389-1411.

Scott, D.L., Rosendahl, B.R., 1989. North Viking Graben: An East African Perspective. AAPG Bulletin, 73, 155-165.

Sengör, A.M.C., 1995. Sedimentation and tectonics of fóssil rift. In: Busby, C. & Ingersoll, R., (Eds.), Tectonics of Sedimentary Basins, p. 53-177, Black Well Science.

Sibson, R.H., 1977. Fault rocks and fault mechanisms. Journal of the Geological Society, 133, 191-213. https://doi.org/10.1144/gsjgs.133.3.0191

Soliva, R., Ballas, G., Fossen, H., Philit, S., 2016. Tectonic regime controls clustering of deformation bands in porous sandstone. Geology, 44, 423-426. doi:10.1130/G37585.1

Steiner, S. dos S., 2012. Morfotectônica de províncias distensionais ativas: implicações para os modelos de preenchimento de bacias tipo rift. PhD thesis. Universidade de São Paulo.

Szatmari, P., Françolin, J.B.L., Zanotto, O., Wolff, S., 1987. Evolução tectônica da margem equatorial brasileira, in Carneiro, C.R., ed., First symposium on the evolution of the South Atlantic Ocean, 1985. Revista Brasileira de Geociências. 17, 180-188.

Szatmari, P., Milani, E.J., 1999. Microplate rotation in northeast Brazil during South Atlantic rifting: Analogies with the Sinai microplate. Geology 27, 1115–1118. doi:https://doi.org/10.1130/0091-7613(1999)027<1115:MRINBD>2.3.CO;2

Szatmari, P., Milani, E., Lana, M., Conceição, J., Lobo, A., 1985. How South Atlantic rifting affects Brazilian oil reserves distribution. Oil and Gas Journal, Jan 14, pp. 107-113.

Twiss, R.J., Unruh, J.R., 1998. Analysis of fault slip inversions; do they constrain stress or strain rate? Journal of Geophysical Research 103 (B6), 12,205-12,222.

Vollmer, F.W., 2017. Ellipsefit 3.4.0: strain and fabric analysis software. http://www.frederickvollmer.com/ellipsefit/index.html.

Wernicke, B., 1981. Low-angle normal faults in the Basin and Range province: Nappe tectonics in an extending orogen. Nature, 291, 645-648.

Younes, A.I., Mcclay, K., Younes, A.I., 2002. Development of accommodation zones in the Gulf of Suez–Red Sea rift, Egypt. AAPG Bulletin 6, 1003–1026.

Zuluaga, L. F., Fossen, H., Rotevatn, A. 2014. Progressive evolution of deformation band populations during Laramide fault-propagation folding: Navajo Sandstone, San Rafael monocline, Utah, U.S.A. Journal of Structural Geology 68, 66-81. doi:10.1016/j.jsg.2014.09.008

8. Appendices

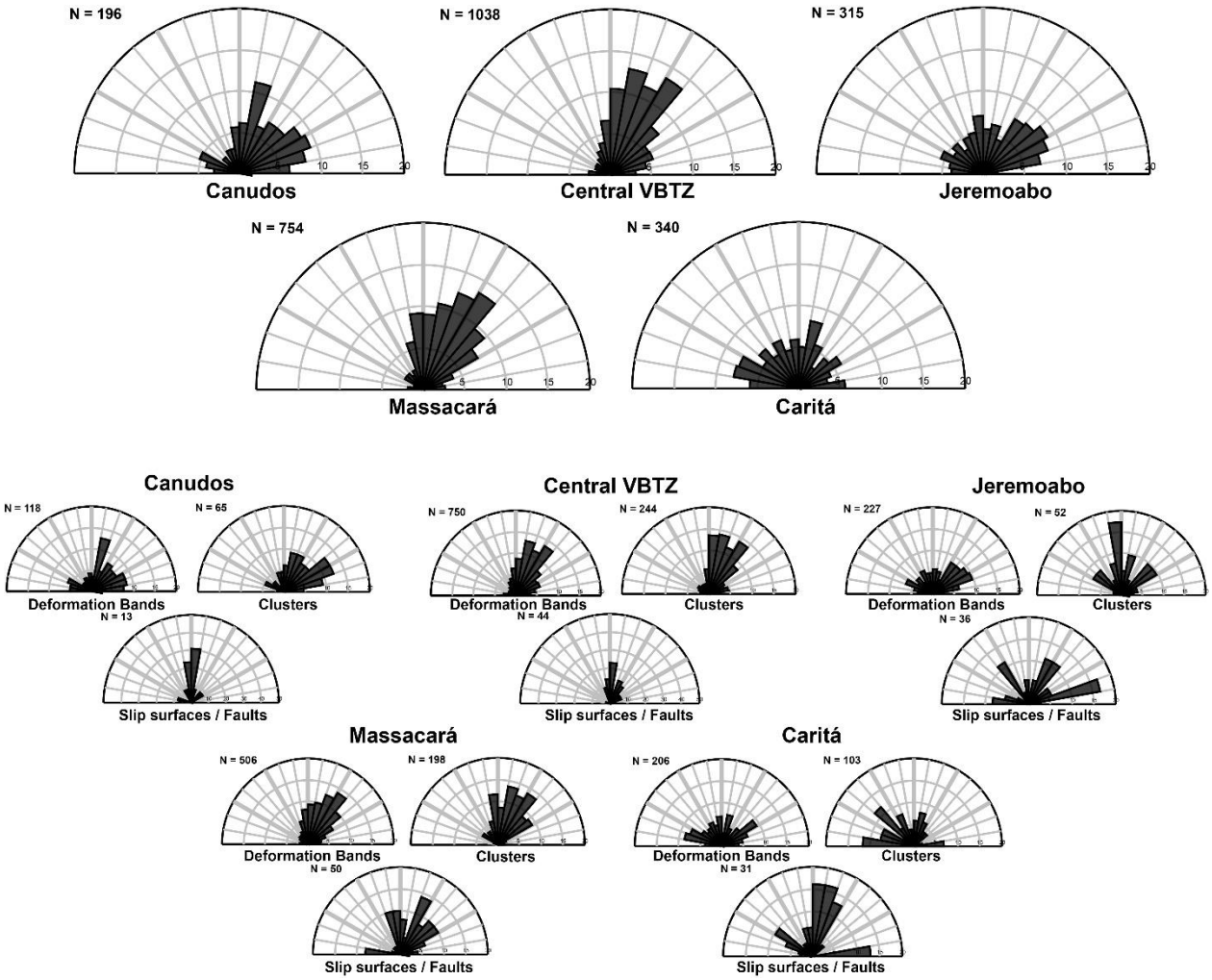

A. Normal sense subseismic structures rose diagrams separated by locality and type.

Localities	Lat	Long	Nº of Deformation Bands	Nº of Conjugate Sets	Unit deformed	σ 1	σ 2	σ 3
1-2	-10,471977	-38,758813	9	1	São Sebastião Fm.	72/179	17/021	06/289
8	-10,302617	-38,10838	12	1	Sergi Fm.	87/308	03/115	01/205
13	-10,027626	-38,546706	56	1	São Sebastião Fm.	14/034	64/273	22/129
15	-10,181829	-38,577962	13	2	São Sebastião Fm.	80/350	08/200	05/109
18-19	-10,021542	-38,585138	13	2	São Sebastião Fm.	68/347	22/172	02/082
20	-9,990259	-38,639378	30	1	São Sebastião Fm.	71/007	18/203	05/111
35	-9,925	-39,075278	43	5	Ilhas Gp.	σ_v	$\sigma_2 = \sigma_3$	$\sigma_3 = \sigma_2$
53	-10,089992	-38,196138	108	2	Sergi Fm.	89/114	01/267	01/357

B. Stress axes orientation calculated from conjugate sets of deformation bands.

Localities	Lat	Long	Nº of Fault Slip data	Unit deformed	Z	Y	X
1	-10,471977	-38,758813	8	São Sebastião Fm.	78/182	07/059	10/328
3	-10,442984	-38,893525	7	São Sebastião Fm.	73/225	14/007	10/099
4	-10,513558	-38,846031	3	São Sebastião Fm.	47/084	18/194	38/299
6-7	-10,551471	-38,646083	10	Banzaê Mb.	85/285	03/043	05/133
8	-10,302617	-38,10838	15	Sergi Fm.	77/042	02/303	12/213
9	-10,305432	-38,111304	4	Sergi Fm.	77/250	03/351	13/081
11	-10,207528	-38,213281	9	Sergi Fm.	72/124	07/012	17/280
13	-10,027626	-38,546706	9	São Sebastião Fm.	46/056	43/242	03/149
14	-10,036001	-38,554055	4	São Sebastião Fm.	50/093	01/001	40/270
15	-10,181829	-38,577962	1	São Sebastião Fm.	04/191	79/078	10/282
17	-10,162061	-38,545033	1	São Sebastião Fm.	53/297	05/200	36/106
18	-10,021542	-38,585138	5	São Sebastião Fm.	63/033	25/235	09/141
19-20	-10,009634	-38,592035	3	São Sebastião Fm.	81/029	09/213	01/123
22	-9,910075	-38,772744	4	São Sebastião Fm.	62/293	06/191	27/098
23	-9,898706	-38,834373	1	São Sebastião Fm.	61/322	01/231	29/140
24	-9,877778	-38,897944	9	São Sebastião Fm.	85/279	01/179	05/088
25	-9,929444	-39,078611	2	Ilhas Gp.	04/061	78/313	12/152
27-28	-10,14391	-38,29277	9	São Sebastião Fm.	51/329	38/167	09/070
30	-10,101347	-38,457391	4	São Sebastião Fm.	62/066	27/264	08/170
32	-10,551218	-38,806629	7	São Sebastião Fm.	67/241	11/360	20/094
35	-9,925	-39,075278	1	Ilhas Gp.	09/003	62/254	09/003
36	-9,923553	-39,070704	2	Ilhas Gp.	67/305	08/054	22/147
38	-9,921535	-39,074665	3	Ilhas Gp.	63/091	25/244	11/339
39	-9,906037	-39,039933	4	Ilhas Gp.	23/040	54/274	26/142
40	-10,525958	-38,855449	3	São Sebastião Fm.	80/181	08/037	06/307
42	-10,475456	-38,798053	3	São Sebastião Fm.	73/269	01/177	17/086
45-46	-10,479522	-38,777379	8	São Sebastião Fm.	71/315	05/209	18/117
47	-10,46154	-38,76304	2	São Sebastião Fm.	52/205	01/113	38/023
50	-10,086219	-38,314831	5	Sergi Fm.	61/068	24/212	15/309
52	-10,089893	-38,181588	4	Sergi Fm.	70/288	06/034	19/126
53	-10,089992	-38,196138	2	Sergi Fm.	76/245	04/140	14/049
54	-10,088183	-38,203013	16	Sergi Fm.	89/258	01/079	00/349
55	-10,095558	-38,25963	3	Sergi Fm.	08/256	68/005	21/164
57	-10,104952	-38,269565	4	Sergi Fm.	61/119	01/211	29/302
58-59	10,086135	-38,282563	6	Sergi Fm.	63/272	19/043	19/139
60	-10,417626	-38,005574	1	Sergi Fm.	66/302	12/062	20/156
62	-10,257113	-38,233409	4	Sergi Fm.	40/340	50/158	01/249
65	-10,260122	-38,172576	1	Sergi Fm.	67/044	04/304	23/213
66	-10,283175	-38,148417	3	Sergi Fm.	78/351	00/082	12/172
67	-10,096405	-38,408505	4	São Sebastião Fm.	73/165	01/074	17/344
69	-10,056167	-38,416677	1	São Sebastião Fm.	15/031	74/185	07/299
72	-9,955769	-38,692326	1	São Sebastião Fm.	78/340	12/169	02/078
Total			196				

C. Strain axes orientation inversion from striated slip surfaces (fault slip).

Samples	Localities	Description	Dip	Dipdir	Unit
CLB-01	1	Single band			São Sebastião Fm.
CLB-02A	4	HR + cluster	70	272	São Sebastião Fm.
CLB-02B	4	HR + cluster	70	272	São Sebastião Fm.
CLB-03	4	HR + cluster	88	277	São Sebastião Fm.
CLB-04	4	HR + cluster	42	111	São Sebastião Fm.
CLB-05	5	HR + single bands			Banzaê Mb. - Marizal Fm.
CLB-06	8	HR + thick cluster	14	358	Sergi Fm.
CLB-07	11	Cemented ? HR + thick cluster	77	292	Sergi Fm.
CLB-08a	11	Slip surface	77	200	Sergi Fm.
CLB-08b	11	HR + slip surface	77	200	Sergi Fm.
CLB-08b2	11	HR + slip surface	77	200	Sergi Fm.
CLB-09	11	HR + single bands			Sergi Fm.
CLB-10A	25	Big cluster	72	245	Ilhas Gp.
CLB-10B	25	Big cluster	72	245	Ilhas Gp.
CLB-11	35	Cluster	72	0	Ilhas Gp.
CLB-12	45	Cluster	20	295	São Sebastião Fm.
CLB-16	66	Cluster - Rotated normal sense ladder structures	77	140	Sergi Fm.
CLB-17	68	Cluster - Dextral deformation bands cutting cluster	59	108	São Sebastião Fm.

D. Selected samples for petrographic descriptions and SEM image analysis (thin sections).

Upper Jurassic Sergi Fm. - Locality 8	Host rock permeability (md)	Subseismic structure permeability (md)	DB/HR
8 - Slip Surface	8018,5	2,8	3,49E-04
Early Cretaceous Ilhas Gp. - Locality 35			**DB/HR**
11 - Cluster	10615,9	4,9	4,62E-04
Early Cretaceous São Sebastião - Locality 4			**DB/HR**
4-1 - Slip Surface	2027,5	59,1	2,91E-02
4-2 - Cluster	4448,2	44,6	1,00E-02
4-3 - Deformation Band	4448,2	26,2	5,89E-03
4-4 - Deformation Band	8722,7	7,4	8,48E-04
4-5 - Deformation Band	1294,2	162,3	1,25E-01
4-6 - Deformation Band	873,7	3,3	3,78E-03
4-7 - Cluster	409,6	2,1	5,13E-03
4-8 - Slip Surface	8018,5	2,8	3,49E-04
4-9 - Deformation Band	9758,8	7,4	7,58E-04

E. Tinyperm data: permeability contrasts between undeformed host rock (HR) and subseismic structures (deformation bands, clusters and slip surfaces).